

THE UNIVERSITY OF CALGARY

**A COMPREHENSIVE SILICON DIODE MODEL**

by

Edmond Edwin Clarke

A THESIS

SUBMITTED TO THE FACULTY OF GRADUATE STUDIES  
IN PARTIAL FULFILLMENT OF THE REQUIREMENTS FOR THE  
DEGREE OF MASTER OF SCIENCE

DEPARTMENT OF ELECTRICAL ENGINEERING

CALGARY, ALBERTA

MARCH, 1987

© Edmond Edwin Clarke 1987

THE UNIVERSITY OF CALGARY

Permission has been granted to the National Library of Canada to microfilm this thesis and to lend or sell copies of the film.

The author (copyright owner) has reserved other publication rights, and neither the thesis nor extensive extracts from it may be printed or otherwise reproduced without his/her written permission.

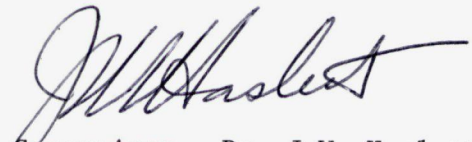
L'autorisation a été accordée à la Bibliothèque nationale du Canada de microfilmer cette thèse et de prêter ou de vendre des exemplaires du film.

L'auteur (titulaire du droit d'auteur) se réserve les autres droits de publication; ni la thèse ni de longs extraits de celle-ci ne doivent être imprimés ou autrement reproduits sans son autorisation écrite.

ISBN 0-315-35925-0

THE UNIVERSITY OF CALGARY  
FACULTY OF GRADUATE STUDIES

The undersigned certify that they have read, and recommended to the Faculty of Graduate Studies for acceptance, a thesis entitled, "*A Comprehensive Silicon Diode Model*" submitted by Edmond Edwin Clarke in partial fulfillment of the requirements for the degree of Master of Science.



Supervisor - Dr. J.W. Haslett  
Electrical Engineering Dept.



Dr. R.H. Johnston  
Electrical Engineering Dept.



Dr. J. Kendall  
Computer Science Dept.



Dr. F.N. Trofimenkoff  
Electrical Engineering Dept.

Date: Apr 30, 1987

## ABSTRACT

A Comprehensive silicon diode model is introduced. It mathematically portrays the steady state behavior of diodes for a wide range of applied bias and temperature. It is the summation of an improved diode equation and a refined depletion region recombination - generation (RG) equation which are both derived from the existing theoretical foundation. The improved diode equation extends the modelling capability of the popular ideal diode equation into the high level injection domain, and the refined depletion region RG equation describes the very low current region. The extended capability of the comprehensive diode model is demonstrated by a computer assisted comparison of the theoretical and measured characteristics of diodes exposed to elevated temperatures.

This work was motivated by the University of Calgary Electrical Engineering Department's interest in high temperature electronics for energy sector applications. Since PN junctions are a fundamental building block of both discrete and integrated semiconductor devices, a thorough knowledge of diode behavior is essential to the understanding of semiconductor electronics.

The ideal diode equation governs only the central part of the forward characteristic where low level injection prevails; here the current is larger than that which is attributable to depletion region RG but less than that which results from high level injection. A high level injection equation is derived here and combined with the ideal diode equation to create the improved diode equation. This equation continuously describes both low and high level injection, and it also accounts for series resistance. The development of the high level injection equation and the improved diode equation is believed to be original work.

It is shown that the temperature dependent DC characteristics of a diode can be modelled outside of the influence of depletion region RG by the improved diode equation, when that equation is supplied with the high and low level injection intercepts of a single measured forward characteristic. The validity of the improved diode equation is rigorously tested by comparing the measured high and low level injection intercepts with values calculated using their theoretical formulae. These formulae must be supplied with the junction area, substrate doping, and the high and low level injection lifetimes. This creates the need for a new high level injection transient analysis, which is presented here, and which relates lifetime to the measured charge storage delay time. Non-uniform doping is accounted for, and the effects of this make it impossible to show exactly that the calculated and measured intercepts agree; however, it is shown that the theoretical predictions are reasonable.

Like the ideal diode equation, the improved diode equation does not model the depletion region RG current that dominates the low current portion of the diode characteristic; here the applied bias is a small positive voltage or a negative voltage that does not exceed the reverse breakdown voltage. A rigorous analysis of the depletion region process yields, possibly for the first time, a refined depletion region RG equation. Values generated by this equation when it is supplied with the junction area, doping gradient, lifetime, and trap energy level are in good agreement with observed currents. Current that leaks around the junction is modelled by a parallel resistor.

The improved diode equation extends diode modelling capability into the high injection region where many devices normally operate; high injection dominates the forward characteristic at high temperatures. The refined depletion region RG equation is expected to improve the reverse biased diode modelling capability.

## **ACKNOWLEDGMENTS**

I am grateful to my supervisor, Dr. J. W. Haslett, and to my teacher, Dr. F. N. Trofimenkoff, for their guidance and for their contributions to this work.

## **DEDICATION**

To my wife June.

## TABLE OF CONTENTS

	Page
I LIST OF TABLES	viii
II LIST OF FIGURES	viii
III LIST OF SYMBOLS	xii
1 INTRODUCTION	1
2 THE DC EQUATIONS OF STATE	4
2.1 The Transport Equations	4
2.2 The Continuity Equations	7
2.3 Boundary Conditions	10
3 THE DIODE EQUATIONS	14
3.1 Solutions of the Low Injection State Equations	14
3.2 Solutions of the High Injection State Equations	17
3.3 The Low Injection (Ideal) Diode Equation	20
3.4 The High Injection Diode Equation	22
3.5 The Improved Diode Equation	24
3.6 Voltage Drops in the Bulk Regions and Contacts	28
3.7 Diode Equation Summary	30
3.8 Diodes of Finite Length	30
4 TRANSIENT AND SMALL SIGNAL ANALYSIS	33
4.1 The Time Dependent Equations of State	33
4.2 Low Injection Transient Analysis	33
4.3 High Injection Transient Analysis	37
4.4 Thin Base Diode Transient Analysis	39
4.5 Small Signal Junction Capacitance	41

	Page
5 DIFFUSED JUNCTION DIODES	43
5.1 The Equations of State for Non-uniform Doping	45
5.2 Low Injection DC Solutions of the Equations of State	46
5.3 Low Injection Transient Solutions of the State Equations	48
5.4 Low Injection Diode Equations for Non-uniform Doping	51
5.5 High Injection Diode Equations for Non-uniform Doping	51
5.6 Linearly Graded Junction Capacitance	53
6 DIODE EQUATION EVALUATION	57
6.1 Modelling With $I_h$ and $I_s$ at Room Temperature	57
6.2 The Temperature Dependence of $I_h$ and $I_s$	59
6.3 Calculation of $I_h$ and $I_s$ at Room Temperature	62
6.4 Series Resistance	69
6.5 Diode Parameter Measurement Considerations	70
7 THE LOW CURRENT DOMAIN	76
7.1 The Standard Depletion Region RG Equation	77
7.2 The Refined Depletion Region RG Equation	82
7.3 Surface Leakage Current	89
8 CONCLUSION	91
8.1 Summary	91
8.2 Applications	94
8.3 Suggestions for Further Research	96
9 LABORATORY INSTRUMENTATION	98
10 REFERENCES	101

## LIST OF TABLES

	Page
6.1	Summary of Measured and Calculated Diode Parameters. 68
6.2	Measured Series Resistance at Elevated Temperatures. 69
7.1	Depletion Region Width and Voltage for a 1N5369 Diode. 80

## LIST OF FIGURES

1.1	Measured Forward Characteristics of a 1N5281 Diode at 25° C Illustrating the Departures From Ideal.	2
1.2	Measured Forward Characteristic of a 1N5281 Diode at 250° C.	3
3.1	Typical Approximate Hole Distribution for High Injection	20
3.2	Hole and Electron Current Densities for the Case of Low Level Injection on Both Sides of the Junction.	21

	Page
3.3 Hole and Electron Current Densities for the Case of High Injection on the N side of a p <sup>+</sup> n Junction.	22
3.4 The Relationship Between Carrier Concentration and Current.	25
3.5 Illustration of High and Low Injection Intercepts	27
5.1 Doping Profile for a Typical p <sup>+</sup> n Diode.	43
5.2 Exponential Approximation to the Doping Profile of a typical p <sup>+</sup> n Diode.	44
5.3 High Injection Hole distribution and Doping Profile.	52
5.4 Doping Concentration in the Vicinity of the Depletion Region.	53
6.1 A Measured Forward Characteristic Showing the Tangent Lines and High and Low Injection Intercepts.	58
6.2 A Comparison of the Measured Currents and the Improved Diode Equation With Zero Series Resistance.	58
6.3 A Comparison of the Measured Currents and Those Generated by the Improved Diode Equation With the Series Resistance Accounted for.	59
6.4 A Comparison of the Measured Currents and Those Generated by the Low [Ideal] and High Injection Equations.	61

	Page	
6.5	A Comparison of the Measured Currents and Those Generated by the Improved Diode Equation.	61
6.6	High Injection Charge Storage Delay Time vs $T^{3/2}$ .	62
6.7	Physical Geometry of the Tested Diodes.	63
6.8	The Measured Small Signal Junction Capacitance	64
6.9	The Relationship Between Delay Time and Injection Level.	65
6.10	Measured Delay Times for a 0.5W and a 5W Zener Diode.	71
6.11	Junction Capacitance Characteristics for Reverse Biased 0.5W and 5W Zener Diodes.	72
6.12	Measured Currents and Theoretical Currents Generated by the Improved Diode Equation for 0.5W and 5W Zener Diodes.	73
7.1	A Comparison of the Measured Forward and Reverse Characteristics With those Generated by the Improved Diode Equation Showing the Influence of Depletion Region $R_G$ at Low Current and at Moderate Temperatures.	76
7.2	Depletion and Bulk Region Currents for a p <sup>+</sup> n Diode.	78
7.3	Junction Capacitance Characteristic for a Reverse Biased 51V 5W Zener Diode.	79

	Page
7.4 The Relationship Between Charge Storage Delay Time and Injection Level for a 51V 5W Zener Diode.	80
7.5 A Comparison of the Theoretical Depletion Region RG Current, the Improved Diode Equation and the Measured Forward Characteristic of a 51V 5W Zener Diode.	81
7.6 The Space Charge, Electric Field and Potential Distribution for a Linearly Graded Junction.	83
7.7 A Comparison of the Improved Diode Equation, the Refined Depletion Region RG Equation and Measured 1N5369 Data.	84
7.8 A Comparison of the Comprehensive Diode Model with the Measured Characteristics of a 51V 5W Diode.	85
7.9 A Comparison of the Comprehensive Diode Model with the Measured Characteristics of a 25V 5W Diode.	86
7.10 A Comparison of the Comprehensive Diode Model with the Measured Characteristics of a 25V 0.5W Diode.	89
7.11 A Comparison of the Measured Characteristics of a 25V 0.5W Diode with the Comprehensive Diode Model and an Added Surface Leakage Component.	90
9.1 DC Characteristic Data Acquisition.	98
9.2 Charge Storage Delay Time Measurement Schematic and Waveforms.	99

## LIST OF SYMBOLS

A	Area of the PN junction
a	Linearly graded junction doping gradient
$C_j$	Junction Capacitance
$C_{j0}$	Equilibrium Junction Capacitance
D	Geometric mean of the hole and electron diffusivities
$D_p$	Hole diffusivity
$D_n$	Electron diffusivity
E	Electric Field
$E_g$	Band gap energy
$E_i$	Intrinsic Fermi Level
$E_t$	Trap energy level
$\epsilon$	Permittivity of silicon
$\phi_p$	Quasi Fermi potential for holes
$\phi_n$	Quasi Fermi potential for electrons
$\gamma$	Ratio of reverse to forward switching current
$I_h$	High injection intercept of the forward characteristic
$I_n$	Electron current
$I_p$	Hole current
$I_{RG}$	Depletion region RG current
$I_s$	Low injection intercept or reverse saturation current
$I_{SL}$	Surface leakage Current
$J_p$	Hole current density
$J_{pn}$	Hole current density in the N region
$J_{pp}$	Hole current density in the P region
$J_{pRG}$	Hole current density difference across the depletion region
$J_n$	Electron current density
$J_{nn}$	Electron current density in the N region
$J_{np}$	Electron current density in the P region
$J_t$	Total current

$k$	Boltzmann's constant
$L_n$	Low Injection diffusion length in the P region
$L_p$	Low injection diffusion length in the N region
$L$	High injection diffusion length
$\lambda$	Exponential doping diffusion length
$N_a$	Acceptor concentration
$N_b$	Substrate background doping
$N_d$	Donor concentration
$N_{do}$	Depletion region edge exponential doping concentration
$N_c$	Effective density of conduction band states
$N_t$	Trap Density
$N_v$	Effective density of valence band states
$n$	Electron concentration
$n_i$	Intrinsic carrier concentration
$n_o$	Equilibrium electron concentration
$n_n$	Electron concentration in the N region
$n_p$	Electron concentration in the P region
$n_{po}$	Equilibrium electron concentration in the P region
$\Delta n$	Excess electron concentration
$\Delta n_n$	Excess electron concentration in the N region
$\Delta n_p$	Excess electron concentration in the P region
$p$	Hole concentration
$p_o$	Equilibrium hole concentration
$p_n$	Hole concentration in the N region
$p_p$	Hole concentration in the P region
$p_{no}$	Equilibrium hole concentration in the N region
$\Delta p$	Excess hole concentration
$\Delta p_n$	Excess hole concentration in the N region
$\Delta p_p$	Excess hole concentration in the P region
$q$	Electron charge
$R_s$	Diode series resistance
$R_{SL}$	Surface leakage resistance
$\rho_p$	Space charge density in the P region

$\rho_n$	Space charge density in the N region
$t_{dH}$	High injection charge storage delay time
$t_{dL}$	Low injection charge storage delay time
$U$	Net recombination rate for holes or electrons
$\sigma$	High injection factor
$\sigma_p$	Capture cross section for holes
$\sigma_n$	Capture cross section for electrons
$T$	Temperature
$\tau$	High Injection lifetime
$\tau_n$	Low injection lifetime in the P region
$\tau_p$	Low injection lifetime in the N region
$\tau_0$	Average Low injection lifetime
$\tau_t$	Trap lifetime
$\mu_p$	Hole mobility
$\mu_n$	Electron mobility
$V$	Voltage across the depletion region
$V_n$	Voltage drop across the N bulk region
$V_a$	Applied diode voltage
$V_{pb}$	Forward characteristic breakpoint voltage for hole current
$V_t$	Potential corresponding to the trap energy difference from $E_i$
$\psi$	Intrinsic Fermi potential
$\psi_{bi}$	Built in potential
$\psi_{b10}$	Equilibrium built in potential
$\psi_{np}$	Potential across the depletion region
$W$	Depletion region width
$W_n$	Length of the N bulk region
$W_b$	Effective high injection length of the N bulk region
$v_{th}$	Thermal velocity of carriers
$\xi$	High Injection current factor
$\chi$	High injection field factor
$\zeta$	Non-uniform doping factor

## 1 INTRODUCTION

The equation that is extensively used to model the DC characteristics of PN junctions is the familiar ideal diode equation [[1 pp91]]. A typical diode is doped more heavily on the P side than on the N side, and for such a p<sup>+</sup>n junction the ideal diode equation is

$$I_p = I_s \left[ e^{qV/kT} - 1 \right], \quad (1.1)$$

where  $I_p$  is the hole dominated diode current,  
 $I_s$  is the the reverse saturation current,  
 $V$  is the voltage across the depletion region,  
 $T$  is the absolute temperature,  
 $k$  is Boltzman's constant, and  
 $q$  is the electron charge.

If  $V$  is greater than zero by even a small amount, the ideal diode equation can be approximated by

$$I_p = I_s e^{qV/kT} \quad (1.2)$$

Taking the logarithm of both sides gives the linear relationship

$$\text{Log } I_p = \text{Log } I_s + \frac{q}{kT} \left[ \text{Log } e \right] V. \quad (1.3)$$

Hence, a plot of  $\text{Log } I_p$  vs  $V$  is a straight line having intercept  $I_s$  and slope  $(q/kT) \text{Log } e$ .

Actual diodes typically exhibit ideal diode behavior for only part of the forward bias range. This is illustrated in Figure 1.1 where two tangent lines have been drawn on the measured forward characteristic of a

silicon diode. This diode characteristic has the  $(q/kT) \text{ Log } e$  slope predicted by the Ideal diode equation in the region where the current is moderate. For larger current the slope decreases to  $(q/2kT) \text{ Log } e$  because of the effects of high level injection [1 pp96]. As the bias is increased further the slope falls below  $(q/2kT) \text{ Log } e$  because of series resistance [5 pp70]. The departure from ideal observed at very low current results from depletion region recombination [1 pp95].

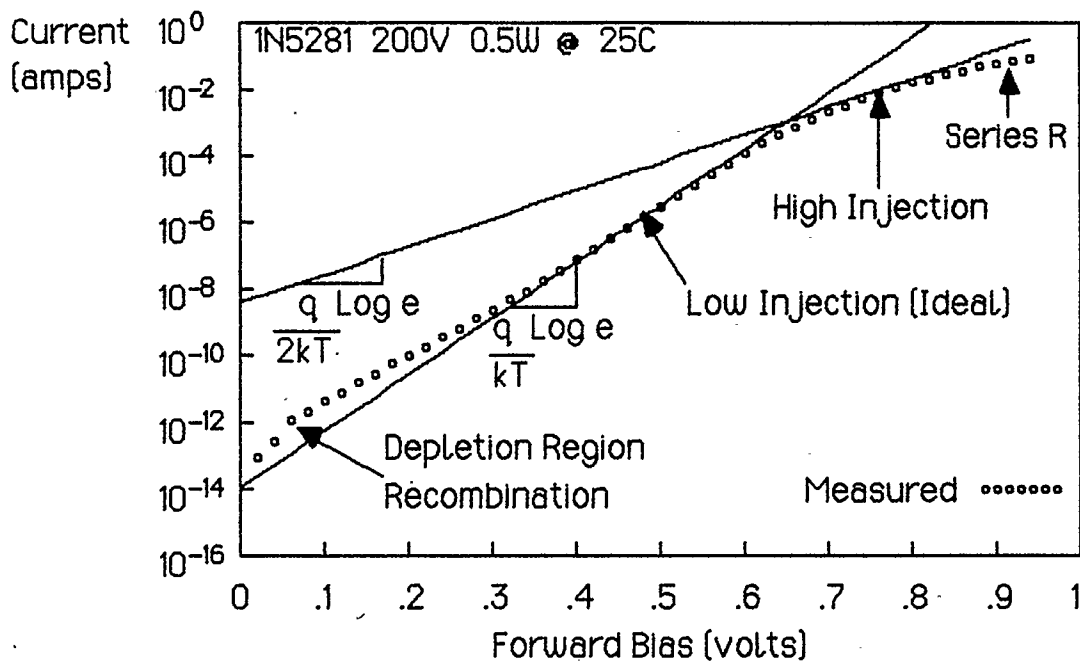


**Figure 1.1** Measured Forward Characteristic of a 1N5281 Diode at 25°C Illustrating the Departures From Ideal.

Figure 1.2 uses a different current scale to show the slopes of the forward characteristic of the same diode measured at a much higher temperature. At this temperature most of the forward characteristic has the  $(q/2kT) \text{ Log } e$  slope that signifies high level injection, and the ideal diode equation is useful only in the region of small forward bias. Depletion region recombination current is not evident at higher temperatures.

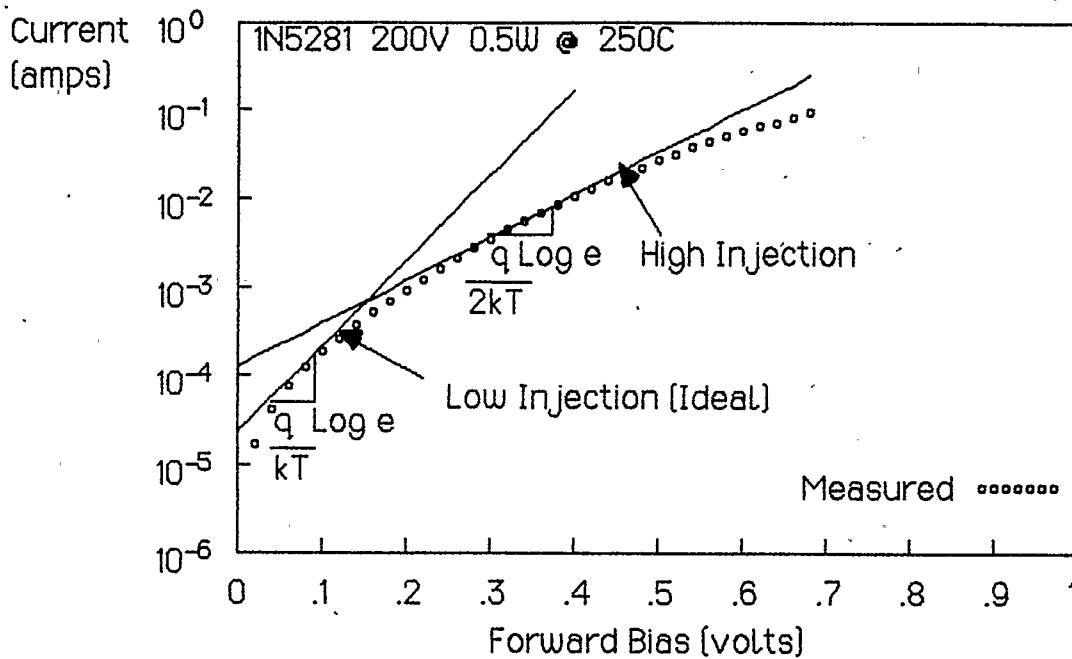


**Figure 1.2** Measured Forward Characteristic of a 1N5281 Diode at 250°C.

The reasons for the departures from ideal are well known, but a single equation that models diode behavior in both the low and high level injection regions has not been reported. The improved diode equation described here is intended to overcome this deficiency. This equation is derived by applying appropriate boundary conditions to the steady state simultaneous solutions of the transport and continuity equations in the charge neutral regions for both low and high level injection. The low and high level injection solutions are then combined using a boundary condition that is applicable to both to yield the desired result. The refined depletion region RG current equation presented here predicts the low current portion of the characteristic more accurately than does the approximate equation given in most texts.

Although the low level injection solutions are widely publicized, they are included here for comparison with and for combination with the unfamiliar high level injection solutions.

## 2 THE DC EQUATIONS OF STATE

The diode equations are derived from the steady state transport and continuity equations. These equations and their boundary conditions are required for both holes and electrons for each of three cases:

$$p \ll n, \quad n \ll p, \quad n = p,$$

where  $p$  is the hole concentration and  
 $n$  is the electron concentration.

The  $p \ll n$  situation occurs only on the N side during low level injection;  $n \ll p$  occurs only on the P side also during low level injection;  $n = p$  occurs on any side that is biased well into high level injection. The initial requirement is that the materials be uniformly doped.

### 2.1 The Transport Equations

The basic transport equations for holes and electrons are [[1 Ch3]]

$$J_p = q \mu_p p E - q D_p \frac{dp}{dx}, \quad (2.1)$$

$$J_n = q \mu_n n E + q D_n \frac{dn}{dx}, \quad (2.2)$$

where  $J_p$  is the hole current density,  
 $\mu_p$  is the hole mobility,  
 $D_p$  is the hole diffusivity,  
 $E$  is the electric field,  
 $J_n$  is the electron current density,  
 $\mu_n$  is the electron mobility, and  
 $D_n$  is the electron diffusivity.

To preserve current continuity the total current density is [[3 pp96]]

$$J_t = J_p + J_n, \quad (2.3)$$

and  $J_t$  is independent of  $x$ . Since [[3 pp28]]

$$\frac{D}{\mu} = \frac{kT}{q}, \quad (2.4)$$

then

$$\frac{\mu_p}{\mu_n} = \frac{D_p}{D_n}. \quad (2.5)$$

The charge balance equations for the donor doped N side [[3 pp17]],

$$n_n = p_n + N_d, \quad (2.6)$$

and the acceptor doped P side [[3 pp17]],

$$p_p = n_p + N_a \quad (2.7)$$

can be differentiated to give

$$\frac{dp}{dx} = \frac{dn}{dx}, \quad (2.8)$$

if  $N_d$  and  $N_a$  are constant,

where  $p_n$  is the hole concentration in the N region,  
 $n_n$  is the electron concentration in the N region,  
 $p_p$  is the hole concentration in the P region,  
 $n_p$  is the electron concentration in the P region,  
 $N_d$  is the donor doping concentration, and  
 $N_a$  is the acceptor doping concentration.

Adding Equations (2.1) and (2.2) and applying Equations (2.3) and (2.8) gives

$$E = \frac{J_t + q[D_p - D_n] \frac{dp}{dx}}{q[\mu_p p + \mu_n n]} \quad (2.9)$$

Substituting the expression for E from Equation (2.9) into Equation (2.1) and applying Equation (2.5) yields

$$J_p = \left[ \frac{J_t}{1 + \frac{D_n n}{D_p p}} \right] + \left[ \frac{D_p - D_n - D_p}{1 + \frac{D_n n}{D_p p}} \right] q \frac{dp}{dx} \quad (2.10)$$

This reduces to three transport equations for holes:

$$J_{pn} = -q D_p \frac{dp_n}{dx} \quad \text{for } p \ll n, \quad (2.11)$$

$$J_{pp} = J_t - q D_n \frac{dp_p}{dx} \quad \text{for } n \ll p, \quad (2.12)$$

$$J_p = \frac{J_t}{1 + \frac{D_n}{D_p}} - q D \frac{dp}{dx} \quad \text{for } n = p, \quad (2.13)$$

where

$$D \equiv \frac{2 D_n D_p}{D_n + D_p}, \quad (2.14)$$

the geometric mean of the hole and electron diffusivities,  $J_{pp}$  is the hole current density in the P region, and  $J_{pn}$  is the hole current density in the N region.

Substituting the expression for E from Equation (2.9) into Equation (2.2) and applying Equations (2.5) and (2.8) yields

$$J_n = \left[ \frac{J_t}{1 + \frac{D_p p}{D_n n}} \right] + \left[ \frac{D_p - D_n}{1 + \frac{D_p p}{D_n n}} + D_n \right] q \frac{dn}{dx} \quad (2.15)$$

This reduces to three transport equations for electrons:

$$J_{np} = q D_n \frac{dn_p}{dx} \quad \text{for } n \ll p, \quad (2.16)$$

$$J_{nn} = J_t + q D_p \frac{dn_n}{dx} \quad \text{for } p \ll n, \quad (2.17)$$

$$J_n = \frac{J_t}{1 + \frac{D_p}{D_n}} + q D \frac{dn}{dx} \quad \text{for } n = p, \quad (2.18)$$

where  $J_{np}$  is the electron current density in the P region, and  $J_{nn}$  is the electron current density in the N region.

## 2.2 The Continuity Equations

The continuity equations require expressions for the net recombination rates for holes and electrons on both sides of the junction. On any particular side, the net recombination rate for holes must be the same as that for electrons, since there must be no net increase in the concentration of one carrier type over the other. To maintain charge neutrality in the bulk regions of the biased diode, the change in hole concentration must equal the change in electron concentration on any particular side of the junction; that is

$$p - p_0 = \Delta p = n - n_0 = \Delta n, \quad (2.19)$$

where  $p_0$  is the equilibrium hole concentration,  
 $n_0$  is the equilibrium electron concentration,  
 $\Delta p$  is the excess hole concentration, and  
 $\Delta n$  is the excess electron concentration.

In silicon, recombination occurs indirectly via recombination centers or traps created by impurities and crystal lattice defects. The net recombination rate is described by the Shockley-Hall-Read equation [1 pp51] [6]

$$U = \frac{pn - n_i^2}{\tau_n \left[ p + n_i e^{\frac{E_t - E_f}{kT}} \right] + \tau_p \left[ n + n_i e^{\frac{E_t - E_f}{kT}} \right]}, \quad (2.20)$$

where

$$\tau_p = \frac{1}{v_{th} \sigma_p N_t} \quad \text{and} \quad \tau_n = \frac{1}{v_{th} \sigma_n N_t}, \quad (2.21)$$

and  $U$  is the net recombination rate,  
 $n_i$  is the intrinsic carrier concentration,  
 $v_{th}$  is the carrier thermal velocity,  
 $N_t$  is the trap density,  
 $\sigma_p$  is the capture cross section for holes,  
 $\sigma_n$  is the capture cross section for electrons,  
 $E_f$  is the intrinsic Fermi level,  
 $E_t$  is the trap energy level,  
 $\tau_p$  is the low injection lifetime on the N side, and  
 $\tau_n$  is the low injection lifetime on the P side.

To simplify this, assume that the capture cross sections are the same for holes and electrons by letting  $\tau_n = \tau_p = \tau_0$  [1 pp93]. Then Equation (2.20) becomes

$$U = \frac{pn - n_i^2}{\tau_0 \left[ p + n + 2n_i \cosh \left[ \frac{E_i - E_t}{kT} \right] \right]} \quad (2.22)$$

The term containing the hyperbolic can be neglected if it is much less than either  $p$  or  $n$ , and one of these will be at least as large as the doping. This term will be less than even a light doping if  $(E_i - E_t) < \pm 10 kT$ ; that is, if the traps have energy levels within about the center half of the energy band gap. Traps near the band gap edges are ineffective, because they result in a small value for  $U$ . The net recombination rate in the charge neutral region for mid gap traps can be expressed as

$$U = \frac{pn - n_i^2}{\tau_n [p + n_i] + \tau_p [n + n_i]} \quad (2.23)$$

Equation (2.30) reduces to

$$U = \frac{\Delta p_n}{\tau_p} = \frac{\Delta n_n}{\tau_p} \quad \text{for } p \ll n, \quad (2.24)$$

$$U = \frac{\Delta n_p}{\tau_n} = \frac{\Delta p_p}{\tau_n} \quad \text{for } n \ll p, \quad (2.25)$$

$$U = \frac{p}{\tau} \quad \text{or} \quad U = \frac{n}{\tau} \quad \text{for } p = n, \quad (2.26)$$

where  $\Delta p_n$  is the excess hole concentration in the N region,  $\Delta p_p$  is the excess hole concentration in the P region,  $\Delta n_n$  is the excess electron concentration in the N region,  $\Delta n_p$  is the excess electron concentration in the P region, and  $\tau$  is defined as the high injection lifetime,  $\tau \equiv \tau_p + \tau_n$ .

The steady state continuity equations are [[1 ch3]]

$$\frac{dJ_p}{dx} = -qU \quad \text{for holes,} \quad [2.27]$$

$$\frac{dJ_n}{dx} = qU \quad \text{for electrons.} \quad [2.28]$$

### 2.3 Boundary Conditions

The boundary conditions needed to solve the transport and continuity equations are the excess carrier concentrations at both of the depletion region edges under the influence of the applied voltage.

The equilibrium mass action equation [[1 pp19]],

$$n_0 p_0 = n_i^2, \quad [2.29]$$

is valid everywhere in the diode at equilibrium. The non-equilibrium carrier concentrations are [[2 pp45]]

$$p = n_i e^{(\phi_p - \psi) q/kT}, \quad [2.30]$$

$$n = n_i e^{(\psi - \phi_n) q/kT}, \quad [2.31]$$

where  $\phi_p$  is the quasi Fermi potential for holes,  
 $\phi_n$  is the quasi Fermi potential for electrons, and  
 $\psi$  is the intrinsic Fermi potential.

At any particular location,  $\psi$  is the same for  $n$  and  $p$ , and their product is

$$np = n_i^2 e^{(\phi_p - \phi_n)q/kT} \quad [2.32]$$

The voltage across the junction,  $V$ , is equal to the difference between  $\phi_p$  on one side of the depletion region and  $\phi_n$  on the other side. Since the depletion region is narrow, the change in both  $\phi_p$  and  $\phi_n$  across this region is small. Hence, [[1 pp94]]

$$np = n_i^2 e^{qV/kT} \quad [2.33]$$

everywhere in the depletion region.

Consider first the N side boundary conditions. In the charge-neutral N region for low level injection  $p \ll n$ , and Equation [2.6] becomes

$$n_n = N_d \quad [2.34]$$

The corresponding equilibrium hole concentration is obtained by substituting Equation [2.34] into [2.29] to give

$$p_{no} = \frac{n_i^2}{N_d} \quad [2.35]$$

The non-equilibrium hole concentration at the depletion region edge, that is at  $x = 0$ , is obtained by substituting Equation [2.34] into [2.33] to give

$$p_n(0) = \frac{n_i^2}{N_d} e^{qV/kT} \quad [2.36]$$

Therefore, the excess carrier concentration at the depletion region edge in response to an applied voltage is [[1 pp90]]

$$\Delta p_n(0) = \frac{n_i^2}{N_d} \left[ e^{qV/kT} - 1 \right] = \Delta n_n(0). \quad (2.37)$$

For large forward bias  $p_n$  exceeds  $N_d$  at the depletion region edge, and Equations (2.6) and (2.7) become

$$n(0) = p(0). \quad (2.38)$$

Substituting this into Equation (2.33) yields the high level injection boundary condition

$$p(0) = n_i e^{qV/2kT} = n(0). \quad (2.39)$$

For the general case which applies to low and high level injection, it is only necessary to substitute Equation (2.6) into (2.29) and (2.33) and solve for  $p_{no}$  and  $p_n(0)$ :

$$p_{no} = \frac{-N_d + \sqrt{N_d^2 + 4n_i^2}}{2}, \quad (2.40)$$

$$p_n(0) = \frac{-N_d + \sqrt{N_d^2 + 4n_i^2 e^{qV/kT}}}{2}, \quad (2.41)$$

$$\Delta p_n(0) = \frac{\sqrt{N_d^2 + 4n_i^2 e^{qV/kT}} - \sqrt{N_d^2 + 4n_i^2}}{2} = \Delta n_n(0). \quad (2.42)$$

The excess carrier concentrations at the P side edge of the depletion region are similarly derived. The low injection, high injection and general case boundary conditions are respectively

$$\Delta n_p(0) = \frac{n_i^2}{N_a} \left[ e^{qV/kT} - 1 \right] = \Delta p_p(0), \quad (2.43)$$

$$n(0) = n_i e^{qV/2kT} = p(0). \quad [2.44]$$

$$\Delta n_p(0) = \frac{\sqrt{N_a^2 + 4n_i^2 e^{qV/kT}} - \sqrt{N_a^2 + 4n_i^2}}{2} = \Delta p_p(0). \quad [2.45]$$

### 3 THE DIODE EQUATIONS

The improved diode equation is the combination of the low and high level injection diode equations. The word "level" is henceforth dropped, and the two injection levels are referred to as high injection and low injection. These diode equations are derived by solving the DC state equations for hole and electron current in terms of the total current in the N and P charge-neutral regions. The total current is then obtained by equating either the N and P region hole currents or the N and P region electron currents at the junction of the P and N material. The coordinate system used consistently throughout has the N region along the positive x axis, the P region along the negative x axis, and the depletion region concentrated at  $x = 0$ . Finite length considerations follow the derivations for infinitely long uniformly doped diodes.

#### 3.1 Solutions of the Low Injection State Equations

The transport equation for low injection hole current in the charge-neutral N region is Equation (2.11) which is repeated here for convenience:

$$J_{pn} = -q D_p \frac{dp_n}{dx} \quad (2.11)$$

The corresponding continuity equation is obtained by substitution of Equation (2.24) into (2.27) to give

$$\frac{dJ_{pn}}{dx} = -q \frac{\Delta p_n}{\tau_p} \quad (3.1)$$

Substitution of the derivative of the current density given by the transport equation into the continuity equation produces the second order linear differential equation,

$$\frac{d^2 \Delta p_n}{dx^2} - \frac{\Delta p_n}{D_p \tau_p} = 0, \quad [3.2]$$

which has the solution

$$\Delta p_n = C_1 e^{-x/L_p} + C_2 e^{x/L_p}, \quad [3.3]$$

where the N region diffusion length,  $L_p$ , is

$$L_p = \sqrt{D_p \tau_p}. \quad [3.4]$$

If the N region is long, the boundary conditions are [[1 ch3]]

$$\Delta p_n = 0 \text{ at } x = \infty \text{ and}$$

$$\Delta p_n = \Delta p_n(0) \text{ at } x = 0;$$

and applying these to Equation (3.3) gives the N side excess hole distribution

$$\Delta p_n = \Delta p_n(0) e^{-x/L_p}. \quad [3.5]$$

When the derivative of this expression for  $\Delta p_n$  is substituted back into the transport equation, Equation (2.11), the hole current density results:

$$J_{pn} = q \frac{D_p}{L_p} \Delta p_n(0) e^{-x/L_p}. \quad [3.6]$$

The transport equation for low injection hole current in the charge-neutral P region is Equation (2.12) which is repeated here for convenience:

$$J_{pp} = J_t - q D_n \frac{dp_p}{dx} \quad (2.12)$$

The corresponding continuity equation is obtained by substitution of Equation (2.25) into (2.28) to give

$$\frac{dJ_{pp}}{dx} = -\frac{\Delta p_p}{\tau_n} \quad (3.7)$$

Solving these as before but using the boundary conditions [[1 ch3]]

$$\Delta p_p = 0 \text{ at } x = -\infty \text{ and}$$

$$\Delta p_p = \Delta p_p(0) \text{ at } x = 0$$

gives the P side excess hole distribution

$$\Delta p_p = \Delta p_p(0) e^{x/L_n}, \quad (3.8)$$

where the P region diffusion length,  $L_n$ , is

$$L_n = \sqrt{D_n \tau_n} \quad (3.9)$$

When the derivative of this expression for  $\Delta p_p$  is substituted back into the transport equation, Equation (2.12), the hole current density results:

$$J_{pp} = J_t - q \frac{D_n}{L_n} \Delta p_p(0) e^{x/L_n} \quad (3.10)$$

Because  $\Delta n_n = \Delta p_n$  and  $\Delta n_p = \Delta p_p$  for the preservation of charge neutrality, the excess electron current density distributions are now

easily obtained by substitution of Equations (3.5) and (3.8) into the appropriate transport equations, Equations (2.17) and (2.16) respectively to give

$$J_m = J_t - q \frac{D_p}{L_p} \Delta n_n(0) e^{-x/L_p}, \quad (3.11)$$

$$J_{np} = q \frac{D_n}{L_n} \Delta n_p(0) e^{x/L_n}. \quad (3.12)$$

### 3.2 Solutions of the High Injection State Equations

High level injection implies that the forward bias is sufficient to cause the injected minority carrier concentration to exceed the doping at the depletion region edge. When this occurs, Equations (2.6) and (2.7) predict that the hole and electron concentrations become equal at the depletion region edge. As the bias is increased further, the equality of hole and electron concentrations extends further into the charge-neutral region until eventually  $n = p$  essentially everywhere in that region. Further justification for the use of  $n = p$  in the entire charge-neutral region follows the derivations of the high injection carrier concentration and current density distributions.

When  $n = p$  the transport equation for holes is given by Equation (2.13) which is repeated here:

$$J_p = \frac{J_t}{1 + \frac{D_n}{D_p}} - q D \frac{dp}{dx}. \quad (2.13)$$

The corresponding continuity equation is obtained by combining Equations (2.26) and (2.27) to give

$$\frac{dJ_p}{dx} = -q \frac{p}{\tau} \quad (3.13)$$

The high injection state equations are the same on both sides of the junction; when  $n = p$  the doping has no influence. Substitution of the derivative of the current density given by the transport equation into the continuity equation produces the second order linear differential equation

$$\frac{d^2 p}{dx^2} - \frac{p}{D \tau} = 0 \quad (3.14)$$

which has the solution

$$p = C_1 e^{-x/L} + C_2 e^{x/L} \quad (3.15)$$

where the high injection diffusion length on either side is

$$L = \sqrt{D \tau} \quad (3.16)$$

The boundary conditions for long diodes are

$$p = p(0) \text{ at } x = 0,$$

$$p_n \approx 0 \text{ at } x = \infty \text{ on the N side,}$$

$$p_p \approx 0 \text{ at } x = -\infty \text{ on the P side.}$$

Therefore

$$p_n = p(0) e^{-x/L}, \quad (3.17)$$

$$p_p = p(0) e^{x/L}. \quad (3.18)$$

Substituting the derivatives of these back into the transport equation, Equation (2.13) gives

$$J_{pn} = \frac{J_t}{1 + \frac{D_n}{D_p}} + q \frac{D}{L} p(0) e^{-x/L}, \quad (3.19)$$

$$J_{pp} = \frac{J_t}{1 + \frac{D_n}{D_p}} - q \frac{D}{L} p(0) e^{x/L}. \quad (3.20)$$

Since  $p_n = n_n$ ,  $p_p = n_p$ , and  $p(0) = n(0)$  then substitution of the derivatives of equations (3.17) and (3.18) into the high injection electron transport equation, Equation (2.18) gives the electron current densities

$$J_{nn} = \frac{J_t}{1 + \frac{D_p}{D_n}} - q \frac{D}{L} n(0) e^{-x/L}, \quad (3.21)$$

$$J_{np} = \frac{J_t}{1 + \frac{D_p}{D_n}} + q \frac{D}{L} n(0) e^{x/L}. \quad (3.22)$$

The N side high injection hole distribution is illustrated in Figure 3.1. If  $p_n(0)$  is sufficiently greater than  $N_d$ , then  $p_n$  exceeds  $N_d$  and  $n = p$  throughout all of the distribution, except in the tail below  $N_d$  where low injection begins and the shape of the curve changes. The integral of the continuity equation

$$\int_0^{\infty} dJ_p = -\frac{q}{\tau} \int_0^{\infty} p_n dx \quad (3.23)$$

shows that the current density is proportional to the area under the hole distribution. This area is not significantly influenced by the change in the shape of the tail of the hole distribution if  $p_n(0)$  is one or more orders of magnitude above  $N_d$ . The higher the bias the closer is the relative approach of  $N_d$  to the  $x$  axis, and the better is the  $p = n$  approximation. Note that similar considerations apply to the low injection equations; that is, it can be safely stated that  $p \ll n$  in the entire charge-neutral region only if  $p_n(0)$  is sufficiently less than  $N_d$ .

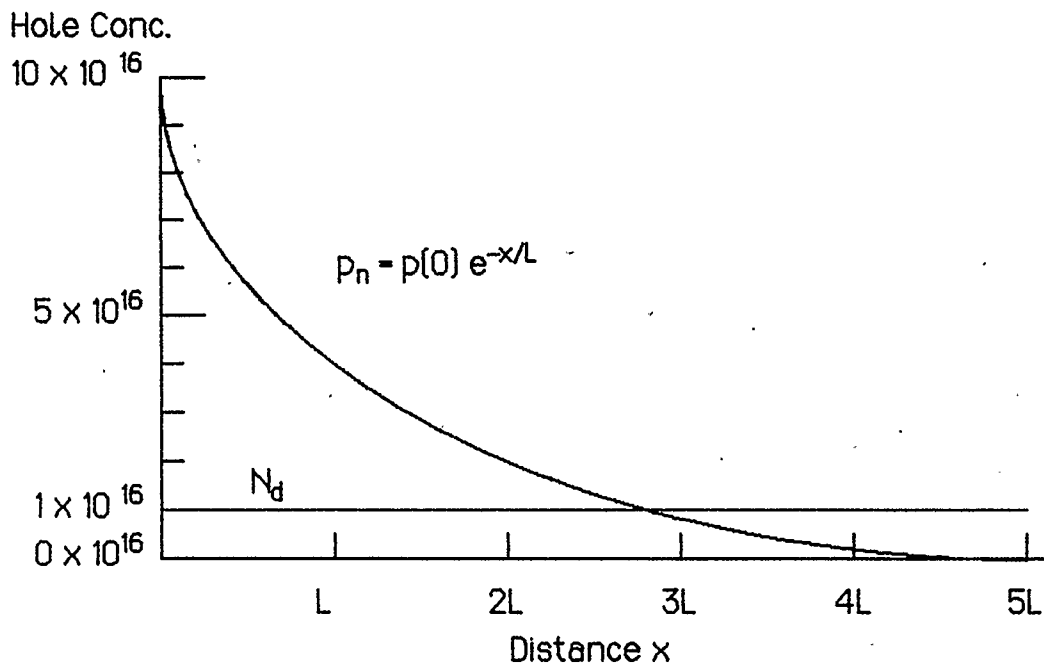


**Figure 3.1** Typical Approximate Hole Distribution for High Injection.

### 3.3 The Low Injection (Ideal) Diode Equation

Equating at  $x = 0$  the N side and P side low injection hole current densities given by Equations (3.6) and (3.10) and solving for  $J_t$  gives

$$J_t = q \frac{D_p}{L_p} \Delta p_n(0) + q \frac{D_n}{L_n} \Delta p_p(0). \quad (3.24)$$

Inserting the depletion region edge boundary conditions from Equations (2.37) and (2.43) and multiplying by the area,  $A$ , yields the familiar Ideal diode equation for infinitely long uniformly doped diodes

$$I = A q \left[ \frac{D_p}{L_p} \frac{n_i^2}{N_d} + \frac{D_n}{L_n} \frac{n_i^2}{N_a} \right] \left[ e^{qV/kT} - 1 \right]. \quad (3.25)$$

The same result could have been achieved by equating the electron current densities at  $x = 0$ . The P side of a diode is often doped heavier than the N side. If both sides of a  $p^n$  diode are experiencing low level injection, the current density distributions will appear approximately as those depicted in Figure 3.2.

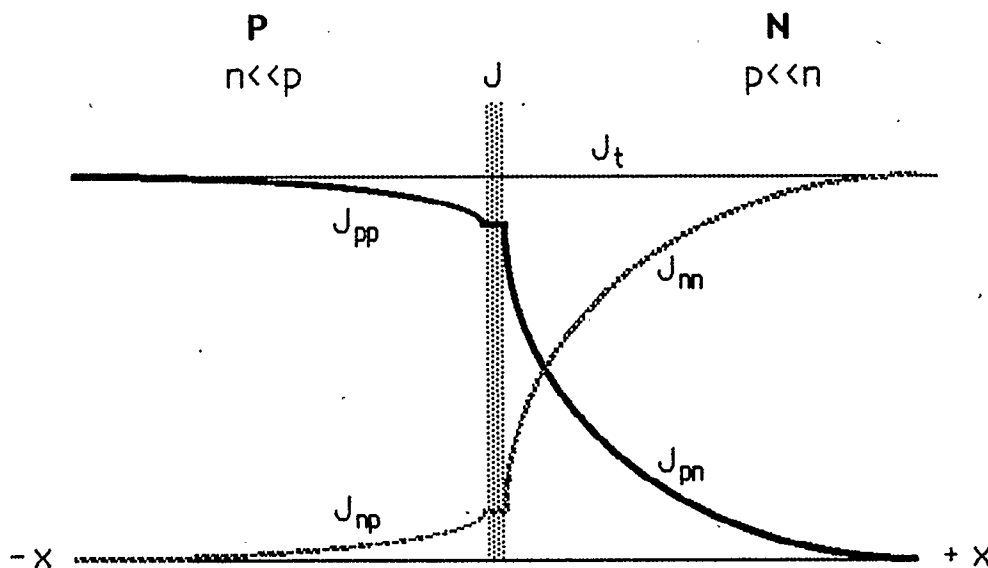


**Figure 3.2** Hole and Electron Current Densities for the Case of Low Level Injection on Both Sides of the Junction.

### 3.4 The High Injection Diode Equation

With increasing forward bias, a  $p^+n$  diode will achieve high injection on the N side while the P side remains in a state of low injection. For this situation, the hole current at  $x = 0$  will be much larger than the electron current, and  $J_t \approx J_p(0)$ . The N side high injection hole and electron current densities expressed by Equations (3.19) and (3.21) will be as illustrated in Figure 3.3.

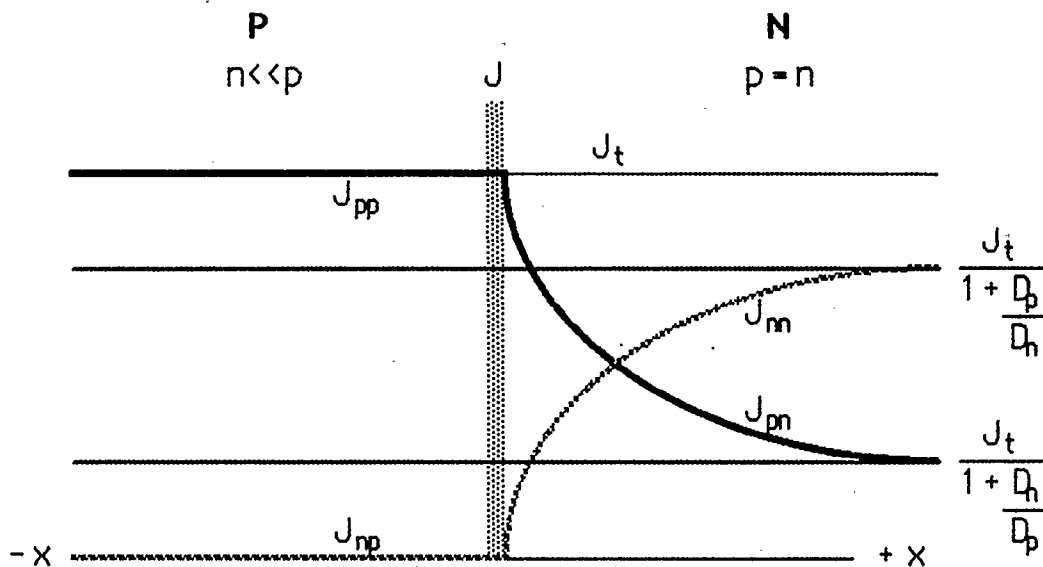


**Figure 3.3** Hole and Electron Current Densities for the Case of High Injection on the N side of a  $p^+n$  Junction.

Equating  $J_{pn}$  to  $J_t$  at  $x = 0$  in Equation (3.19) and solving for  $J_t$  gives

$$J_t = 2q \frac{D_p}{L} p(0). \quad (3.26)$$

Eliminating  $L$  by applying the definitions for  $D$ ,  $L_p$  and  $L$  gives

$$J_t = \xi q \frac{D_p}{L_p} p(0), \quad (3.27)$$

where the high injection current factor is defined to be

$$\xi = \sqrt{2 \left[ 1 + \frac{D_p}{D_n} \right] \frac{\tau_p}{\tau}}. \quad (3.28)$$

Applying the high injection depletion region edge boundary condition from Equation (2.39) and multiplying by the area yields the high injection diode equation

$$I_p = \xi A q \frac{D_p}{L_p} n_i e^{qV/2kT}. \quad (3.29)$$

When the derivative of the high injection hole concentration from Equation (3.17) is substituted into the hole transport equation, Equation (2.1), the result is:

$$J_p(0) = q \mu_p p E + q \frac{D_p}{L} p(0). \quad (3.30)$$

A comparison of this with Equation (3.26) reveals that, under high injection conditions, drift current is responsible for 1/2 of the total current, and diffusion accounts for the remainder, whereas diffusion accounts for all low injection current.

Consider the state of high injection on both sides of the junction. An attempt to equate at  $x = 0$  the N side and P side high injection hole current densities given by Equations (3.19) and (3.20) shows that the two can be equal only if the exponential terms representing the diffusion components of current vanish. Drift current accounts for all of the diode current, the carrier concentrations are independent of the doping on both sides, and the diode behaves like a resistor.

### 3.5 The Improved Diode Equation

According to Equations (3.29) and (3.25), the high and low injection diode equations for a p<sup>+</sup>n diode can be written as

$$I_p = \xi A q \frac{D_p}{L_p} \left[ n_i e^{qV/2kT} \right] \quad \text{and} \quad I_p = A q \frac{D_p}{L_p} \left[ \frac{n_i^2}{N_d} \{ e^{qV/kT} - 1 \} \right]$$

where the terms in the square brackets are the depletion region edge carrier concentrations. Multiplying the low injection equation by  $\xi/\xi$  gives

$$I_p = \xi A q \frac{D_p}{L_p} \left[ n_i e^{qV/2kT} \right] \quad \text{and} \quad I_p = \xi A q \frac{D_p}{L_p} \left[ \frac{n_i^2}{\xi N_d} \{ e^{qV/kT} - 1 \} \right]. \quad (3.31)$$

Therefore, both the low and high injection diode equations can be written as

$$I_p = \xi A q \frac{D_p}{L_p} \Delta p_n(0) \quad (3.32)$$

if  $N_d$  in  $\Delta p_n(0)$  is replaced by  $\xi N_d$ . When  $N_d$  is replaced by  $\xi N_d$  in Equation (2.42), the general form of the depletion region edge excess hole concentration, and the result substituted into Equation (3.32), the improved diode equation is created:

$$I_p = \left[ \xi A q \frac{D_p}{L_p} \right] \frac{\sqrt{[\xi N_d]^2 + 4 n_i^2 e^{qV/kT}} - \sqrt{[\xi N_d]^2 + 4 n_i^2}}{2}. \quad (3.33)$$

This equation is expected to model diode characteristics in both the low and high injection regions of long uniformly doped p<sup>+</sup>n devices.

Figure 3.4 illustrates the relationship between carrier concentration and current. When increasing forward bias is applied, the depletion region edge minority hole concentration rises above its equilibrium value of  $n_i^2/N_d$ ; this causes the current to increase in the low injection region with a slope of  $(q/kT) \text{Log } e$ . When the hole concentration approaches  $N_d$ , the current enters the high injection region, where it exhibits a  $(q/2kT) \text{Log } e$  slope. The location of the breakpoint between the low and high injection regions is governed by the doping concentration,  $N_d$ ; it moves to the left along the high injection characteristic as  $N_d$  is reduced.

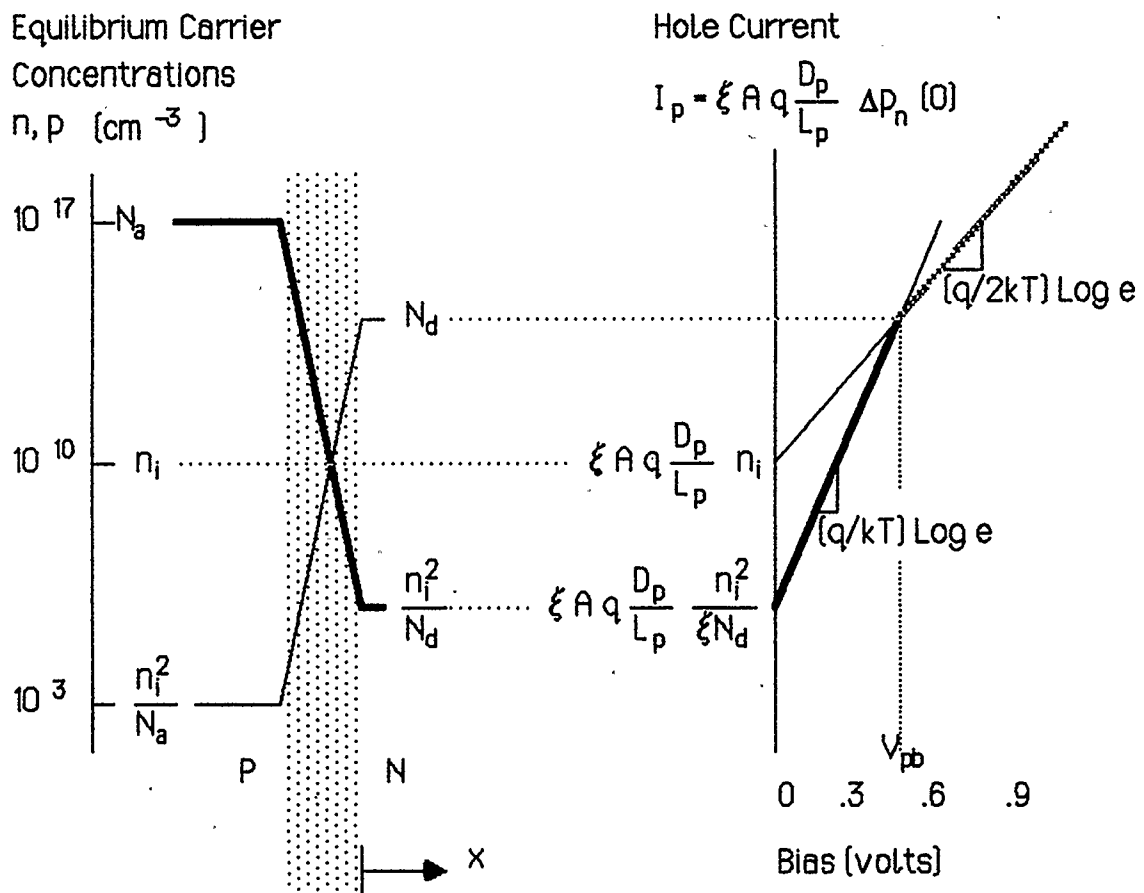


**Figure 3.4** The Relationship Between Carrier Concentration and Current

The breakpoint voltage is determined by equating the low and high

injection diode equations to yield

$$V_{pb} = \frac{kT}{q} \ln \frac{[\xi N_d]^2}{n_i^2} \quad (3.34)$$

which is less than the built in contact potential [[1 pp73]],

$$\psi_{bi} = \frac{kT}{q} \ln \frac{N_a N_d}{n_i^2}, \quad (3.35)$$

of a p<sup>+</sup>n diode for which  $N_d \ll N_a$ .

To model a particular diode, the improved diode equation must be supplied with the two quantities in the square brackets of Equation (3.33). These can be obtained from a measured forward characteristic as follows. According to Equations (3.31), the intercepts of the high and low injection diode equations can be defined respectively as

$$I_h \equiv \xi A q \frac{D_p}{L_p} n_i, \quad (3.36)$$

$$I_s \equiv A q \frac{D_p}{L_p} \frac{n_i^2}{N_d} \quad (3.37)$$

$I_h$  and  $I_s$  can be determined for a particular diode from the intercepts of two tangent lines drawn on the measured forward characteristic as depicted in Figure 3.5. According to Equation (3.36), the quantity  $\{\xi A q D_p/L_p\}$  can be calculated from  $I_h$ , that is

$$\left[ \xi A q \frac{D_p}{L_p} \right] = \frac{I_h}{n_i}. \quad (3.38)$$

The other quantity,  $\{\xi N_d\}$ , can be calculated from the ratio of Equations (3.36) and (3.37), that is

$$\left[\xi N_d\right] = \frac{I_h}{I_s} n_i. \quad (3.39)$$

Substituting these into Equation (3.33) gives the improved diode equation in terms of the high and low injection intercepts:

$$I_p = I_h \left[ \sqrt{\left[\frac{I_h}{2I_s}\right]^2 + e^{qV/kT}} - \sqrt{\left[\frac{I_h}{2I_s}\right]^2 + 1} \right]. \quad (3.40)$$

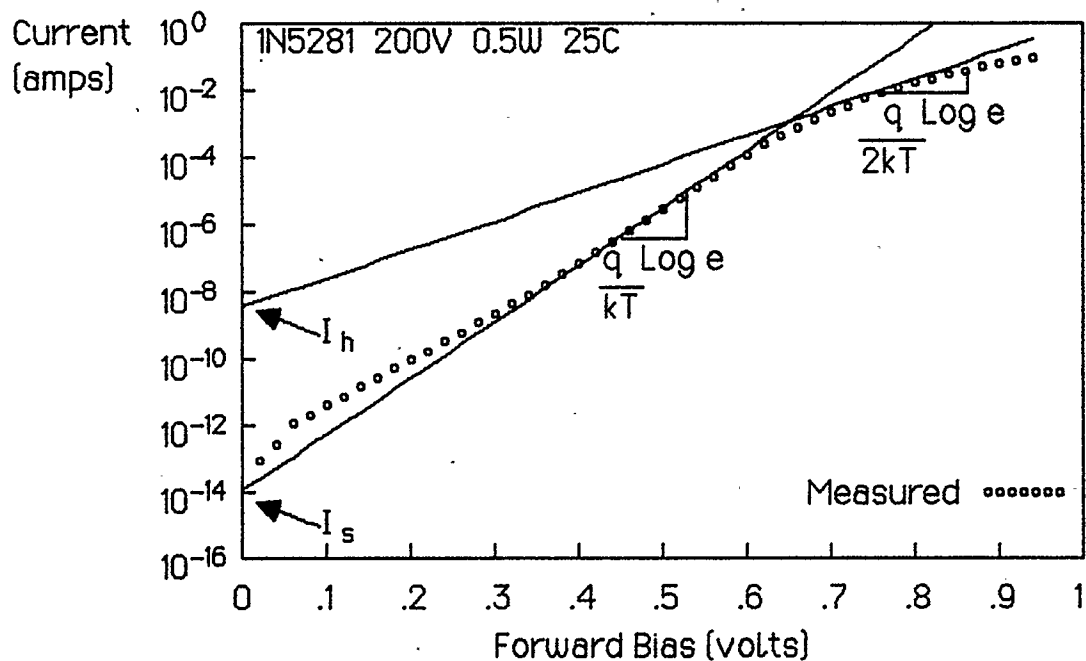


**Figure 3.5** Illustration of High and Low Injection Intercepts.

This modelling method is offered as an alternative to the popular procedure that uses just the ideal diode equation. That procedure requires the determination of the same  $I_s$  from an actual forward

characteristic, but instead of using  $I_h$ , it uses an artificial ideality factor that modifies the slope of the ideal diode equation to that which approximates the average slope of the actual forward characteristic [1 pp95]. The ideality factor does not account for the large difference in the temperature dependence of the low and high injection intercepts.

There is little loss of generality in restricting the derivations to  $p^+n$  diodes, since it is very unlikely that the doping will be the same on both sides. Equation (3.40) also models the electron current,  $I_n$ , of an  $n^+p$  device.

### 3.6 Voltage Drops in the Bulk Regions and Contacts

Thus far the diode equations have been written in terms of  $V$ , the voltage across the depletion region. To express these in terms of the applied voltage,  $V_a$ , it is necessary to account for the voltage drops in the charge-neutral regions and the contacts. These potentials are only significant for high current. The ohmic contacts can be modelled by a small temperature independent series resistance [11] [12]. The heavily doped P charge-neutral region is essentially always in a state of low level injection, and the small resistance of that region can be added to the contact resistance. Hence, to accommodate these two it is only necessary to replace  $V$  by  $V_a - R_s I_p$  [1 pp96]. The E field that accompanies the high injection condition on the N side can produce a significant voltage drop across that region. Letting  $p = n$  in Equation (2.9) yields the high injection E field

$$E_n = \frac{J_t - q[D_n - D_p] \frac{dp_n}{dx}}{q[\mu_p + \mu_n] p_n} \quad (3.41)$$

Substituting into this the expressions for the high injection current density from Equation (3.26) and the high injection hole concentration from Equation (3.17) and its derivative gives

$$E_n = \frac{1}{L} \frac{kT}{q} \left[ \frac{2 D_p}{D_p + D_n} e^{x/L} + \frac{D_n - D_p}{D_p + D_n} \right]. \quad (3.42)$$

Integrating this over the charge-neutral N region gives the voltage drop across that region:

$$V_n = \frac{2 kT}{q} \frac{1}{4} \left[ \frac{W_n}{L} + e^{W_n/L} - 1 \right], \quad (3.43)$$

where use has been made of the approximation,  $D_n \approx 3 D_p$ . Define the high injection field factor

$$\chi \equiv \frac{1}{4} \left[ \frac{W_n}{L} + e^{W_n/L} - 1 \right], \quad (3.44)$$

so that

$$V_n = \frac{2 kT}{q} \chi. \quad (3.45)$$

Replacing  $V$  by  $V - V_n$  in the high injection hole current equation, Equation (3.29) gives

$$I_p = e^{-\chi} \xi A q \frac{D_p}{L_p} n_i e^{qV/2kT}. \quad (3.46)$$

Define the high injection factor

$$\sigma \equiv e^{-\chi} \xi. \quad (3.47)$$

Hence, to accommodate the voltage drops across the bulk regions and the contacts it is necessary to replace  $\xi$  by  $\sigma$  and  $V$  by  $V_a - R_s I_p$  in the diode equations.

### 3.7 Diode Equation Summary

The high and low injection diode equations are

$$I_p = I_h e^{qV/2kT} \quad I_p = I_s \left[ e^{qV/kT} - 1 \right] \quad (3.48)$$

and these can be combined to give the improved diode equation,

$$I_p = I_h \left[ \sqrt{\left[ \frac{I_h}{2I_s} \right]^2 + e^{qV/kT}} - \sqrt{\left[ \frac{I_h}{2I_s} \right]^2 + 1} \right] \quad (3.49)$$

where

$$I_h = \sigma A q \frac{D_p}{L_p} n_i \quad I_s = A q \frac{D_p}{L_p} \frac{n_i^2}{N_d} \quad (3.49)$$

$$\sigma = e^{-x} \xi \quad x = \frac{1}{4} \left[ \frac{W_n}{L} + e^{W_n/L} - 1 \right] \quad \xi = \sqrt{2 \left[ 1 + \frac{D_p}{D_n} \right] \frac{\tau_p}{\tau}} \quad (3.50)$$

$$V = V_o - R_s I_p \quad (3.51)$$

### 3.8 Diodes of Finite Length

If the diffusion length is not significantly less than the actual length of the charge neutral region, the change in the non-equilibrium carrier concentrations cannot be assumed to vanish at  $x = \pm\infty$ . To solve the DC state equations for a finite length diode, it is necessary to know the excess carrier concentration at the end of the charge-neutral region, that is, at the semiconductor-to-metal contact surface. If the surface recombination velocity is very large, the excess carrier concentration will be essentially zero at the contact; the solutions for this situation

follow.

The solution of the low injection state equations for holes in the N charge-neutral region was given by Equation (3.3) which is repeated here for convenience:

$$\Delta p_n = C_1 e^{-x/L_p} + C_2 e^{x/L_p}. \quad (3.3)$$

If the length of the N region is  $W_n$ , the boundary conditions are

$$\Delta p_n = 0 \text{ at } x = W_n \text{ and}$$

$$\Delta p_n = \Delta p_n(0) \text{ at } x = 0.$$

Solving for the constants  $C_1$  and  $C_2$  gives

$$\Delta p_n = \Delta p_n(0) \frac{\sinh \left[ \frac{(W_n - x)}{L_p} \right]}{\sinh \left[ \frac{W_n}{L_p} \right]}. \quad (3.52)$$

Substituting the derivative of this into the transport equation, Equation (2.11), and evaluating the result at  $x = 0$  produces

$$J_{pn}(0) = q \frac{D_p}{L_p \tanh \left[ \frac{W_n}{L_p} \right]} \Delta p_n(0). \quad (3.53)$$

Using the same boundary conditions and procedure to solve the high injection DC state equations for holes, Equations (2.13) and (3.13), yields for a  $p^+n$  diode

$$J_p(0) = 2q \frac{D_p}{L \tanh \left[ \frac{W_n}{L} \right]} p(0). \quad (3.54)$$

These last two expressions will be the same as their infinitely long  $p^+n$

diode equivalents, Equations (3.24) and (3.26), only if  $\tanh \{W_n/L_p\}$  is close to unity. Since  $\tanh 2 = 0.96$ , the long diode equations will adequately apply as long as  $L_p \ll W_n/2$ .

If  $L_p > W_n$ , the hole distribution on the N side is approximately linear, recombination is insignificant, and the hole current is constant. Setting  $J_p = J_t = \text{constant}$  in the low injection hole transport equation, Equation (2.11) gives

$$J_{pn} = J_t = -q D_p \frac{dp_n}{dx} \quad (3.55)$$

Integrating this equation

$$\int_0^{W_n} J_t dx = -q D_p \int_{p_n(0)}^{p_n(W_n)} dp \quad (3.56)$$

produces the low injection  $p^+n$  thin base diode equation

$$I_p = A q \frac{D_p}{W_n} \Delta p_n(0) \quad (3.57)$$

The high injection equation for this diode is similarly derived by integrating the high injection transport equation, Equation (2.13), using  $J_p = J_t = \text{constant}$ ; the result is

$$I_p = 2 A q \frac{D_p}{W_n} p(0) \quad (3.58)$$

Therefore, the diode equations for a uniformly doped thin base  $p^+n$  diode are the same as those for a long diode, except that  $W_n$  replaces  $L_p$  and  $\xi = 2$ .

## 4 TRANSIENT AND SMALL SIGNAL ANALYSIS

To check the agreement between the measured and theoretical intercepts given by Equations (3.49) it is necessary to supply these equations with estimates for the lifetimes and the junction area. The minority carrier lifetime,  $\tau_p$ , can be determined from the time taken to switch a diode from the low injection forward biased state to the reverse biased state. The high injection lifetime,  $\tau$ , is similarly determined using high injection currents. The relationship between switching time and lifetime is governed by the solutions of the time dependent low and high injection equations of state. The junction area can be deduced from the measured small signal junction capacitance and confirmed from the physical dimensions of the die.

### 4.1 The Time Dependent Equations of State

The transport equations are the same as the steady state ones, but current density and carrier concentration are understood to be functions of both distance,  $x$ , and time,  $t$ . The time dependent continuity equations for holes and electrons are [[4 pp85]]

$$\frac{\partial J_p}{\partial x} = -qU - q \frac{\partial p}{\partial t}, \quad (4.1)$$

$$\frac{\partial J_n}{\partial x} = qU + q \frac{\partial n}{\partial t}. \quad (4.2)$$

### 4.2 Low Injection Transient Analysis [[7]] [[8]]

Without loss of generality and in the interest of simplicity the transient

analysis is performed for a p<sup>+</sup>n diode. The transport equation appropriate for low injection hole current in the N region is given by Equation (2.11) which is repeated here:

$$J_{pn} = -q D_p \frac{dp_n}{dx} \quad (2.11)$$

Substituting the derivative of this into Equation (4.1) and using the net recombination rate from Equation (2.24) yields the partial differential equation

$$\frac{\partial^2 \Delta p_n}{\partial x^2} - \frac{\Delta p_n}{D_p \tau_p} = \frac{1}{D_p} \frac{\partial \Delta p_n}{\partial t} \quad (4.3)$$

The Laplace transform of this is

$$\frac{d^2 \Delta p_n}{dx^2} - \left[ \frac{1}{D_p \tau_p} + \frac{s}{D_p} \right] \Delta p_n = - \frac{\Delta p_n(x,0)}{D_p} - \frac{\Delta p_n(0,0)}{D_p} e^{-\frac{x}{L_p}} \quad (4.4)$$

where the bold symbols represent transformed variables, and use has been made of Equation (3.5). The solution to Equation (4.4) is

$$\Delta p_n = C_1 e^{-\frac{\sqrt{s+1/\tau_p}}{\sqrt{D_p}} x} + C_2 e^{\frac{\sqrt{s+1/\tau_p}}{\sqrt{D_p}} x} + \frac{\Delta p_n(0,0)}{s} e^{-\frac{x}{L_p}} \quad (4.5)$$

For an infinitely long charge-neutral N region

$$\Delta p_n = 0 \text{ at } x = \infty, \quad \therefore C_2 = 0.$$

The second boundary condition is determined from the ratio of the forward and reverse currents as follows. For  $t < 0$ , steady state forward current,  $I_{fwd}$ , flows in the diode. The steady state low injection

p+n diode equation derivation showed that

$$I_{\text{fwd}} = -A q D_p \left[ \frac{\partial \Delta p_n}{\partial x} \right]_{x=0, t < 0} = A q D_p \frac{\Delta p_n(0,0)}{L_p} \quad (4.6)$$

At  $t = 0$  the current is switched to  $I_{\text{rev}} = -\gamma I_{\text{fwd}}$ , so for  $t > 0$

$$I_{\text{rev}} = -A q D_p \left[ \frac{\partial \Delta p_n}{\partial x} \right]_{x=0, t > 0} = -\gamma I_{\text{fwd}} \quad (4.7)$$

Therefore

$$\left[ \frac{\partial \Delta p_n}{\partial x} \right]_{x=0, t > 0} = \frac{\gamma \Delta p_n(0,0)}{s L_p} \quad (4.8)$$

Equating this to the derivative evaluated at  $x = 0$  of  $\Delta p_n$  from Equation (4.5) yields  $C_1$ , and Equation (4.5) becomes

$$\Delta p_n(x,s) = \frac{-\{1 + \gamma\} \Delta p_n(0,0)}{\sqrt{\tau_p} s \sqrt{s + 1/\tau_p}} e^{-\frac{\sqrt{s + 1/\tau_p}}{\sqrt{D_p}} x} + \frac{\Delta p_n(0,0)}{s} e^{-\frac{x}{L_p}} \quad (4.9)$$

Hence, at  $x = 0$

$$\Delta p_n(0,s) = \frac{\Delta p_n(0,0)}{s} \left[ 1 - \frac{\{1 + \gamma\}}{\sqrt{\tau_p} \sqrt{s + 1/\tau_p}} \right], \quad (4.10)$$

and the inverse transform of this is [[9 pp673]]

$$\Delta p_n(0,t) = \Delta p_n(0,0) \left[ 1 - \{1 + \gamma\} \text{erf} \sqrt{\frac{t}{\tau_p}} \right] \quad (4.11)$$

When the depletion region edge carrier concentration,  $\Delta p_n(0,t)$ , decays to zero, the diode voltage crosses zero, and  $t = t_{dL}$ , the low injection charge storage delay time. Setting  $\Delta p_n(0,t) = 0$  in Equation (4.11) produces

$$\operatorname{erf} \sqrt{\frac{t_{dL}}{\tau_p}} = \frac{1}{1 + \gamma}. \quad (4.12)$$

Hence, for a uniformly doped infinitely long p+n diode,  $\tau_p$  can be deduced from a measurement of  $t_{dL}$  using

$$\tau_p = \frac{t_{dL}}{\left[ \operatorname{erf}^{-1} \frac{1}{1 + \gamma} \right]^2}. \quad (4.13)$$

If the approximate form of the error function,

$$\operatorname{erf} \sqrt{\frac{t_{dL}}{\tau_p}} = \frac{1}{1 + \gamma} \approx \frac{2}{\sqrt{\pi}} \sqrt{\frac{t_{dL}}{\tau_p}}, \quad (4.14)$$

is introduced, the resulting equation,

$$\sqrt{\tau_p} = \sqrt{t_{dL}} \frac{2(1 + \gamma)}{\sqrt{\pi}}, \quad (4.15)$$

will generate values for  $\tau_p$  that are about 15% high for  $\gamma$ 's near 1; this amounts to about a 4% error in  $L_p$ , which is not very significant for this measurement.

Substituting Equation (4.15) into the low injection diode equation yields an expression for that equation in terms of the delay time:

$$I_p = A q \frac{\sqrt{D_p}}{\sqrt{t_d}} \frac{n_i^2}{2(1+\gamma) N_d} \left[ e^{qV/kT} - 1 \right]. \quad (4.16)$$

### 4.3 High Injection Transient Analysis

Proceeding in the same way as for the low injection case by combining the appropriate transport equation, continuity equation and net recombination rate given respectively by Equations (2.13), (4.1) and (2.26) results in the partial differential equation

$$\frac{\partial^2 p_n}{\partial x^2} - \frac{p_n}{D\tau} = \frac{1}{D} \frac{\partial p_n}{\partial t}. \quad (4.17)$$

As for the low injection case, the solution to the Laplace transform of this equation for an infinitely long diode is

$$p_n = C_1 e^{\frac{-\sqrt{s+1/\tau}}{\sqrt{D}} x} + \frac{p(0,0)}{s} e^{-\frac{x}{L}}. \quad (4.18)$$

Setting  $J_p(0) = J_t$  in the transport equation, Equation (2.13), and multiplying by  $A$  gives

$$I_{fwd} = -A q 2 D_p \left[ \frac{\partial p_n}{\partial x} \right]_{x=0, t < 0} = A q 2 D_p \frac{p(0,0)}{L}. \quad (4.19)$$

At  $t = 0$  the current is switched to  $I_{rev} = -\gamma I_{fwd}$ , so for  $t > 0$

$$I_{rev} = -A q 2 D_p \left[ \frac{\partial p_n}{\partial x} \right]_{x=0, t > 0} = -\gamma I_{fwd}. \quad (4.20)$$

Therefore

$$\left[ \frac{\partial p_n}{\partial x} \right]_{x=0, t>0} = \frac{\gamma p(0,0)}{sL}$$

Equating this to the derivative evaluated at  $x = 0$  of  $p_n$  from Equation (4.18) yields  $C_1$ , and Equation (4.18) becomes

$$p_n(x,s) = \frac{-(1+\gamma) p_n(0,0)}{\sqrt{\tau} s \sqrt{s+1/\tau}} e^{-\frac{\sqrt{s+1/\tau}}{\sqrt{D}} x} + \frac{p(0,0)}{s} e^{-\frac{x}{L}} \quad (4.21)$$

Comparing this with Equation (4.9) shows that the relationship between  $\tau$  and  $t_{dH}$ , the high injection charge storage delay time, is the same as that between  $\tau_p$  and  $t_{dL}$ , that is

$$\sqrt{\tau} = \sqrt{t_{dH}} \frac{2\{1+\gamma\}}{\sqrt{\pi}} \quad (4.22)$$

Substituting Equation (4.22) into the high injection diode equation yields an expression for that equation in terms of the delay time:

$$I_p = e^{-x} \sqrt{2 \left[ 1 + \frac{D_p}{D_n} \right]} A q \frac{\sqrt{D_p}}{\sqrt{t_{dH}} \frac{2\{1+\gamma\}}{\sqrt{\pi}}} n_i e^{qV/2kT} \quad (4.23)$$

When measuring the high injection charge storage delay time, the forward current must be large enough to ensure that the hole charge stored in the N side due to high injection current substantially exceeds that due to low injection. The charge stored is equal to the area under the hole concentration distribution. Figure 3.1 is a reminder that high injection will be responsible for most of this area if the forward current

exceeds the breakpoint by about one order of magnitude.

#### 4.4 Thin Base Diode Transient Analysis

It was previously argued that a thin base diode has a linear excess carrier distribution and behaves as if its lifetime were very large.

Letting  $\tau_p \rightarrow \infty$  in Equation (4.3) gives

$$\frac{\partial^2 \Delta p_n}{\partial x^2} = \frac{1}{D_p} \frac{\partial \Delta p_n}{\partial t} \quad (4.24)$$

The Laplace transform of this is

$$\frac{d^2 \Delta p_n}{dx^2} - \frac{s}{D_p} \Delta p_n = - \frac{\Delta p_n(x,0)}{D_p} \quad (4.25)$$

At  $t = 0$  the linear excess carrier concentration changes from  $\Delta p_n(0,0)$  at  $x = 0$  to 0 at  $x = \infty$ , so its distribution must be

$$\Delta p_n(x,0) = \Delta p_n(0,0) - \frac{\Delta p_n(0,0)}{W_n} x \quad (4.26)$$

and the transformed differential equation becomes

$$\frac{d^2 \Delta p_n}{dx^2} - \frac{s}{D_p} \Delta p_n = \frac{\Delta p_n(0,0)}{D_p W_n} x - \frac{\Delta p_n(0,0)}{D_p} \quad (4.27)$$

for which the solution is

$$\Delta p_n = C_1 e^{-\sqrt{s/D_p} x} + C_2 e^{\sqrt{s/D_p} x} + \frac{\Delta p_n(0,0)}{s} \left[ 1 - \frac{x}{W_n} \right]. \quad (4.28)$$

The boundary condition for the derivative of this equation is again obtained from the ratio of the reverse to the forward current, that is

$$\left[ \frac{\partial \Delta p_n}{\partial x} \right]_{x=0, t>0} = \frac{\gamma \Delta p_n(0,0)}{s W_n}. \quad (4.29)$$

The other boundary condition is

$$\Delta p_n = 0 \text{ at } x = W_n,$$

and solving for the constants  $C_1$  and  $C_2$  gives

$$\Delta p_n(x,s) = \frac{-(1+\gamma) \Delta p_n(0,0) \sinh \left[ \sqrt{s/D_p} (x - W_n) \right]}{W_n s \sqrt{s/D_p} \cosh \left[ \sqrt{s/D_p} W_n \right]} + \frac{\Delta p_n(0,0)}{s} \left[ 1 - \frac{x}{W_n} \right] \quad (4.30)$$

which at  $x = 0$  becomes

$$\Delta p_n(0,s) = \frac{\Delta p_n(0,0)}{s} \left[ 1 - \frac{(1+\gamma) \tanh \left[ W_n \sqrt{s/D_p} \right]}{W_n \sqrt{s/D_p}} \right]. \quad (4.31)$$

The inverse transform of this is obtained using the first two terms of the expansion

$$\tanh z = 1 - 2 e^{-2z} + \dots,$$

to give

$$\Delta p_n(0,t) \approx \Delta p_n(0,0) \left[ 1 - (1 + \gamma) \frac{2 D_p}{W_n} \sqrt{\frac{t}{\pi}} \right]. \quad (4.32)$$

Letting  $\Delta p_n(0,0) = 0$  when  $t = t_d$  yields the relationship between the width of the charge-neutral N region and the charge storage delay time for a uniformly doped thin base diode

$$\frac{W_n^2}{D_p} \approx t_d \frac{4 (1 + \gamma)^2}{\pi}. \quad (4.33)$$

Note the similarity between this and Equation (4.15). Equation (4.33) can also be derived using the high injection equations;  $W_n$  is obviously independent of the injection level.

#### 4.5 Small Signal Junction Capacitance

The junction of uniformly doped P and N materials is abrupt. The space charge densities in the depletion region on the P and N sides of the junction are respectively [[1 pp80]]

$$\rho_p = -q N_a \quad \text{and} \quad \rho_n = q N_d. \quad (4.34)$$

For a p<sup>+</sup>n diode  $N_d \ll N_a$ , and since the total space charge must be the same on both sides of the junction, then the depletion region width on the P side contributes very little to the total depletion region width,  $W$ , and the potential across the P side can be neglected. The N side electric field is given by the integral of the space charge, that is

$$E_n = \frac{-q N_d W}{\epsilon} \left[ 1 - \frac{x}{W} \right], \quad (4.35)$$

where  $\epsilon$  is the permittivity of silicon, and the E field vanishes at the depletion region edge. The potential distribution in the N side of the depletion region is obtained by integrating Equations (4.35) to yield

$$\psi - \phi = \frac{q N_d W}{\epsilon} \left[ x - \frac{x^2}{2W} \right], \quad (4.36)$$

where  $\phi$  is the potential at  $x = 0$ . The potential across the narrow P side is approximately zero, so the potential difference across the depletion region is the difference in potential between the points  $x = W$  and  $x = 0$ , that is

$$\psi_{np} = \frac{q N_d W^2}{2 \epsilon} \text{ which also equals } \psi_{bi} - V, \quad (4.37)$$

where  $\psi_{bi}$  is given by Equation (3.35). Solving Equation (4.37) for  $W$  gives

$$W = \sqrt{\frac{2 \epsilon \{ \psi_{bi} - V \}}{q N_d}}. \quad (4.38)$$

Because the junction capacitance is [1 pp83]

$$C_J = \frac{\epsilon A}{W}, \quad (4.39)$$

then

$$\frac{1}{C_J^2} = \frac{2}{q N_d \epsilon A^2} \psi_{bi} - \frac{2}{q N_d \epsilon A^2} V, \quad (4.40)$$

and a plot of  $1/C_J^2$  vs  $V$  will be linear for an abrupt junction diode.

## 5 DIFFUSED JUNCTION DIODES

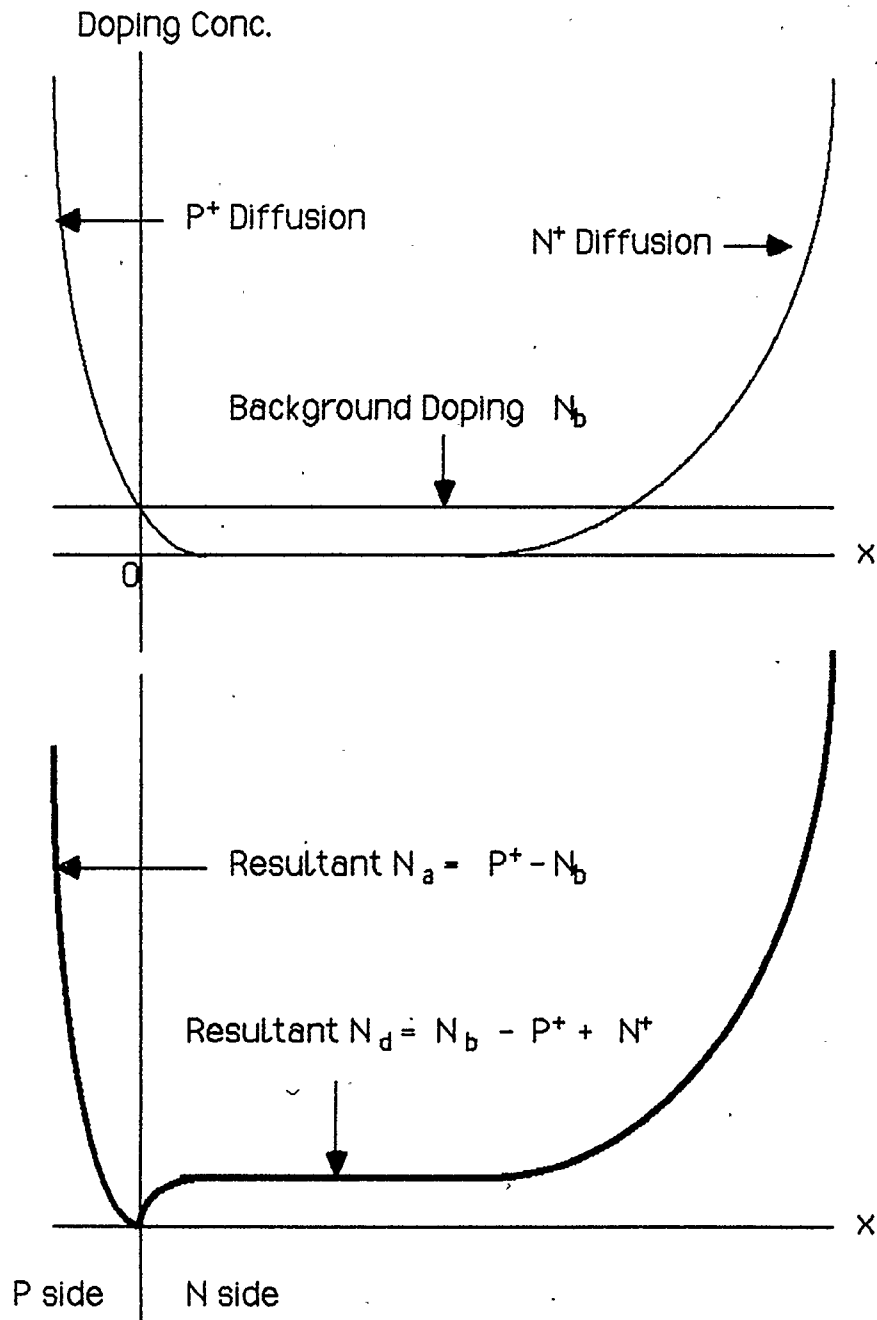
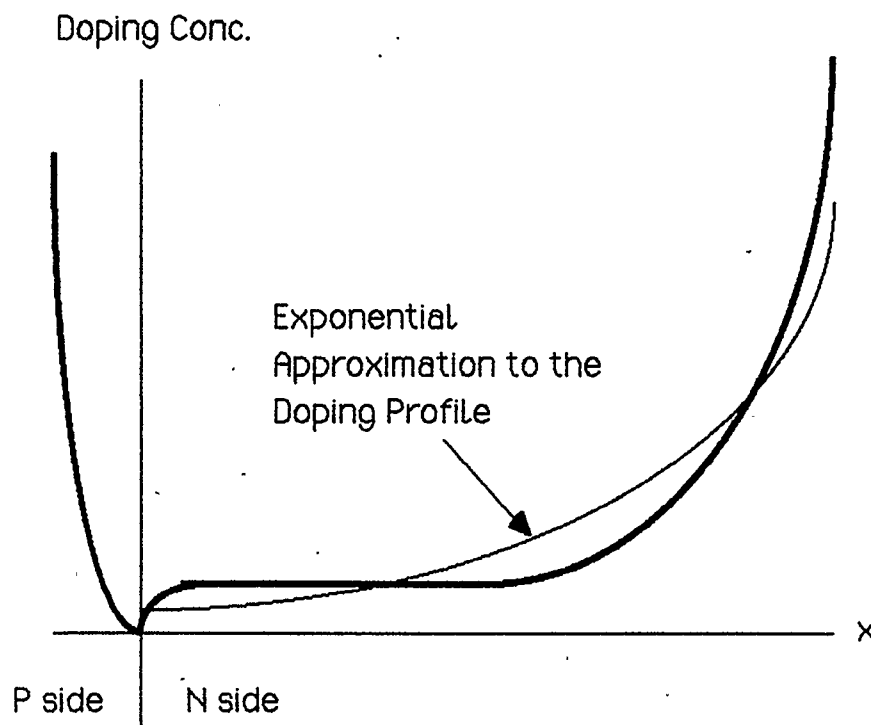


Figure 5.1 Doping Profile for a Typical  $p^+n$  Diode

Figure 5.1 serves to illustrate the non-uniformity of the doping for a typical diffused junction  $p^+n$  diode. The anode is formed by a  $P^+$  diffusion into the N substrate. The  $P^+$  concentration at the anode surface is made large enough to produce a non-rectifying ohmic contact [1 pp170]. The  $N^+$  diffusion is required for a non-rectifying cathode contact.

Neither the ideal diode equation nor the improved diode equation accounts for the small electric field in the bulk regions created by the doping gradients. Accurate knowledge of the doping profile is required to solve the equations of state for a non-uniformly doped device, and simple closed form solutions will not always be possible. However, an understanding of the influence of non-uniform doping can be achieved through consideration of a particular diode - one that is exponentially doped. Manageable solutions are attainable for this device. Actual Gaussian and erfc doping profiles do approximate exponential curves



**Figure 5.2** Exponential Approximation to the Doping Profile of a typical  $p^+n$  Diode.

sufficiently far from the contact, and the exponential doping profile illustrated in Figure 5.2 is not very unlike that of a realistically doped diode.

### 5.1 The Equations of State for Non-uniform Doping

The most general form of the hole transport equation is deduced as it was for uniform doping except that now  $N_d$  is recognized to be a function of  $x$ . Differentiating the charge balance equation, Equation (2.6), gives

$$\frac{dn_n}{dx} = \frac{dp_n}{dx} + \frac{dN_d}{dx} \quad (5.1)$$

When this is used in place of Equation (2.8), the hole transport mechanism for non-uniform doping becomes

$$J_{pn} = \left[ \frac{J_t}{1 + \frac{D_n n_n}{D_p p_n}} \right] + \left[ \frac{D_p - D_n}{1 + \frac{D_n n_n}{D_p p_n}} - D_p \right] q \frac{dp_n}{dx} - \left[ \frac{D_n}{1 + \frac{D_n n_n}{D_p p_n}} \right] q \frac{dN_d}{dx} \quad (5.2)$$

Low level injection and charge neutrality imply that

$$p_n \ll n_n \quad \text{and} \quad n_n = N_d,$$

and applying these conditions to Equation (5.2) gives

$$J_{pn} = -q \left[ \frac{kT}{q} \frac{1}{N_d} \frac{dN_d}{dx} \right] \mu_p p_n - q D_p \frac{dp_n}{dx} \quad (5.3)$$

The term within the square brackets is recognized as the equilibrium electric field, obtainable also by setting  $J_n = 0$  in the electron transport

equation, Equation (2.2). This field remains undisturbed even when current flows as long as  $n_p = N_d$ . There must of course be some departure from charge neutrality to generate the space charge for the electric field. An exponential doping profile in the N region will be described by

$$N_d = N_{d0} e^{x/\lambda}, \quad (5.4)$$

where  $\lambda$  is the doping diffusion length and  $N_{d0}$  is the donor doping concentration at  $x = 0$ .

Substituting this into Equation (5.3) yields the low injection hole transport equation

$$J_p = -q \frac{D_p}{\lambda} p_n - q D_p \frac{dp_n}{dx}. \quad (5.5)$$

The DC and time dependent continuity equations are independent of the doping gradient.

## 5.2 Low Injection DC Solution of the Equations of State

Substituting the derivative of  $J_p$  from Equation (5.5) into the steady state continuity equation, Equation (2.27), and using the low injection net recombination rate of Equation (2.24) gives

$$\frac{d^2 p_n}{dx^2} + \frac{1}{\lambda} \frac{dp_n}{dx} - \frac{1}{L_p^2} p_n = -\frac{1}{L_p^2} p_{no}, \quad (5.6)$$

where

$$p_{no} = \frac{n_i^2}{N_d} = \frac{n_i^2}{N_{d0}} e^{-x/\lambda}. \quad (5.7)$$

Note that

$$\frac{d\Delta p_n}{dx} = \frac{dp_n}{dx} \quad \text{since} \quad \frac{dp_{no}}{dx} = 0.$$

The boundary conditions for an infinitely long diode are

$$p_n - p_{no} = 0 \quad \text{at} \quad x = \infty \quad \text{and} \quad p_n = p_n(0) \quad \text{at} \quad x = 0,$$

so the solution is

$$p_n = \frac{n_i^2}{N_{do}} e^{-x/\lambda} + \Delta p_n(0) e^{-\left[\frac{1}{2\lambda} + \frac{1}{2} \sqrt{\frac{1}{\lambda^2} + \frac{4}{L_p^2}}\right] x} \quad (5.8)$$

Substituting this and its derivative evaluated at  $x = 0$  into the transport equation, Equation (5.5), yields the depletion region edge hole current density for an exponentially doped  $p^+n$  diode:

$$J_{pn}(0) = q \frac{D_p}{L_p} \left[ \sqrt{1 + \left[\frac{L_p}{2\lambda}\right]^2} - \frac{L_p}{2\lambda} \right] \Delta p_n(0). \quad (5.9)$$

Define the non-uniform doping factor

$$\zeta \equiv \sqrt{1 + \left[\frac{L_p}{2\lambda}\right]^2} - \frac{L_p}{2\lambda}, \quad (5.10)$$

and Equation (5.9) can be written as

$$J_{pn}(0) = q \frac{D_p}{L_p} \zeta \Delta p_n(0). \quad (5.11)$$

### 5.3 Low Injection Transient Solution of the Equations of State

Substituting the derivative of  $J_p$  from Equation (5.5) into the time dependent continuity equation, Equation (4.1), and using the low injection net recombination rate of Equation (2.24) gives

$$\frac{\partial^2 p_n}{\partial x^2} + \frac{1}{\lambda} \frac{\partial p_n}{\partial x} - \frac{1}{L_p^2} p_n = -\frac{1}{L_p^2} p_{no} + \frac{1}{D_p} \frac{\partial p_n}{\partial t} \quad (5.12)$$

The Laplace transform of this partial differential equation is

$$\frac{d^2 P_n}{dx^2} + \frac{1}{\lambda} \frac{dP_n}{dx} - \left[ \frac{1}{L_p^2} + \frac{s}{D_p} \right] P_n = -\frac{P_{no}}{s L_p^2} - \frac{P_n(x,0)}{D_p} \quad (5.13)$$

Substituting into this  $P_n(x,0)$  from Equation (5.8),

$P_{no}$  from Equation (5.7),

and using  $P_n - P_{no} = 0$  at  $x = \infty$  for a long diode,

delivers the solution to Equation (5.13):

$$P_n = C_1 e^{-\left[ \frac{1}{2\lambda} + \frac{1}{2} \sqrt{\frac{1}{\lambda^2} + \frac{4}{L_p^2} + \frac{4s}{D_p}} \right] x} + \frac{P_n(x,0)}{s} \quad (5.14)$$

According to the governing transport equation, Equation (5.5)

$$\left[ \frac{\partial p_n}{\partial x} \right]_{x=0, t < 0} + \frac{1}{\lambda} p_n(0,0) = -\frac{J_{pn}(0,0)}{q D_p} = -\frac{J_{fwd}}{q D_p} \quad (5.15)$$

$$\left[ \frac{\partial p_n}{\partial x} \right]_{x=0, t>0} + \frac{1}{\lambda} p_n(0,t) = -\frac{J_{rev}}{q D_p} = \gamma \frac{J_{fwd}}{q D_p}. \quad (5.16)$$

Therefore

$$\left[ \frac{dp_n}{dx} \right]_{x=0} + \frac{1}{\lambda} p_n(0,s) = -\frac{\gamma}{s} \left[ \left[ \frac{\partial p_n}{\partial x} \right]_{x=0, t<0} + \frac{1}{\lambda} p_n(0,0) \right]. \quad (5.17)$$

Substituting into this

$p_n$  and its derivative evaluated at  $x = 0$  from Equation (5.14)

and

$p_n$  and its derivative evaluated at  $x = 0$  from Equation (5.8)

yields  $C_1$ , and Equation (5.14) becomes at  $x = 0$

$$p_n(0,s) = \frac{p_n(0,0)}{s} - \frac{\Delta p_n(0,0) \{1 + \gamma\} \left[ \sqrt{\frac{D_p}{4\lambda^2} + \frac{1}{\tau_p}} - \sqrt{\frac{D_p}{4\lambda^2}} \right]}{s \left[ \sqrt{\frac{D_p}{4\lambda^2} + \frac{1}{\tau_p} + s} - \sqrt{\frac{D_p}{4\lambda^2}} \right]}. \quad (5.18)$$

This reduces to its uniformly doped equivalent, Equation (4.10), for large  $\lambda$ . In general [[9 pp673]]

$$\frac{a-b}{s \left[ \sqrt{s+a^2} - b \right]} \Leftrightarrow \frac{1}{a+b} \left[ b + a \operatorname{erf} [a \sqrt{t}] - b e^{[b^2-a^2]t} \operatorname{erfc} [-b \sqrt{t}] \right] \quad (5.19)$$

which is of the same form as Equation (5.18) for

$$a = \sqrt{\frac{D_p}{4\lambda^2} + \frac{1}{\tau_p}} \quad \text{and} \quad b = \sqrt{\frac{D_p}{4\lambda^2}} \quad (5.20)$$

Also, when  $p_n(0,t)$  decays to  $n_i^2/N_{d0}$  then  $t = t_d$ ; therefore,

$$\frac{1}{a+b} \left[ b + a \operatorname{erf} \left[ a \sqrt{t_d} \right] - b e^{-t_d/\tau_p} \operatorname{erfc} \left[ -b \sqrt{t_d} \right] \right] = \frac{1}{1+\gamma} \quad (5.21)$$

If  $t_d$  is somewhat less than  $\tau_p$ , as it is for uniformly doped diodes, then

$$\operatorname{erf} \left[ a \sqrt{t_d} \right] = \frac{2}{\sqrt{\pi}} a \sqrt{t_d},$$

$$\operatorname{erfc} \left[ -b \sqrt{t_d} \right] = 1 + \frac{2}{\sqrt{\pi}} b \sqrt{t_d},$$

$$e^{-t_d/\tau_p} = 1,$$

and Equation (5.21) becomes

$$\sqrt{\tau_p} - \sqrt{t_d} \frac{2(1+\gamma)}{\sqrt{\pi}} \frac{1}{\sqrt{1 + \left[ \frac{L_p}{2\lambda} \right]^2 + \frac{L_p}{2\lambda}}} \quad (5.22)$$

Invoking the definition for  $\zeta$  from Equation (5.10) gives the result:

$$\sqrt{\tau_p} - \zeta \sqrt{t_d} \frac{2(1+\gamma)}{\sqrt{\pi}} \quad (5.23)$$

For large  $\lambda$  this reduces to its uniformly doped equivalent, Equation (4.15). The charge storage delay time is expected to be greater for an

exponentially doped diode than for a uniformly doped otherwise equivalent part. The value for  $\tau_p$  calculated from the measured delay time is smaller using the formula for the exponentially doped diode.

#### 5.4 The Low Injection Diode Equations for Non-uniform Doping

From Equation (5.11) the exponentially doped low injection diode equation is

$$I_p = \zeta A q \frac{D_p}{L_p} \frac{n_i^2}{N_{do}} \left[ e^{qV/kT} - 1 \right]. \quad (5.24)$$

Combining Equation (5.24) with Equation (5.23) gives the low injection diode equation in terms of the charge storage delay time

$$I_p = A q \frac{\sqrt{D_p}}{\sqrt{t_d} \left[ \frac{2\{1+\gamma\}}{\sqrt{\pi}} \right]} \frac{n_i^2}{N_{do}} \left[ e^{qV/kT} - 1 \right]. \quad (5.25)$$

This is the same as its uniformly doped companion equation, Equation (4.16). From Equations (5.24) and (5.25) the low injection intercept for a non-uniformly doped diode is

$$I_s = \zeta A q \frac{D_p}{L_p} \frac{n_i^2}{N_{do}} = A q \frac{\sqrt{D_p}}{\sqrt{t_d} \left[ \frac{2\{1+\gamma\}}{\sqrt{\pi}} \right]} \frac{n_i^2}{N_{do}}. \quad (5.26)$$

#### 5.5 High Injection Diode Equations for Non-Uniform Doping

If the high injection condition,  $p = n$ , were satisfied everywhere in the charge-neutral N region,  $N_d$  would have no influence, the field due to

the doping gradient would vanish, and the high injection equations would be unchanged for non-uniform doping. However, at some value of  $x < W_n$ , the doping profile of a realistically doped device will rise sharply towards a large degenerate value as illustrated in Figure 5.3. Beyond this point the high injection condition is not satisfied. This will not seriously change the overall shape of the hole distribution because the low and high injection diffusion lengths are much alike. But it will reduce the voltage drop in the charge-neutral N region due to a shortening of the length over which the high injection electric field prevails. That is, to get the voltage drop, Equation (3.42) cannot be integrated over the entire bulk region but only over that part where the high injection condition exists. Hence,  $W_b$ , a value less than  $W_n$  must replace  $W_n$  in Equation (3.43) which in turn reduces  $\chi$  and  $\sigma$ . Otherwise, the high injection equations for uniformly doped diodes apply also to those that are not.

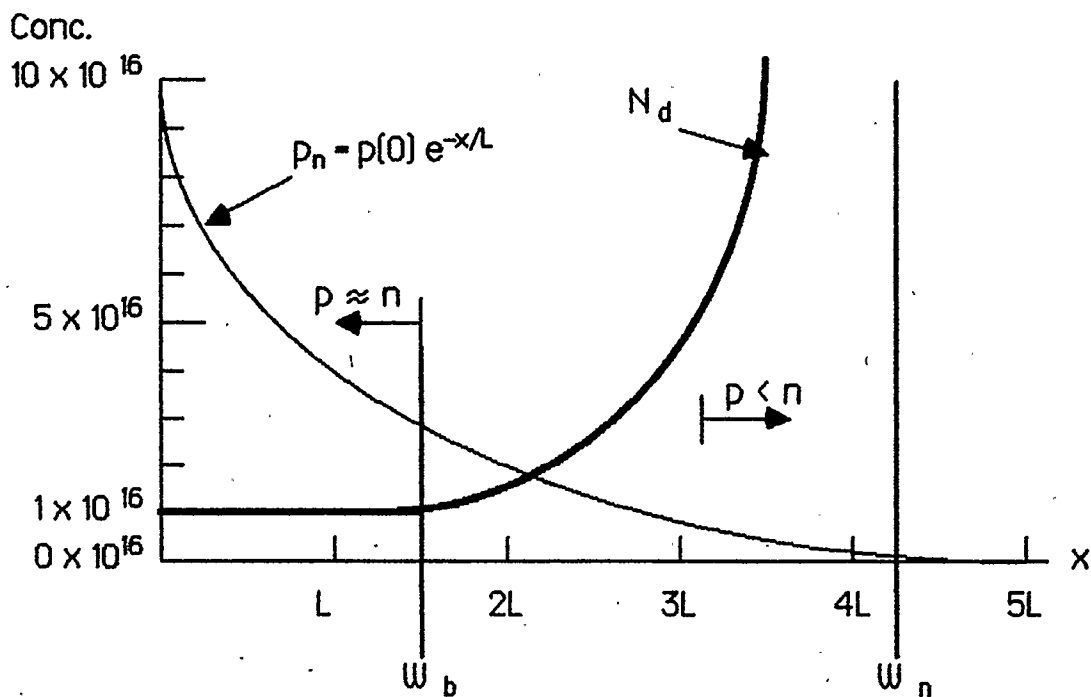


**Figure 5.3** High Injection Hole distribution and Doping Profile.

## 5.6 Linearly Graded Junction Capacitance

Figure 5.4 shows an expanded view of the doping concentration near the depletion region for the diffused junction p<sup>+</sup>n diode. The doping gradient,  $a$ , is approximately linear close to the junction, and the result is a nearly linear space charge distribution, that is

$$\rho = q a x. \quad [5.27]$$

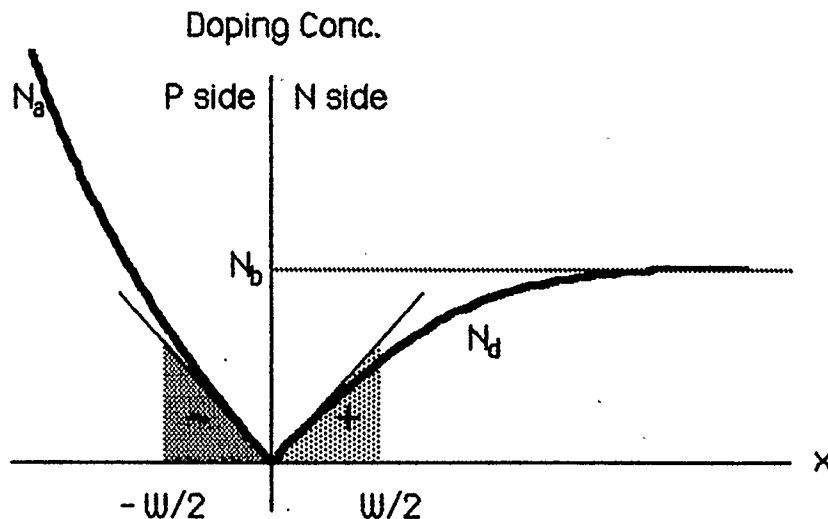


**Figure 5.4** Doping Concentration in the Vicinity of the Depletion Region

Because the doping is linear, then at the depletion region edges

$$N_a(-W/2) = N_d(W/2) = a \frac{W}{2}. \quad [5.28]$$

The usual method for deriving the junction capacitance of a linearly graded junction is to assume that the electric field at the edge of the depletion region is zero [1 pp82] [3 pp88] [5 pp32]. A more rigorous derivation accounts for the finite electric field at the depletion region

edge due to the doping gradient that exists outside of the depletion region; according to Equation (5.3) and (5.28) this field is

$$E(W/2) = -\frac{kT}{q} \frac{1}{N_d(W/2)} \left[ \frac{dN_d}{dx} \right]_{x=W/2} = -\frac{kT}{q} \frac{2}{W} \quad (5.29)$$

Using this boundary condition to integrate the symmetrical linear space charge distribution gives

$$E = \frac{q a}{2 \epsilon} \left[ x^2 - \frac{W^2}{4} \right] - \frac{kT}{q} \frac{2}{W}, \quad (5.30)$$

and the maximum electric field occurs at  $x = 0$ , that is

$$E_{\max} = -\frac{q a W^2}{2 \epsilon \cdot 4} - \frac{kT}{q} \frac{2}{W}. \quad (5.31)$$

Integrating Equation (5.30) gives the potential distribution,

$$\psi - \phi = \frac{q a}{2 \epsilon} \left[ \frac{W^2}{4} x - \frac{x^3}{3} \right] + \frac{kT}{q} \frac{2}{W} x, \quad (5.32)$$

where use has been made of the boundary condition  $\psi = \phi$  at  $x = 0$  which will be useful later. The total potential across the depletion region is

$$\psi_{np} = (\psi - \phi)|_{x=W/2} - (\psi - \phi)|_{x=-W/2} = \frac{q a W^3}{12 \epsilon} + 2 \frac{kT}{q}. \quad (5.33)$$

The built in potential is obtained by combining Equations (3.35) and (5.28) to give

$$\psi_{bi} = 2 \frac{kT}{q} \ln \frac{aW}{2n_i} \quad (5.34)$$

Unlike that of an abrupt junction, the built in potential of a linearly graded junction depends on the width and consequently on the applied voltage. When voltage is applied the potential across the depletion region becomes

$$\psi_{rp} = \psi_{bi} - V, \quad (5.35)$$

and equating this with Equation (5.33) gives

$$W^3 = \frac{12 \epsilon}{q a} \left[ 2 \frac{kT}{q} \ln \frac{aW}{2n_i} - 2 \frac{kT}{q} - V \right], \quad (5.36)$$

where use has been made of Equation (5.34). Equation (5.36) must be solved numerically for  $W$ . Substituting this into Equation (4.39) yields

$$\frac{1}{C_j^3} = \frac{12}{\epsilon^2 A^3 q a} \left[ \psi_{bi} - 2 \frac{kT}{q} \right] - \frac{12}{\epsilon^2 A^3 q a} V; \quad (5.37)$$

hence, a plot of  $1/C_j^3$  vs  $V$  is expected to be linear for a linearly graded junction diode. The doping gradient can be determined from the known breakdown voltage using the empirical relationship between these [1 pp104]. Therefore, once  $a$  is established, the area of the junction can be determined from the slope of the plot of  $1/C_j^3$  vs  $V$ . At  $V = 0$  the vertical intercept of this plot is

$$\frac{1}{C_{j0}^3} = \frac{12}{\epsilon^2 A^3 q a} \left[ \psi_{bi0} - 2 \frac{kT}{q} \right], \quad (5.38)$$

where

$C_{j0}$  is the equilibrium junction capacitance and

$\psi_{\text{bio}}$  is the equilibrium built in potential.

Comparing Equations (5.38) and (5.37) it is apparent that

$$\psi_{\text{bio}} = 2 \frac{kT}{q} + \frac{\text{Intercept}}{\text{slope}} \quad (5.39)$$

## 6. DIODE EQUATION EVALUATION

To test the improved diode equation's ability to predict the forward characteristics of a diode at all temperatures, the equation must be supplied with the essential parameters pertaining to the particular diode. To begin with, the high and low injection intercepts are obtained from a measured forward characteristic, substituted into

$$I_p = I_h \left[ \sqrt{\left[ \frac{I_h}{2I_s} \right]^2 + e^{qV/kT}} - \sqrt{\left[ \frac{I_h}{2I_s} \right]^2 + 1} \right], \quad (3.40)$$

and compared with the measured curve. Then the theoretical temperature dependencies of  $I_h$  and  $I_s$  are tested, and finally the calculated quantities,

$$I_h = \sigma A q \frac{D_p}{L_p} n_i \quad \text{and} \quad I_s = \zeta A q \frac{D_p}{L_p} \frac{n_i^2}{N_{d0}},$$

are compared with their measured values.

### 6.1 Modelling With $I_h$ and $I_s$ at Room Temperature

A 1N4764 100 volt 1 watt zener diode is chosen as a typical part. Figure 6.1 shows its measured room temperature forward characteristic. The two required tangent lines of slope  $(q/2kT) \text{ Log } e$  and  $(q/kT) \text{ Log } e$  have been drawn on the measured curve, and  $I_h$  and  $I_s$  are found to be

$$I_h = 3.1 \times 10^{-9} \text{ amps} \quad \text{and} \quad I_s = 4.1 \times 10^{-15} \text{ amps.}$$

Figure 6.2 shows the result of using these values in Equation (3.40) to generate the theoretical characteristic.

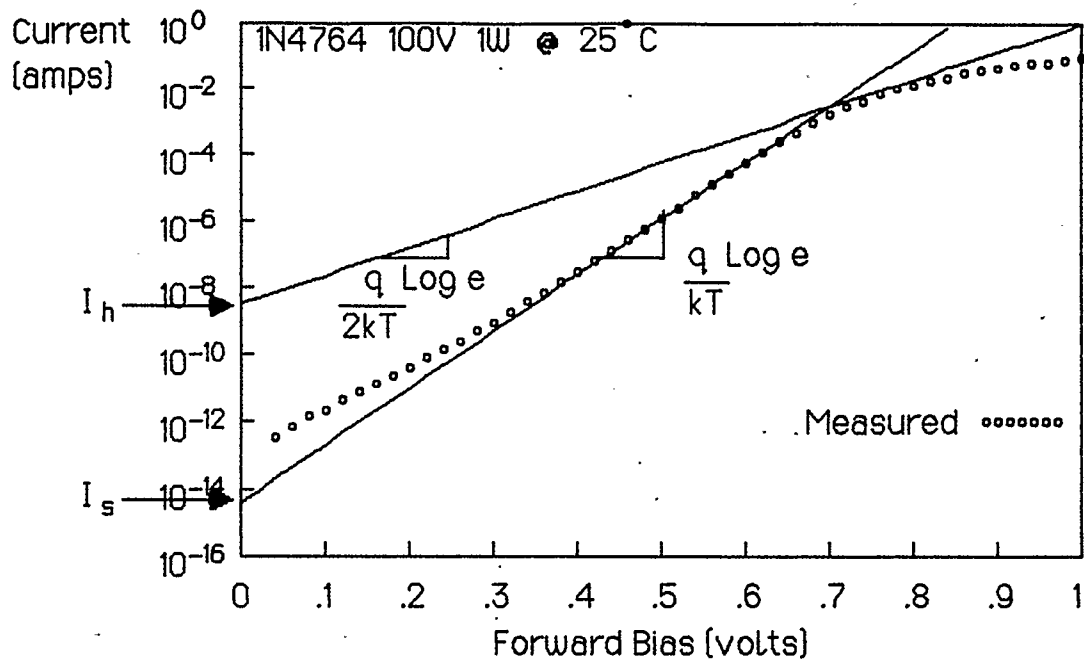


**Figure 6.1** A Measured Forward Characteristic Showing the Tangent Lines and High and Low Injection Intercepts,

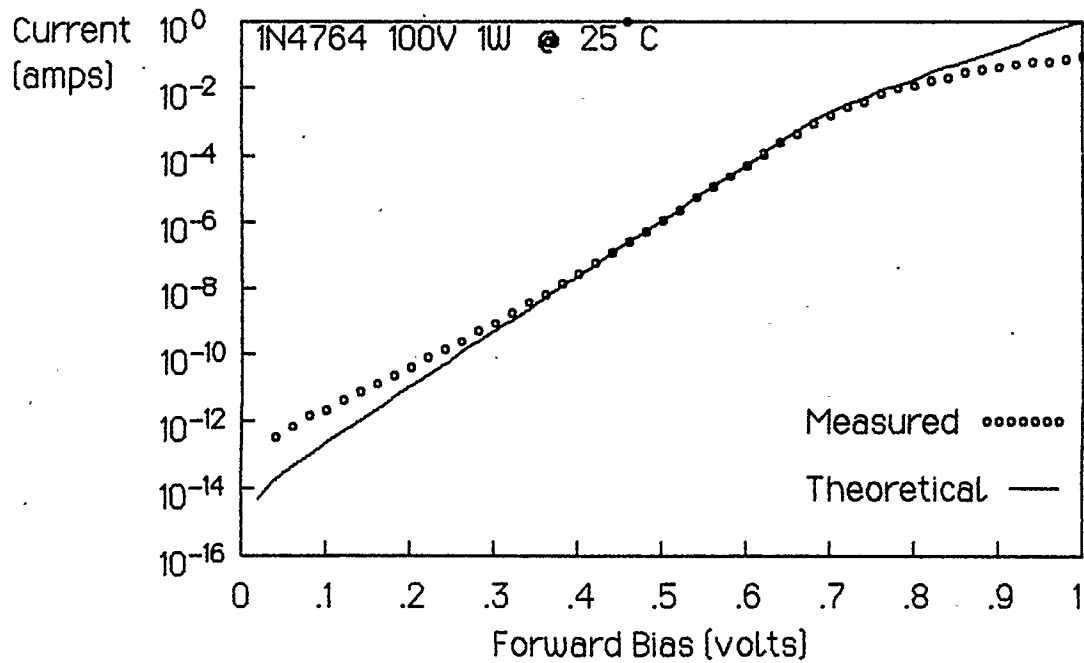


**Figure 6.2** A Comparison of the Measured Currents and the Improved Diode Equation With Zero Series Resistance.

To account for the series resistance, it is necessary to replace  $V$  with  $V_a - R_s I_p$ . This makes the Improved diode equation non-explicit in  $I_p$ , but an iterative solution can be avoided by using the measured values for  $I$  in the expression  $V_a - R_s I_p$ . The result of this is depicted in Figure 6.3. The value of the series resistance is selected by trial and error to cause the theoretical and measured curves to match in the high current region. That value is

$$R = 1.4\Omega \text{ at } 25^\circ \text{C.}$$

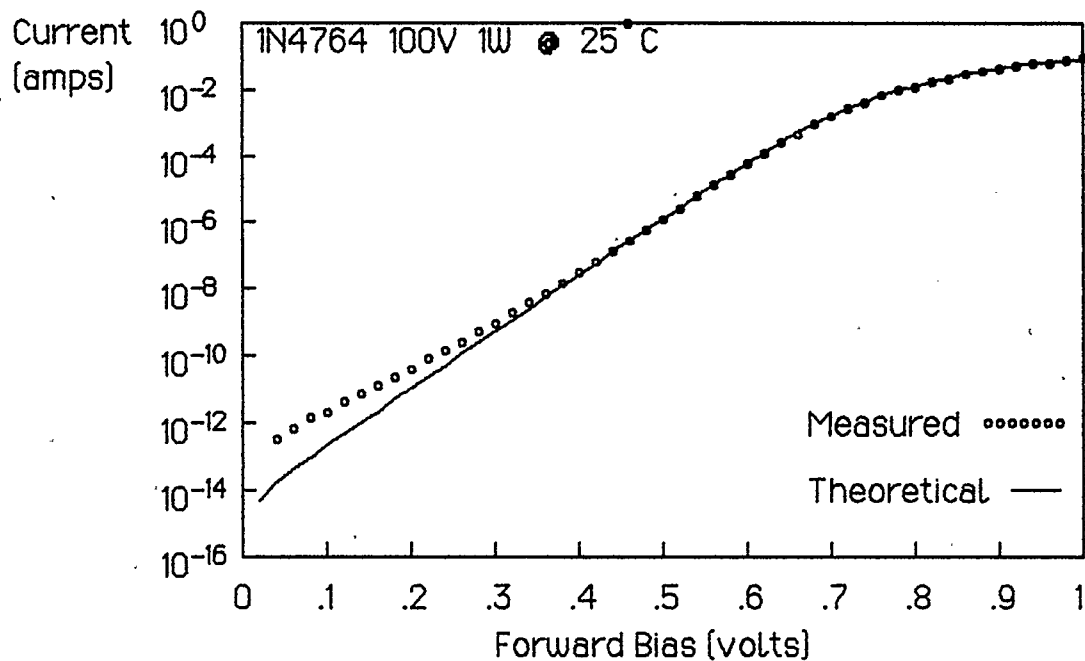


**Figure 6.3** A Comparison of the Measured Currents and Those Generated by the Improved Diode Equation With the Series Resistance Accounted for.

## 6.2 The Temperature Dependence of $I_h$ and $I_s$

The intrinsic carrier concentration has a much greater influence on the temperature dependence of the intercepts than do any of the other parameters.  $n_i$  is given by [1 pp18]

$$n_i^2 = N_c N_v e^{-E_g/kT} = 0.94 \times 10^{32} T^3 e^{-E_g/kT}, \quad (6.1)$$

where the temperature dependence of the band gap energy has been determined to be [1 pp13]

$$E_g = 1.17 - \frac{4.73 \times 10^{-4}}{T + 636}. \quad (6.2)$$

The hole mobility,  $\mu_p$ , is accepted as being proportional to  $T^{-3/2}$  [1 pp32] which, according to the Einstein relation, makes  $D_p$  proportional to  $T^{-1/2}$ . The temperature dependence assigned for now to the lifetime is  $T^{3/2}$ , because the mean time between collisions involving carriers and impurity traps is accepted as being proportional to  $T^{3/2}$  [1 pp33]; experimental support for this follows. The high injection factor,  $\sigma$ , contains two terms:  $\xi$  and  $e^{-x}$ .  $\xi$  contains only ratios of like parameters, so it is independent of temperature. Calculated values of  $e^{-x}$  using  $W_b = L$  at 25°C show that this term varies by less than 20% when the temperature changes from 25°C to 250°C. According to the definition for  $\xi$  its temperature dependence is less than that of  $L_p$  (which is proportional to  $T^{1/2}$ ) and becomes completely temperature independent for appreciable  $\lambda$ . Therefore,

$$I_h \propto \frac{n_i}{T} \quad \text{and} \quad I_s \propto \frac{n_i^2}{T}. \quad (6.3)$$

Using the measured 25°C intercepts for the 1N4764 diode in Equations (6.3) gives

$$I_h = \frac{6.4 \times 10^{-17}}{T} n_i \quad \text{and} \quad I_s = \frac{5.8 \times 10^{-33}}{T} n_i^2.$$

Substitution of these into the low (ideal) and high injection equations,

$$I_p = I_s [e^{qV/kT} - 1] \quad \text{and} \quad I_p = I_h e^{qV/2kT},$$

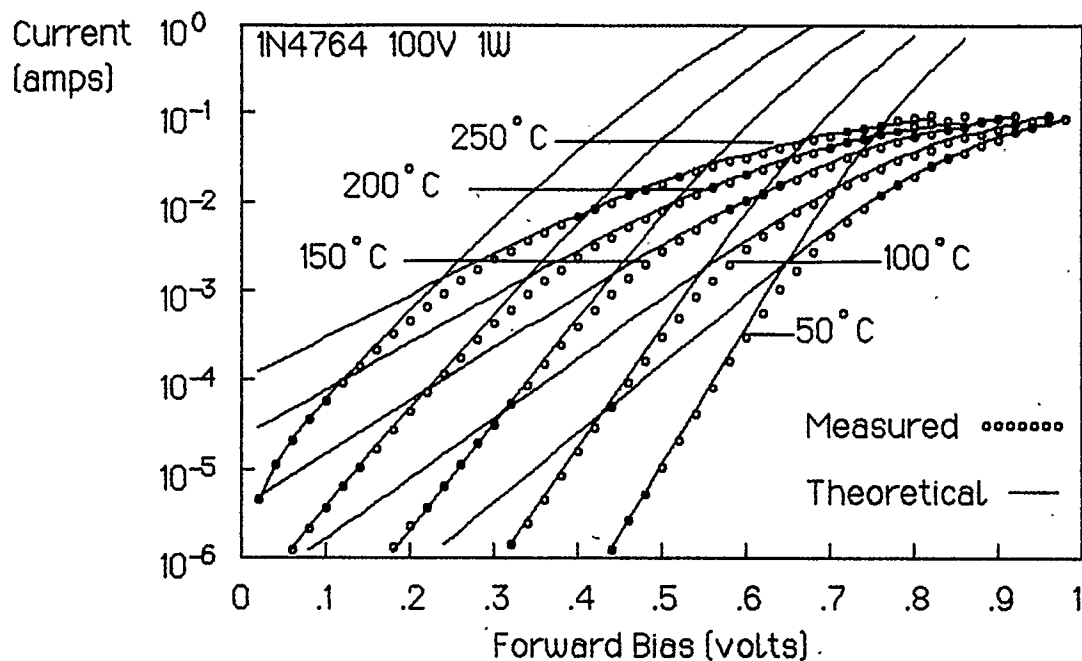


**Figure 6.4** A Comparison of the Measured Currents and Those Generated by the Low (Ideal) and High Injection Equations.

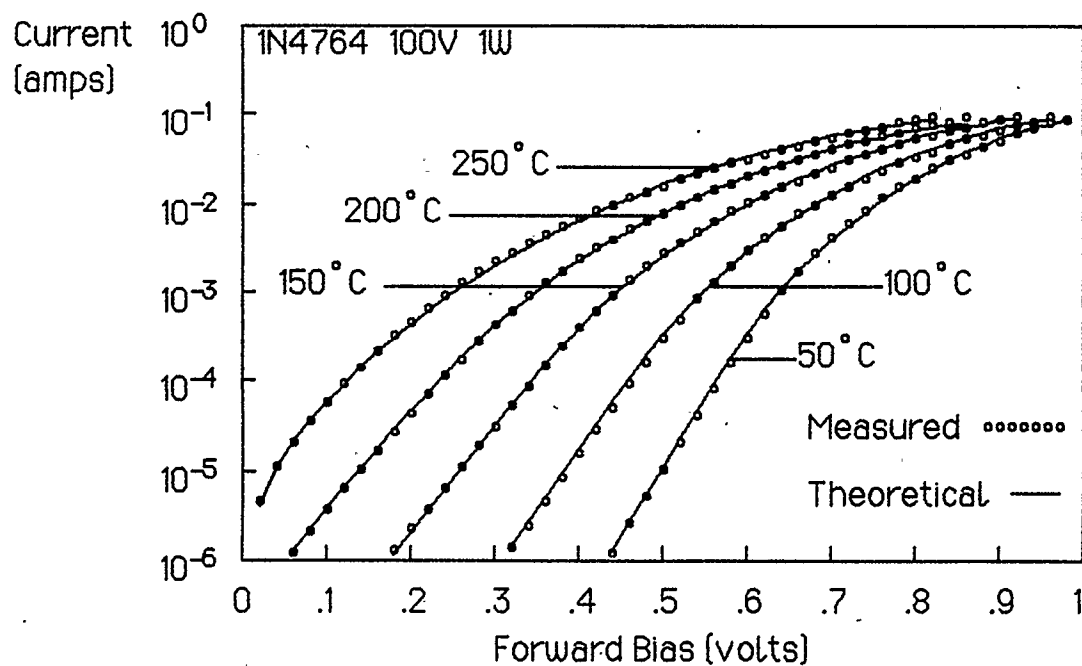


**Figure 6.5** A Comparison of the Measured Currents and Those Generated by the Improved Diode Equation.

results in the theoretical predictions of Figure 6.4. The same expressions for  $I_h$  and  $I_s$  are used in the improved diode equation, Equation (3.40), to generate the theoretical characteristics of Figure 6.5. In both cases series resistance has been accommodated.

The data of Figure 6.6 confirm that the high injection lifetime is nearly proportional to  $T^{3/2}$ . The correlation coefficient is .998, and the linear regression relation is

$$t_d (\mu\text{sec}) = .15 + .000028 T^{3/2}.$$

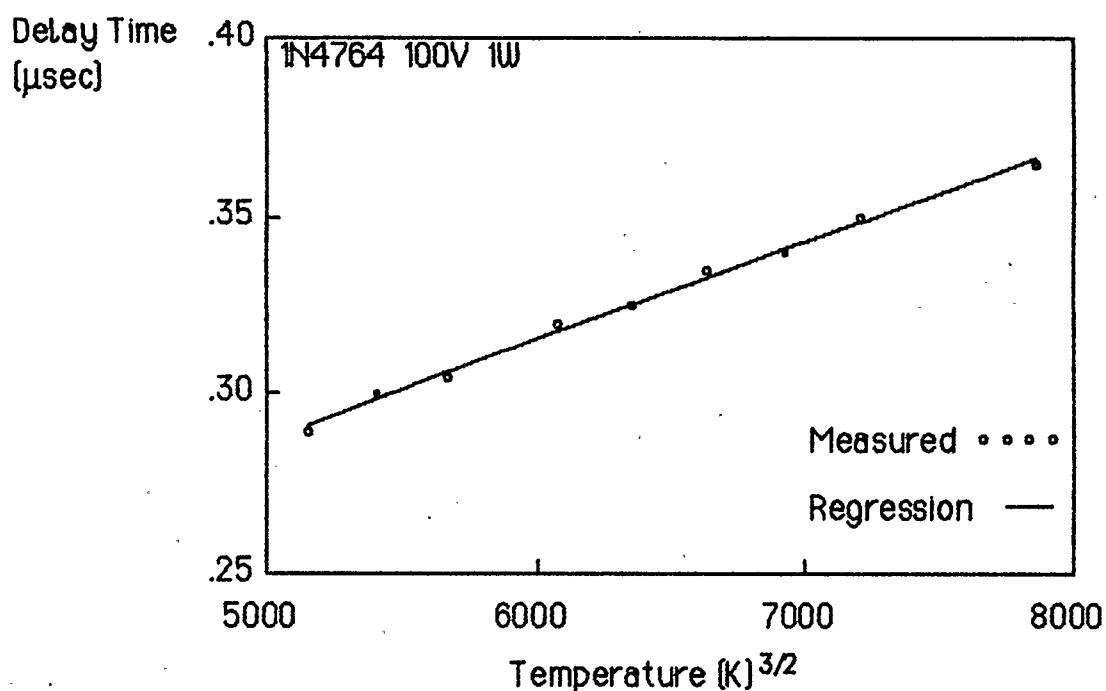


**Figure 6.6** High Injection Charge Storage Delay Time vs  $T^{3/2}$ .

### 6.3 Calculation of $I_h$ and $I_s$ at Room Temperature

Numerical solutions would be required to handle actual doping profiles; otherwise, it is only possible to see if the values of the parameters needed to equate the calculated and measured intercepts are reasonable numbers. Estimates are required for the area, the lifetimes

and the doping. The same 1N4764 diode is considered. The geometry of this device without its metallization is illustrated in Figure 6.7. The square 20 mil wide die has a 12.5 mil wide diffusion window, and the wafer is 8 mils thick, where 1 mil = 1/1000 in [10]. Therefore,

$$A \approx .0010 \text{ cm}^2 \quad \text{and} \quad W_n \approx .02 \text{ cm}.$$

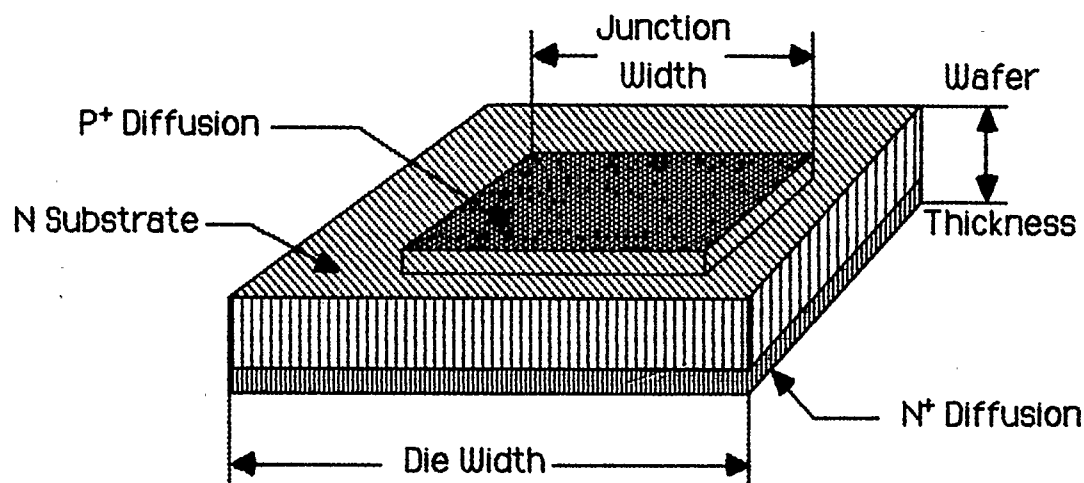


**Figure 6.7** Physical Geometry of the Tested Diodes.

The junction area can also be deduced from the measured small signal junction capacitance for various values of reverse bias. The linear regression relation for the measured data of Figure 6.7 is

$$\frac{1}{C_j^3} = .18 \times 10^{33} + .47 \times 10^{33} |V|,$$

and the correlation coefficient is .9999. This suggests that the junction is linearly graded. The expected doping gradient for a breakdown voltage of 100volts is [1 pp104]

$$a = .9 \times 10^{20} \text{ cm}^{-4}.$$

This value and the actual slope of the regression line can be used with Equation (5.37) to predict the area, and it is

$$A = .0012 \text{ cm}^2.$$

This is about the same as the area of the P<sup>+</sup> diffusion window plus the area due to the actual lateral diffusion of about 10 microns [10].

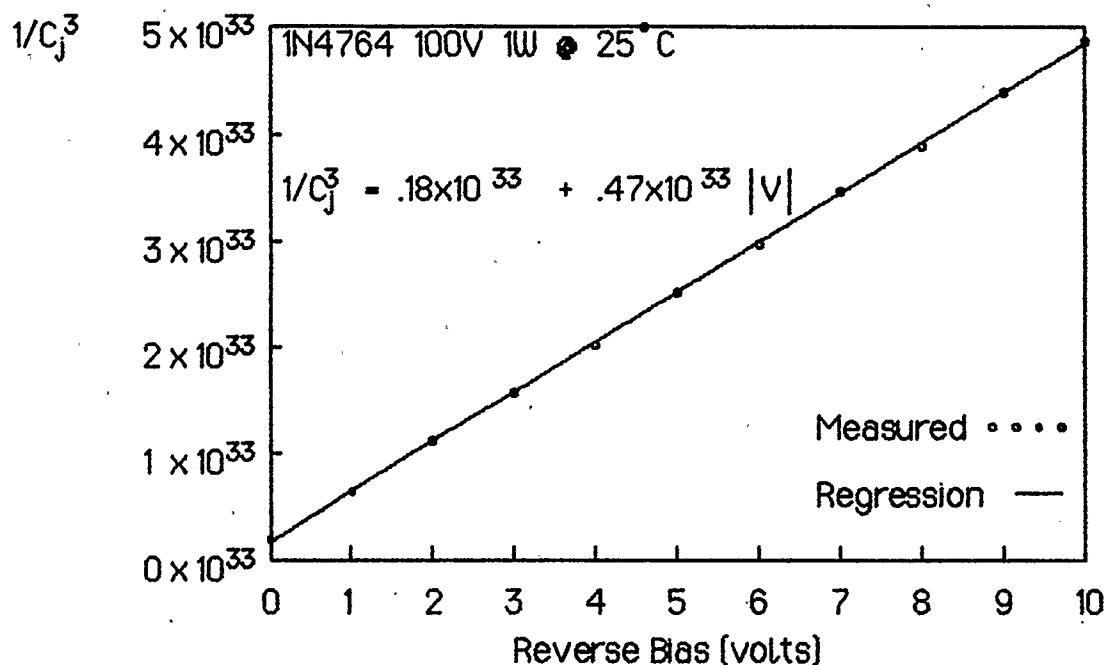


**Figure 6.8** The Measured Small Signal Junction Capacitance

In Figure 6.8, the measured charge storage delay times for various currents are plotted on the same graph as the measured forward characteristic, along with the theoretical low injection diode equation, and the theoretical high injection diode equation in order to show the relationship between delay time and injection level. The high injection lifetime can be obtained from the high injection delay time using Equation (4.22). For the measured  $t_{dH}$  of  $.29 \times 10^{-6}$  sec and the actual  $\gamma$  of 1.1,

$$\tau = 1.6 \times 10^{-6} \text{ sec at } 25^\circ \text{C.}$$

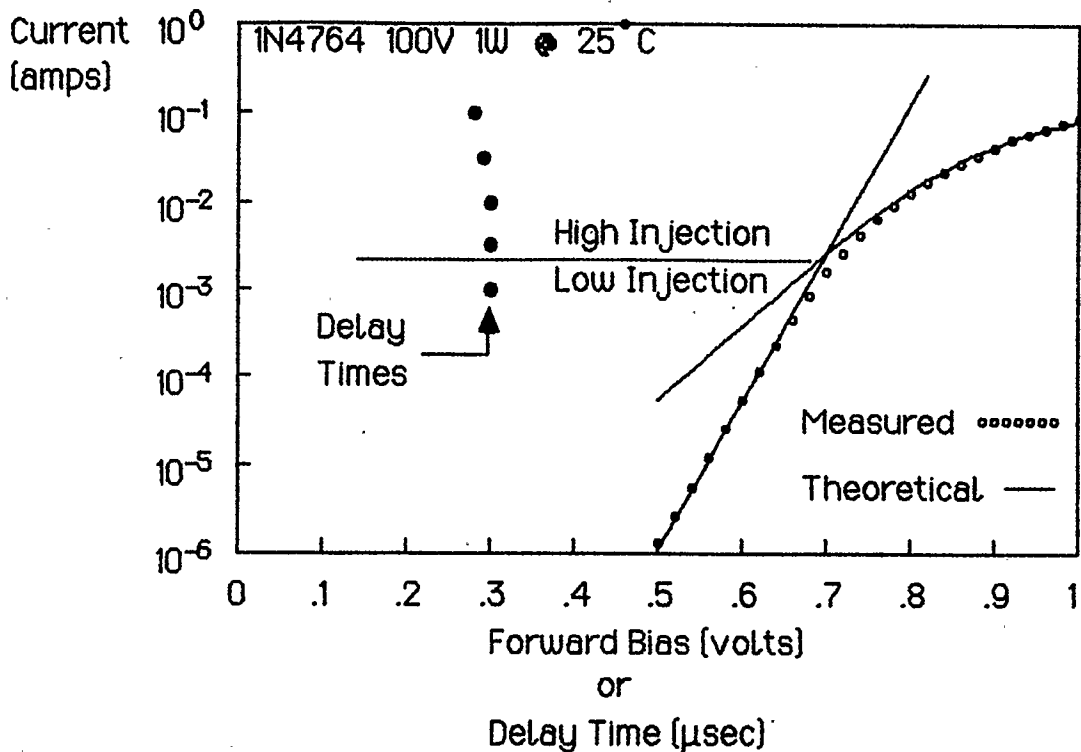


**Figure 6.9** The Relationship Between Delay Time and Injection Level.

According to the measured lifetime, the diffusion length is about 1/4 of the length of the charge-neutral N region. This adequately satisfies the infinitely long diode criteria that requires this fraction to be less than about 1/2.

The manufacturer specifies the substrate resistivity to be between 0.171 and 0.230  $\Omega$  cm [10]. This translates to a background doping,  $N_b$ , of  $2 \times 10^{16}$  to  $4 \times 10^{16}$   $\text{cm}^{-3}$ .

According to Equation (4.23)  $I_h$  can be written as

$$I_h = e^{-x} \sqrt{2 \left[ 1 + \frac{D_p}{D_n} \right]} A q \frac{\sqrt{D_p}}{\sqrt{t_{dH}} \frac{2 \{1 + \gamma\}}{\sqrt{\pi}}} n_i \quad (6.4)$$

But  $D_p/D_n \approx 1/3$ , and  $\gamma = 1.1$  was the ratio used to measure  $t_{dH}$ , hence

$$I_h = e^{-x} 0.69 A q \frac{\sqrt{D_p}}{\sqrt{t_{dH}}} n_i \quad (6.5)$$

Using  $\mu_p = 320$  for  $N_b = 3 \times 10^{16}$  [[4 pp60]],  $A = .0012 \text{ cm}^2$

$$t_{dH} = .29 \times 10^{-6} \text{ sec}, \quad n_i = 1.45 \times 10^{10} \text{ cm}^{-3}$$

gives

$$I_h = e^{-x} 10.2 \times 10^{-9}$$

compared to the measured value of  $3.1 \times 10^{-9}$  obtained from the intercept of the  $(q/2kT)$  Log e tangent line on the actual  $25^\circ \text{C}$  characteristic. If the measured and calculated values for  $I_h$  are to be equal then

$$x = 1.2,$$

and using Equation (3.44) with  $w_n$  replaced by  $w_b$  gives

$$w_b = 1.4 L.$$

But

$$L = \sqrt{D \tau} = .0045 \text{ cm} = \frac{w_n}{4.4},$$

therefore

$$w_b = \frac{w_n}{3}.$$

$I_s$  is calculated using Equation (5.26),

$$I_s = A q \frac{\sqrt{D_p}}{\sqrt{t_d}} \frac{n_i^2}{2(1+\gamma) N_{do} \sqrt{\pi}}, \quad (5.26)$$

which for  $\gamma = 1.1$  translates to

$$I_s = 0.42 A q \frac{\sqrt{D_p} n_i^2}{\sqrt{t_{dl}} N_{db}} \quad (6.6)$$

The measured value of the low injection delay time is

$$t_{dl} = .30 \times 10^{-6} \text{ sec.}$$

The value of  $N_{db}$  needed to make the calculated value of  $I_s$  equal to the measured value obtained from the intercept of the  $(q/kT)$  Log  $e$  tangent line on the actual  $25^\circ \text{C}$  characteristic is

$$N_{db} = 2.3 \times 10^{16} \text{ cm}^{-3}.$$

This compares favorably with the manufacturer's specified background doping range of  $2 \times 10^{16}$  to  $4 \times 10^{16} \text{ cm}^{-3}$ .

Table 6.1 shows a comparison of measured and calculated diode parameters for four different zener diodes of the same family and manufacturer. In each case the known area of the  $P^+$  diffusion window is somewhat smaller than the junction area obtained from the junction capacitance measurements; this is expected, since the difference is due to lateral diffusion. For each diode the value for  $N_{db}$  needed to equate the calculated low injection intercept with the measured value (obtained as shown in Figure 6.1) is either within the range of or just below the background doping specified by the manufacturer; according to Figure 5.2, this is the expected result. The  $W_b/W_n$  ratios needed to equate the calculated high injection intercepts with the measured values (obtained as shown in Figure 6.1) are in the range of 1/5 to 1/3; according to Figure 5.3, these are not unreasonable fractions.

	1N5253 <u>25V 0.5W</u>	1N5360 <u>25v 5W</u>	1N5369 <u>51V 5W</u>	1N4764 <u>100V 1W</u>
$\mu_p$ [[4 pp60]]	135	135	270	320
$a$ $\text{cm}^{-4}$ [[1 pp104]]	$3 \times 10^{21}$	$3 \times 10^{21}$	$4.7 \times 10^{20}$	$9 \times 10^{19}$
Area $\text{cm}^2$ of $P^+$ window	.0010	.014	.014	.0010
Area $\text{cm}^2$ from $C_j$	.0011	.015	.015	.0012
Measured $t_{dL}$ $\mu\text{sec}$	.28	.28	.21	.30
Measured $t_{dH}$ $\mu\text{sec}$	.27	.27	.21	.29
$\tau$ $\mu\text{sec}$ from meas'd. $t_{dH}$	1.5	1.5	1.2	1.6
Measured $I_s$ amps	$3.7 \times 10^{-16}$	$6.5 \times 10^{-15}$	$1.8 \times 10^{-14}$	$4.1 \times 10^{-15}$
Measured $I_h$ amps	$2.4 \times 10^{-9}$	$2.4 \times 10^{-8}$	$3.9 \times 10^{-8}$	$3.1 \times 10^{-9}$
Spec'd. $N_b$ $\text{cm}^{-3}$ [[10]]	$2 \rightarrow 4 \times 10^{17}$	$2 \rightarrow 4 \times 10^{17}$	$5 \rightarrow 8 \times 10^{16}$	$2 \rightarrow 4 \times 10^{16}$
Calculated $N_{b0}$ $\text{cm}^{-3}$	$1.7 \times 10^{17}$	$1.2 \times 10^{17}$	$7.0 \times 10^{16}$	$2.3 \times 10^{16}$
Calculated $W_b/W_n$	1/5	1/4	1/4	1/3
Calc'd. equilibrium $W_0$	$.26 \times 10^{-4}$	$.26 \times 10^{-4}$	$.47 \times 10^{-4}$	$.80 \times 10^{-4}$
Calc'd. equilibrium $\psi_{bio}$	.76	.76	.70	.64
Meas'd. $\psi_{bio}$ from $C_{jo}$	.65	.62	.73	.44

**Table 6.1** Summary of 25° C Diode Parameters.

The equilibrium depletion region widths tabulated in Table 6.1 are calculated using Equation (5.36) with  $V = 0$ . Three of the four values of the equilibrium built in potential,  $\psi_{bi0}$ , calculated using Equation (5.34) with  $W = W_0$  are somewhat larger than those determined from the  $1/C_J^3$  vs  $V$  plots using Equation (5.39). This small discrepancy is of no consequence to this work, and it is not examined further

#### 6.4 Series Resistance

Theory predicts that good ohmic contacts are dominated by the tunneling mechanism and can be modelled by small temperature independent resistors [11] [12]. Most of the measured values of series resistance tabulated in Table 6.2 are independent of temperature. The process of selecting values of series resistance that produce a match of the improved diode equation or the high injection equation to the measured characteristics at large currents turns out to be a method for measuring that series resistance.

	<u>1N5253</u> <u>25V 0.5W</u>	<u>1N5360</u> <u>25v 5W</u>	<u>1N5369</u> <u>51V 5W</u>	<u>1N4764</u> <u>100V 1W</u>
$R_s(50^\circ\text{C}) \Omega$	0.87	0.47	0.60	1.4
$R_s(100^\circ\text{C}) \Omega$	1.1	0.63	0.87	1.7
$R_s(150^\circ\text{C}) \Omega$	1.1	0.63	0.87	1.9
$R_s(200^\circ\text{C}) \Omega$	1.1	0.63	0.87	2.1
$R_s(250^\circ\text{C}) \Omega$	1.1	0.60	0.87	2.2

**Table 6.2** Measured Series Resistance at Elevated Temperatures

## 6.5 Diode Parameter Measurement Considerations

Figures 6.10, 6.11 and 6.12 compare the features of two diodes that are the same in all respects except for their areas. They are both 25V zener diodes, but the 1N5253 is a 0.5W device, and the 1N5360 is a 5W device. These are the same members of the group of four diodes whose parameters were tabulated in Table 6.1. The two parts were not fabricated on the same date.

In Figure 6.10, the measured charge storage delay times for various currents are plotted on the same graph as the measured forward characteristic, along with the theoretical low injection diode equation, and the theoretical high injection diode equation in order to show the relationship between delay time and injection level. This Figure demonstrates that these more heavily doped diodes do not exhibit much high injection current at room temperature in the current range shown. The slope is just beginning to change from  $q/kT \text{ Log } e$  to  $q/2kT \text{ Log } e$  at the top of the characteristic. It is necessary to show enough of the high injection region to facilitate accurate construction of the  $q/2kT \text{ Log } e$  tangent line. To avoid the use of higher current and the possible interference of self heating, it is preferable to measure the diode characteristic at an elevated temperature where high injection is more prevalent. Alternately, even with little high injection exposed, a trial and error match of the improved diode equation with the measured data in a computer that plots both gives good estimates for  $I_h$ ,  $I_s$ , and  $R_s$ .

The measured delay times for the 0.5W diode of Figure 6.10 do not change significantly when the current increases from low to high injection. The high injection lifetime is given by  $\tau = \tau_p + \tau_n$ , and if  $\tau_n \ll \tau_p$  then there would be no noticeable change in the low and high injection delay times. Also, according to Equation (5.23),  $\tau_p$  could be equal to  $\tau/2$  even when  $t_{dL} = t_{dH}$ , provided that  $\zeta = 2^{-1/2}$ . Equation (5.10) predicts that  $\zeta$  will take on this value if  $\lambda \approx L_p$ , and according to Figure 5.3, it is possible for the carrier diffusion length to be similar to the

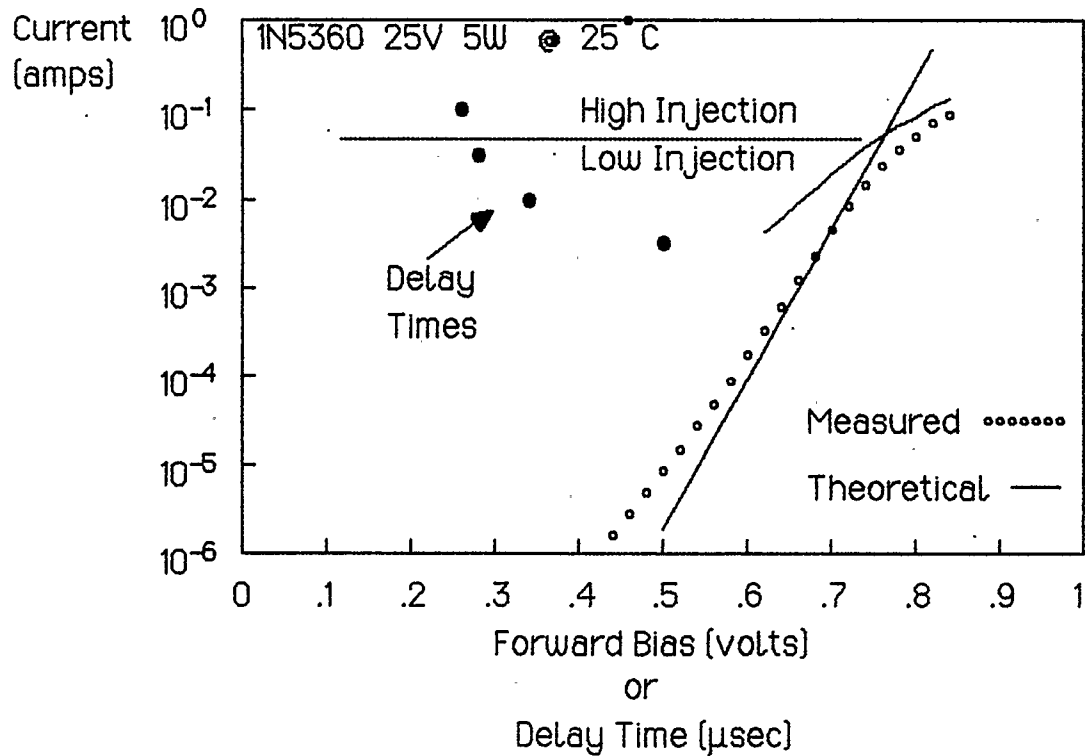
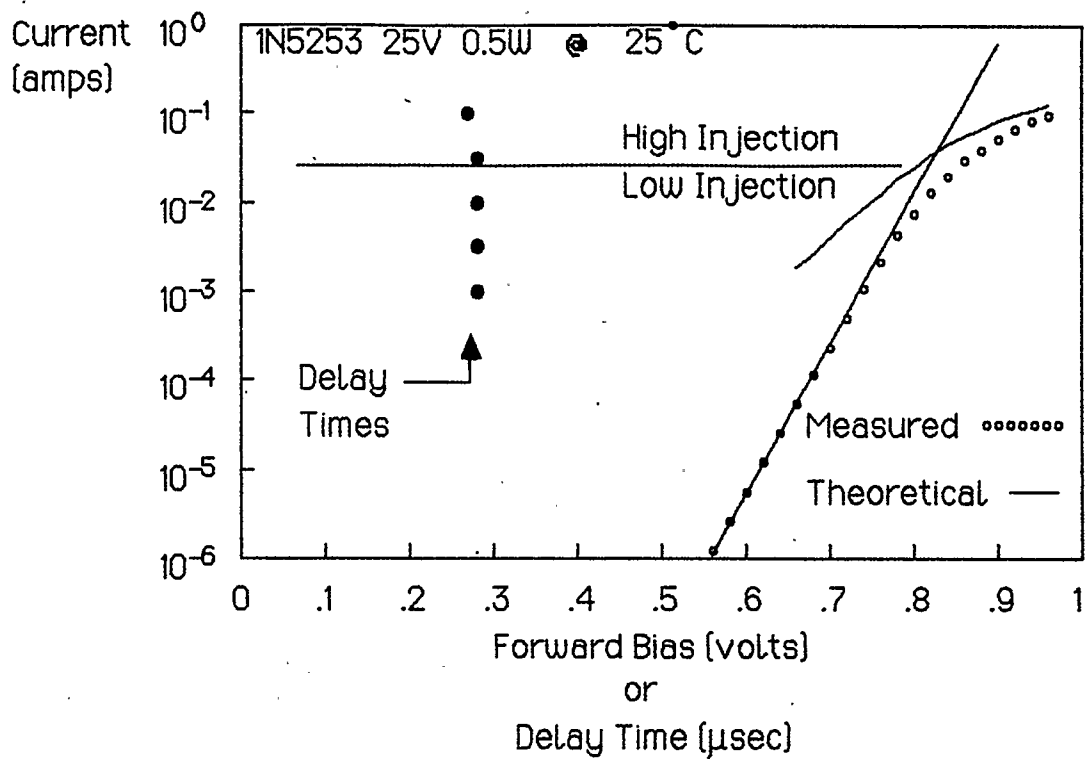


**Figure 6.10** Measured Delay Times for a 0.5W and a 5W Zener Diode.

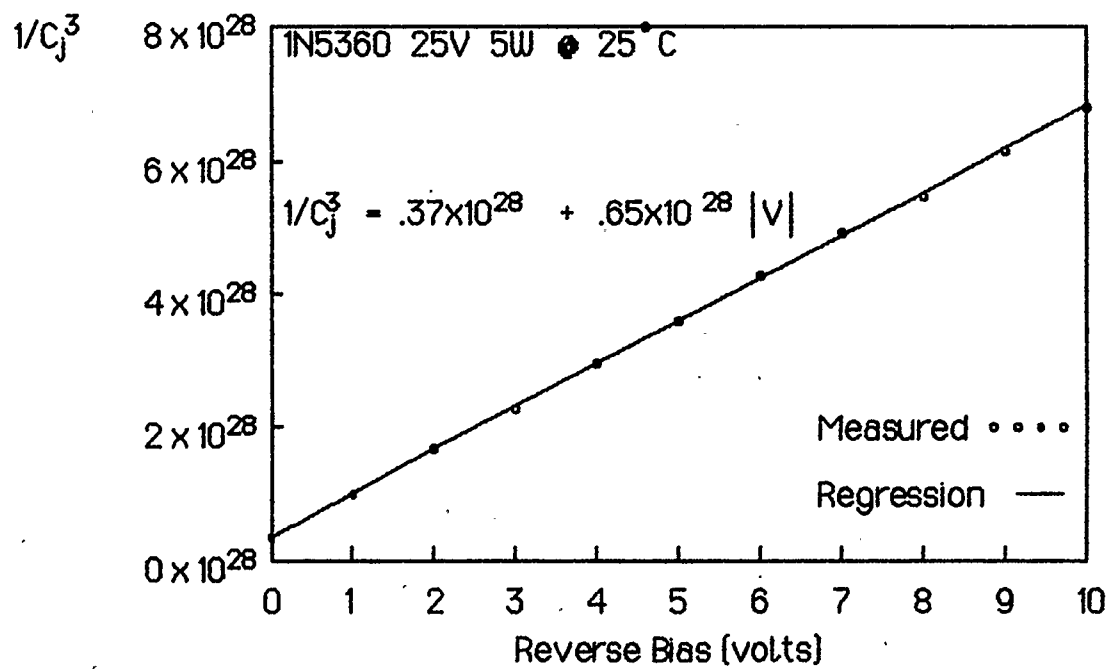
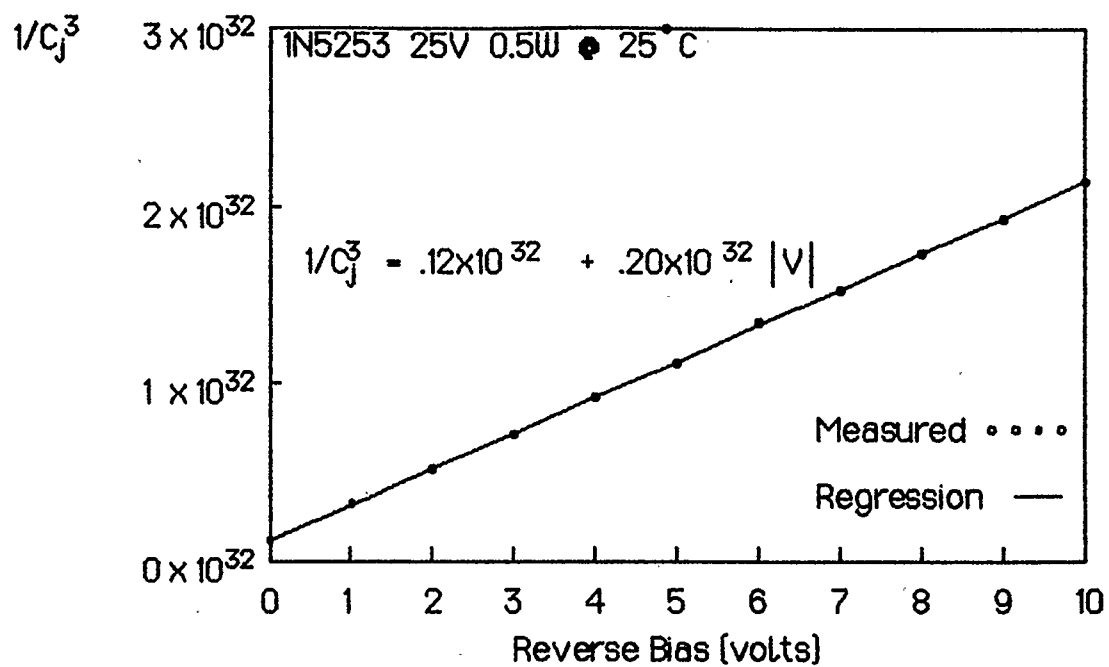


**Figure 6.11** Junction Capacitance Characteristics for Reverse Biased 0.5W and 5W Zener Diodes.

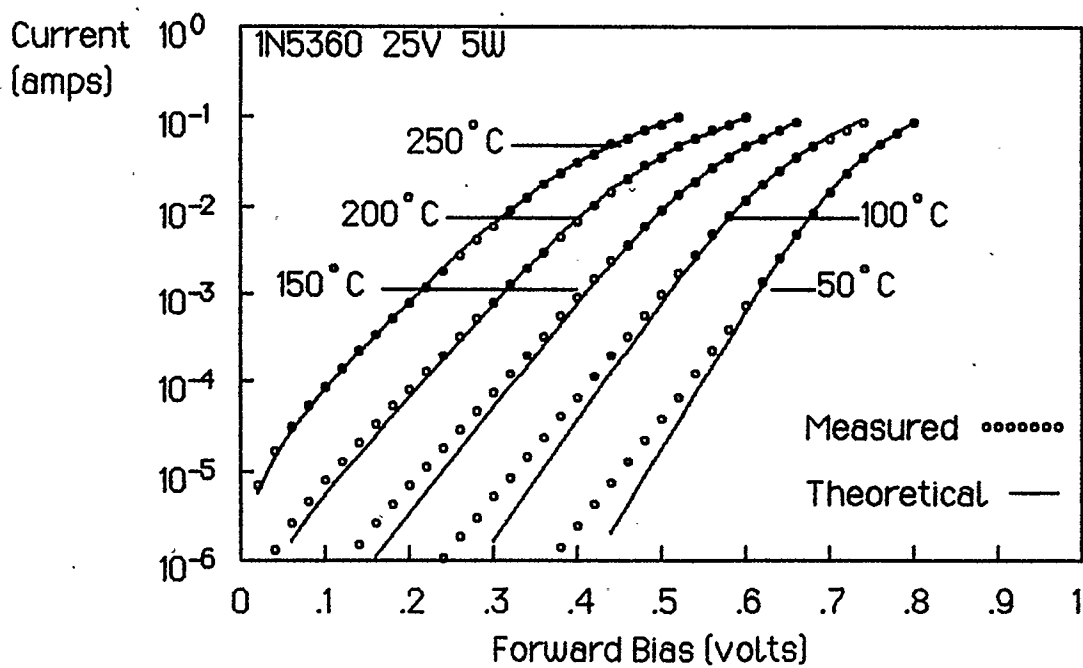
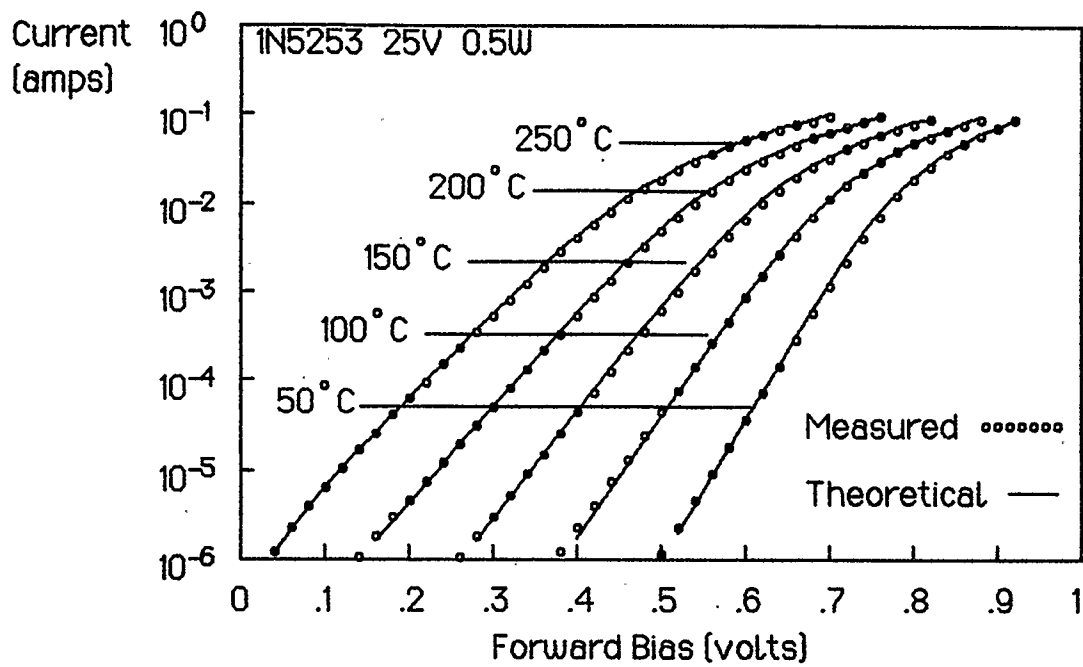


**Figure 6.12** Measured Currents and Theoretical Currents Generated by the Improved Diode Equation for 0.5W, and 5W Zener Diodes.

doping diffusion length. Consideration must be given to the effects of non-uniform doping when calculating  $\tau_p$  from the measured  $t_d$ .

Since the relationship between delay time and lifetime is not area dependent, it is easy to believe that the delay times for the 0.5W and the 5W parts should be the same. However, Figure 6.10 shows that the measured delay times for the 5W diode increase significantly as the current falls, while the 0.5W diode delay times remain constant. When the forward current of a  $p^+n$  diode is suddenly reversed, the reverse current removes the charge stored in the bulk regions, but it must also restore the depletion region space charge. It will be shown that the time required to restore the space charge is insignificant only if the diode area is small.

An estimate of the equilibrium depletion region space charge can be ascertained from the junction area, the equilibrium depletion region width and the doping gradient. These were tabulated in Table 6.1. The charge stored on each side of the depletion region capacitance at equilibrium must be

$$Q_0 = \frac{1}{2} A q a \left[ \frac{W_0}{2} \right]^2 \quad (6.7)$$

Substituting into this the parameters for the two diodes gives

$$Q_0 = 4.5 \times 10^{-11} \text{ coul for the 0.5W diode}$$

and

$$Q_0 = 6.1 \times 10^{-10} \text{ coul for the 5W diode.}$$

As an example, consider a forward current of 3 mA. At this level of bias almost all of the depletion region space charge has been removed from both diodes. The reverse current is  $\gamma \times 3 \text{ mA} = 3.3 \text{ mA}$ . At this current the time required to restore the space charge is

$$t = Q_0 / I_{Rev} \approx 0.01 \mu\text{sec for the 0.5W diode}$$

and

$$t = Q/I_{Rev} \approx 0.18 \mu\text{sec for the 5W diode.}$$

Note that these times increase for smaller current. Figure 6.10 shows that the additional time to restore the space charge for the 0.5W diode is insignificant compared to the measured constant delay time. However, the space charge recovery time for the 5W device is a substantial fraction of the measured delay time, and it seems to be responsible for the increasing delay time with decreasing current. Hence, the space charge recovery time component of the delay time must be considered when lifetime calculations are executed for large diodes.

## 7 THE LOW CURRENT DOMAIN

The diode equations presented thus far model only the charge-neutral region processes and not those of the depletion region. Depletion region RG current,  $I_{RG}$ , dominates the very low current portion of the forward characteristic and also the reverse characteristic as shown in Figure 7.1. The improved diode equation alone accurately models reverse current only at elevated temperatures where  $I_{RG}$  is inconsequential. A good mathematical portrayal of both the low and high current domains would be given by the sum of the current predicted by the improved diode equation,  $I_p$ , and the current predicted by a depletion region RG equation,  $I_{RG}$ . Two depletion region RG models will be compared with measured data.

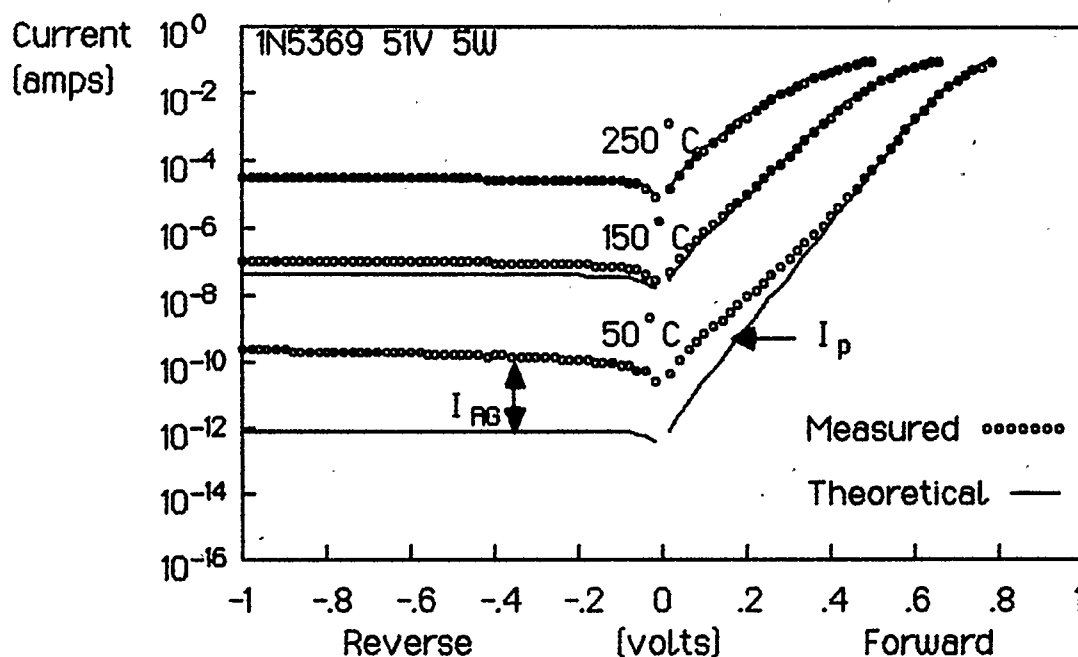


**Figure 7.1** A Comparison of the Measured Forward and Reverse Characteristics With Those Generated by the Improved Diode Equation Showing the Influence of Depletion Region RG at Low Current and at Moderate Temperatures.

## 7.1 The Standard Depletion Region RG Equation

The standard textbook version of the depletion region RG equation is derived as follows [1 pp94]. Equation (2.33),

$$np = n_i^2 e^{qV/kT}, \quad [2.33]$$

is applicable everywhere in the depletion region. Substitution of this equation into the expression for the net recombination rate given by Equation (2.22) gives

$$U = \frac{n_i^2 [e^{qV/kT} - 1]}{\tau_o [p + n + 2n_i]}, \quad [7.1]$$

where equal hole and electron capture cross sections have been assumed; that is,  $\tau_p \approx \tau_n \approx \tau_o$ . Also, the energy level of the recombination centers or traps is assumed to be located at the intrinsic energy level. According to Equation (2.33) the product of  $p$  times  $n$  is a constant, so

$$\frac{d}{dx} (pn) = p \frac{dn}{dx} + n \frac{dp}{dx} = 0. \quad [7.2]$$

$U$  reaches a maximum when the denominator of Equation (7.1) is a minimum, that is when

$$d(p + n) = 0. \quad [7.3]$$

The condition that satisfies Equations (7.2) and (7.3) and maximizes  $U$  is

$$p = n.$$

Combining this with Equations (2.33) and (7.1) gives

$$U_{\max} = \frac{n_i^2 [e^{qV/kT} - 1]}{2 \tau_0 n_i [e^{qV/2kT} + 1]} \approx \frac{e^{qV/2kT}}{2 \tau_0} \quad \text{for } V > 3 kT/q, \quad (7.4)$$

that is, for forward bias. Substitution of this into the hole continuity equation, Equation (2.27) and integrating over the depletion region yields

$$J_{pRG} = qW \frac{n_i e^{qV/2kT}}{2 \tau_0}, \quad (7.5)$$

where  $J_{pRG}$  is the forward depletion region RG hole current density. Similarly, Equation (7.4) could be substituted into the electron continuity equation, Equation (2.28) to yield the same result. The change in hole current across the depletion region must equal the change in electron current because equal numbers of holes and electrons recombine. The forward current density distributions for a  $p^+n$  diode are illustrated in Figure 7.2; it is apparent that the total current density is given by the change in hole current density across the depletion region plus the charge neutral region hole current density at the depletion region edge.

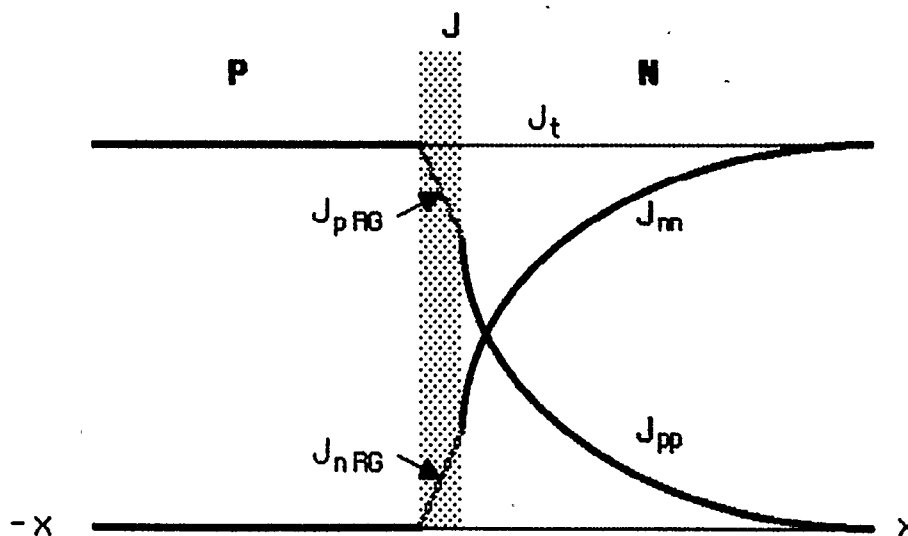


**Figure 7.2** Depletion and Bulk Region Currents for a  $p^+n$  Diode.

Multiplying Equation (7.5) by the area gives the change in forward current across the depletion region, that is,

$$I_{RG\ Fwd} = A q \frac{W}{2 \tau_0} n_i e^{qV/2kT} = A q \frac{W}{\tau} n_i e^{qV/2kT} \quad (7.6)$$

To test the ability of Equation (7.6) to predict the forward  $I_{RG}$ , it is necessary to supply that equation with the area, the depletion region width and the high injection lifetime of the diode used for the test. A diode that exhibits appreciable  $I_{RG}$  at moderate temperatures is the 1N5369. It is a 51V 5W part, it is one of the four diodes listed in Table 6.1, and its forward and reverse characteristics were plotted in Figure 7.1. The measured 1N5369 25°C junction capacitance characteristic of Figure 7.3 is indicative of a linearly graded junction. The measured 25°C delay times for this diode are plotted in Figure 7.4.

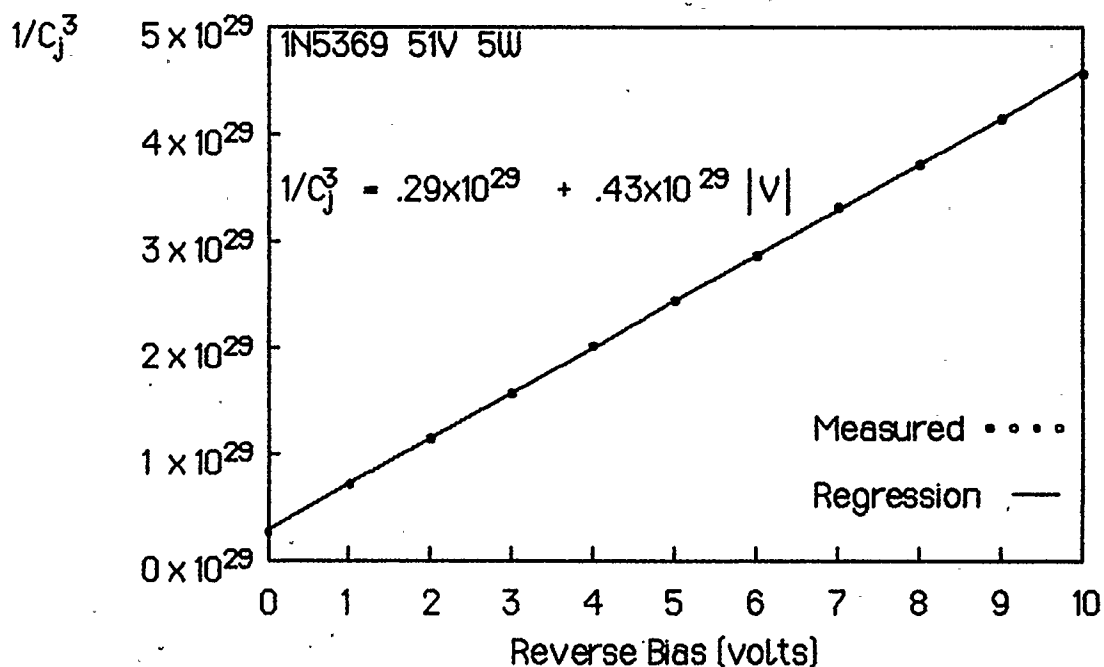


**Figure 7.3** Junction Capacitance Characteristic for a Reverse Biased 51V 5W Zener Diode.

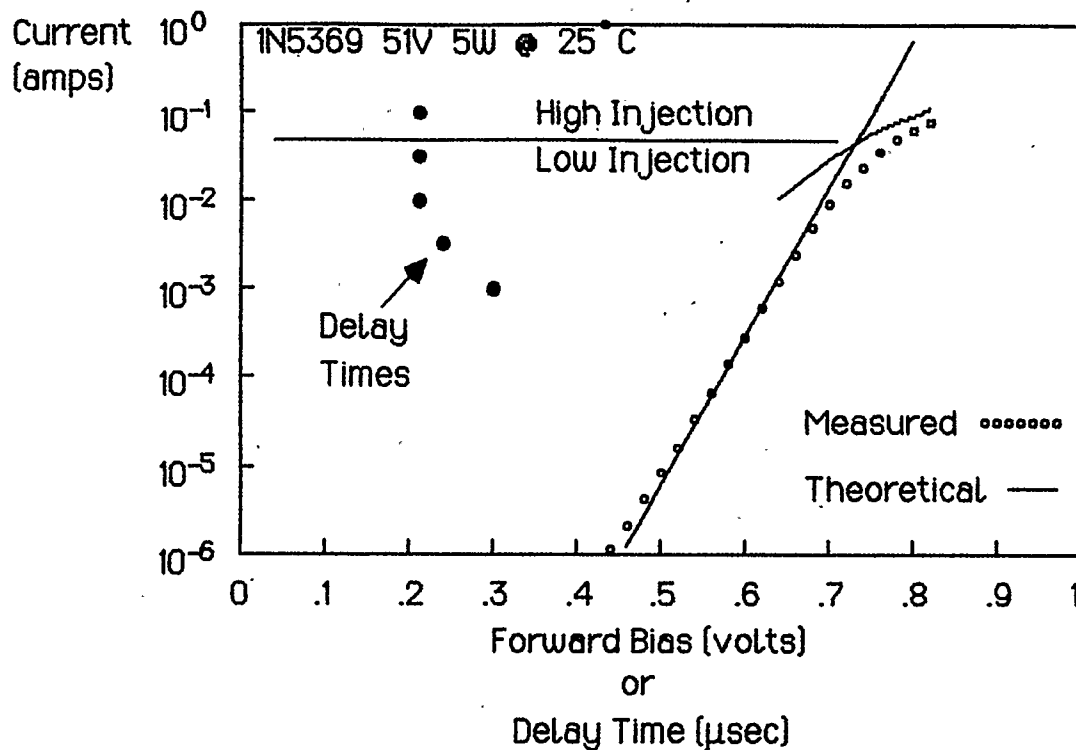


**Figure 7.4** The Relationship Between Charge Storage Delay Time and Injection Level for a 5V 5W Zener Diode.

All of the parameters needed to evaluate the  $I_{FG}$  equation for the 1N5369 diode are listed in Table 6.1, except that Equation (5.36) must be evaluated numerically to determine the depletion region width for each value of the applied voltage. Table 7.1 shows that  $W$  is a weak function of  $V$ .

$V$ (volts)	$W$ (cm)
-1.0	$.65 \times 10^{-4}$
-0.5	$.58 \times 10^{-4}$
0	$.47 \times 10^{-4}$
0.1	$.45 \times 10^{-4}$
0.2	$.42 \times 10^{-4}$
0.3	$.39 \times 10^{-4}$
0.4	$.34 \times 10^{-4}$

**Table 7.1** Depletion Region Width and Voltage for a 1N5369 Diode.

The theoretical depletion region RG current,  $I_{RG}$ , generated by Equation (7.6) and the theoretical charge neutral region current generated by the improved diode equation,  $I_p$ , are compared with the measured data for the 1N5369 diode in Figure 7.5. The prediction of Equation (7.6) is much too large at this temperature, and the slope of the measured forward characteristic in the low current region is larger than that predicted by Equation (7.6). This result is not unexpected, because the net recombination rate used in the derivation of Equation (7.6) was the maximum value of the recombination rate within the depletion region.

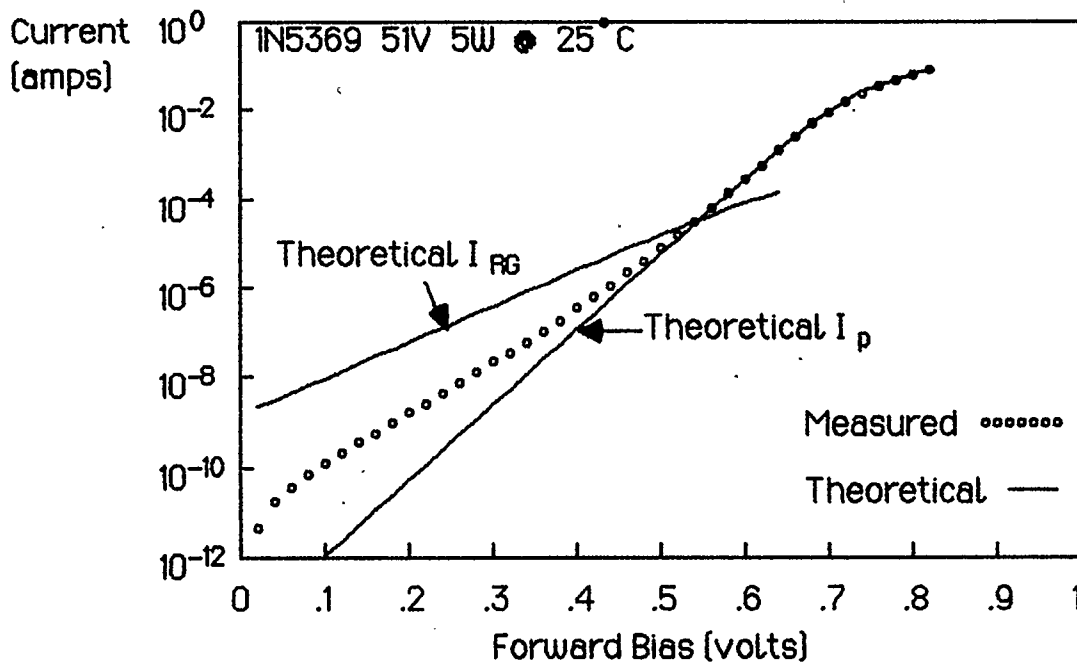


**Figure 7.5** A Comparison of the Theoretical Depletion Region RG Current, the Improved Diode Equation and the Measured Forward Characteristic of a 51V 5W Zener Diode.

In the reverse direction  $n$  and  $p$  are assumed to be much less than  $n_i$ , so the net recombination rate of Equation (2.22) becomes

$$U = -\frac{n_i}{2\tau_0 n_i \cosh\{v_t q/kT\}}, \quad (7.7)$$

where  $v_t$  is the potential corresponding to the trap energy level difference  $E_t - E_i$ . Inserting this expression into the continuity equation and integrating over the depletion region gives

$$I_{RG Rev} = -\frac{A q n_i W}{2 \tau_o \cosh \{v_t q/kT\}} \quad (7.8)$$

This can be forced to agree with the observed reverse current by the appropriate selection of  $v_t$ .

## 7.2 The Refined Depletion Region RG Equation

The net recombination rate can be written as

$$U = \frac{p n - n_i^2}{\tau_n \left[ p + n_i e^{q v_t / kT} \right] + \tau_p \left[ n + n_i e^{-q v_t / kT} \right]} \quad (7.9)$$

Substituting into this the quasi Fermi level expressions for  $p$  and  $n$  from Equations (2.30) and (2.31) and also the  $p n$  product from Equation (2.33) gives

$$U = \frac{n_i \left[ e^{qV/kT} - 1 \right]}{\left[ \tau_n e^{-q\psi/kT} + \tau_p e^{q\psi/kT} \right] + \left[ \tau_n e^{-q(\psi - \phi_p)/kT} + \tau_p e^{q(\psi - \phi_n)/kT} \right]} \quad (7.10)$$

Figure 7.6 shows that for a symmetrical linearly graded junction

$$\phi_p = \phi + \frac{V}{2} \quad \text{and} \quad \phi_n = \phi - \frac{V}{2} \quad (7.11)$$

Substituting Equation (7.10) into the continuity equation and integrating

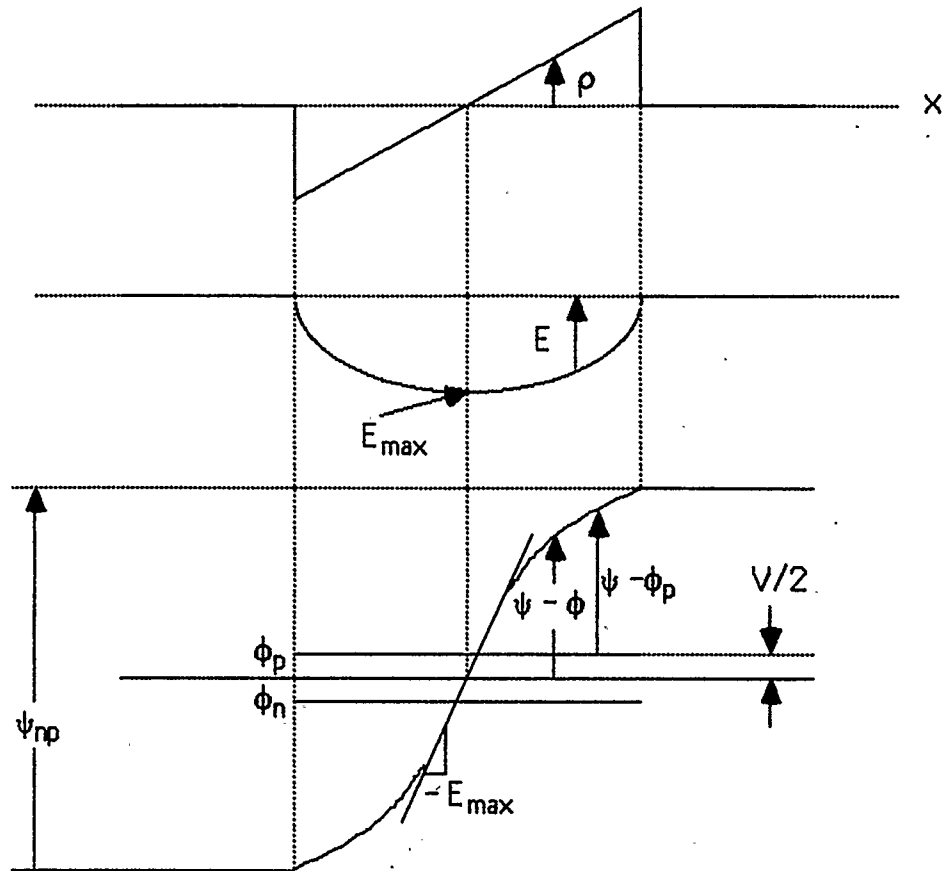


**Figure 7.6** The Space Charge, Electric Field and Potential Distribution for a Linearly Graded Junction.

over the depletion region gives the integral form of the refined depletion region RG equation for a linearly graded junction:

$$I_{RG} = \frac{A q n_i [e^{qV/kT} - 1]}{\tau_t} \int_{-w/2}^{w/2} \frac{dx}{1 + \frac{e^{qV/2kT}}{\tau_t} [\tau_n e^{-q(\psi - \phi)/kT} + \tau_p e^{q(\psi - \phi)/kT}]}, \quad (7.12)$$

where  $\tau_t$  has been defined as

$$\tau_t = \tau_n e^{-\frac{qV_t}{kT}} + \tau_p e^{\frac{qV_t}{kT}}. \quad (7.13)$$

The expression for  $(\psi - \phi)$  as a function of  $x$  for the linearly graded junction was given by Equation (5.32),

$$\psi - \phi = \frac{qa}{2\epsilon} \left[ \frac{W^2}{4} x - \frac{x^3}{3} \right] + \frac{kT}{q} \frac{2}{W} x, \quad (5.32)$$

which can now be substituted into the integral of Equation (7.12) and the result evaluated numerically. The only question is whether or not  $\tau_n$  and  $\tau_p$  have the same value in the depletion region as they have in the charge neutral region. These regions differ by the  $P^+$  diffusion which could introduce impurities that alter the nature of the recombination centers in the substrate. Figure 7.7 shows the result of the numerical

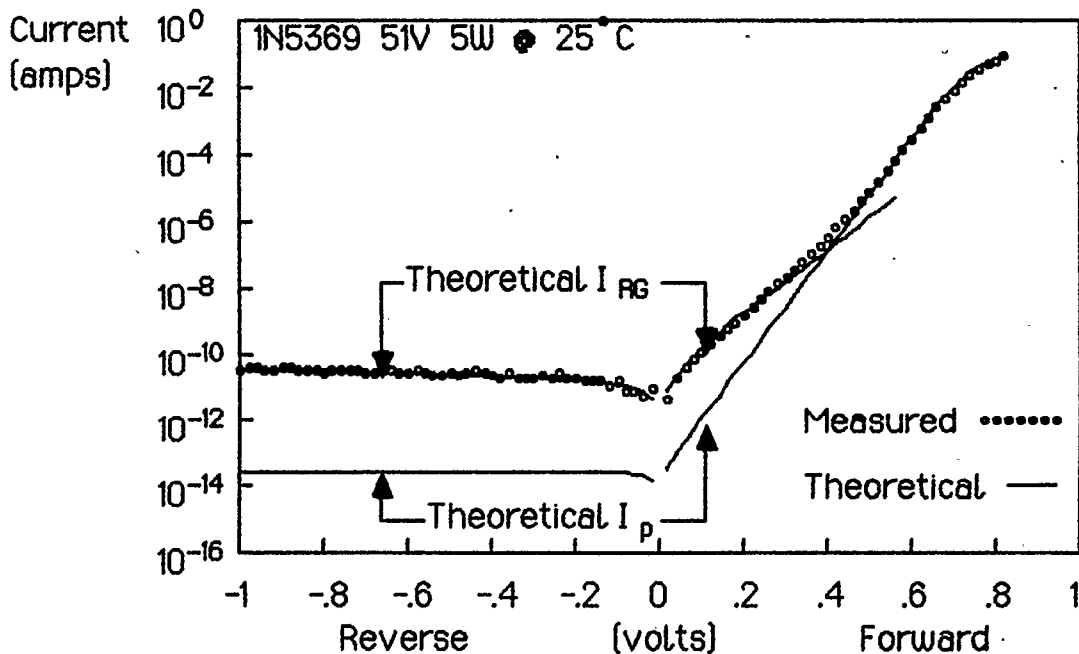


**Figure 7.7** A Comparison of the Improved Diode Equation, the Refined Depletion Region RG Equation and Measured 1N5369 Data.

integration for the 1N5369 diode at 25°C. The set of parameters used to obtain this agreement are not unique; they range from about

$$v_t = .07 \text{ for } \tau_n = \tau_p = 2 \tau, \quad \text{to} \quad v_t = .05 \text{ for } \tau_n = \tau \text{ and } \tau_p = 4 \tau,$$

where  $\tau$  is the high injection lifetime determined from the high injection delay time. Some assumption must be made about the relative magnitudes of  $\tau_p$  and  $\tau_n$  and the sign of  $v_t$  to match the measured and theoretical characteristics. The evidence suggests that the difference between the bulk region and depletion region lifetimes for this diode is not unexpectedly large. The values of  $v_t$  show that the average trap energy level is about  $2kT$  to  $3kT$  away from the intrinsic energy level at 25°C. This is reasonable for typical impurities [1 pp23] [14] and crystal dislocations [15]. It is evident from Figure 7.7 that as the low to high injection breakpoint moves to the left with lower substrate doping, the difference between  $I_p$  and  $I_{RG}$  becomes less significant. Figure 7.8 compares the measured 1N5369 characteristics with the

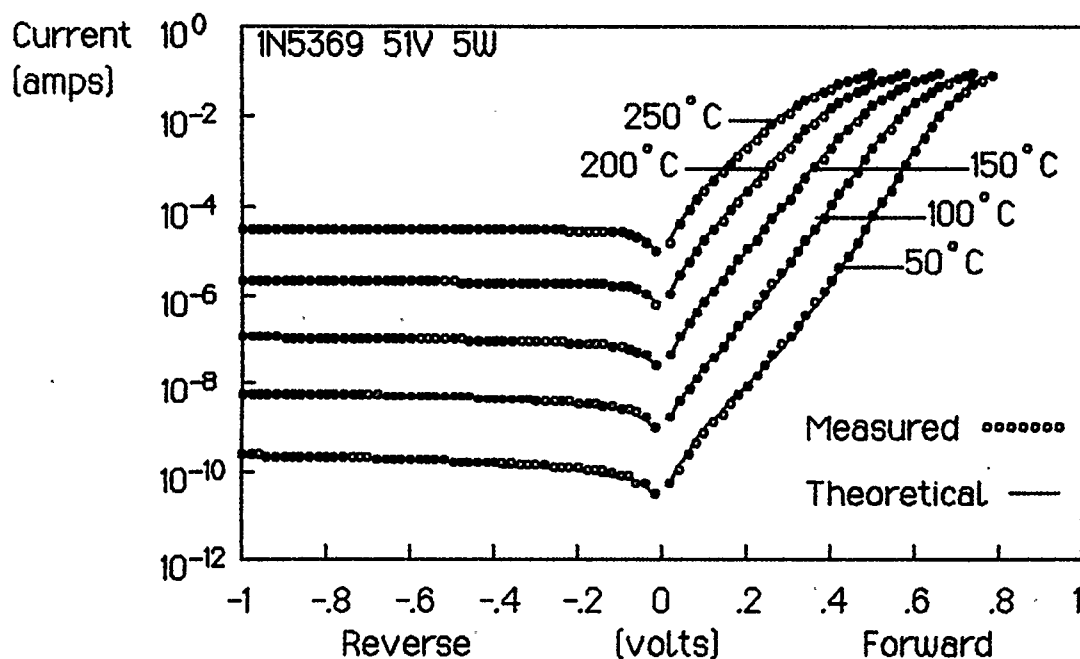


**Figure 7.8** A Comparison of the Comprehensive Diode Model with the Measured Characteristics of a 51V 5W Diode.

theoretical currents generated by the sum of the improved diode equation and the refined depletion region RG equation for a wide range of elevated temperatures. The summation of these two equations is referred to as the integral form of the comprehensive diode model.

Figure 7.9 shows a comparison of the comprehensive diode model with the measured characteristics of a 25V 5W diode. The parameters of this diode were tabulated in Table 6.1, and its delay time, capacitance and forward current characteristics were plotted in Figures (6.10, 11, 12). The parameters used to obtain this fit range from about

$$v_t = .12 \text{ and } \tau_n = \tau_p = .3 \tau, \quad \text{to} \quad v_t = .09 \text{ and } \tau_n = .1 \tau \text{ and } \tau_p = .9 \tau.$$

If the second set of parameters is the correct one, then  $\tau_n + \tau_p$  in the depletion region equals  $\tau$  in the bulk region, and there is no apparent difference in the lifetimes of the two regions of this diode. Also,  $\tau_n < \tau_p$ ,

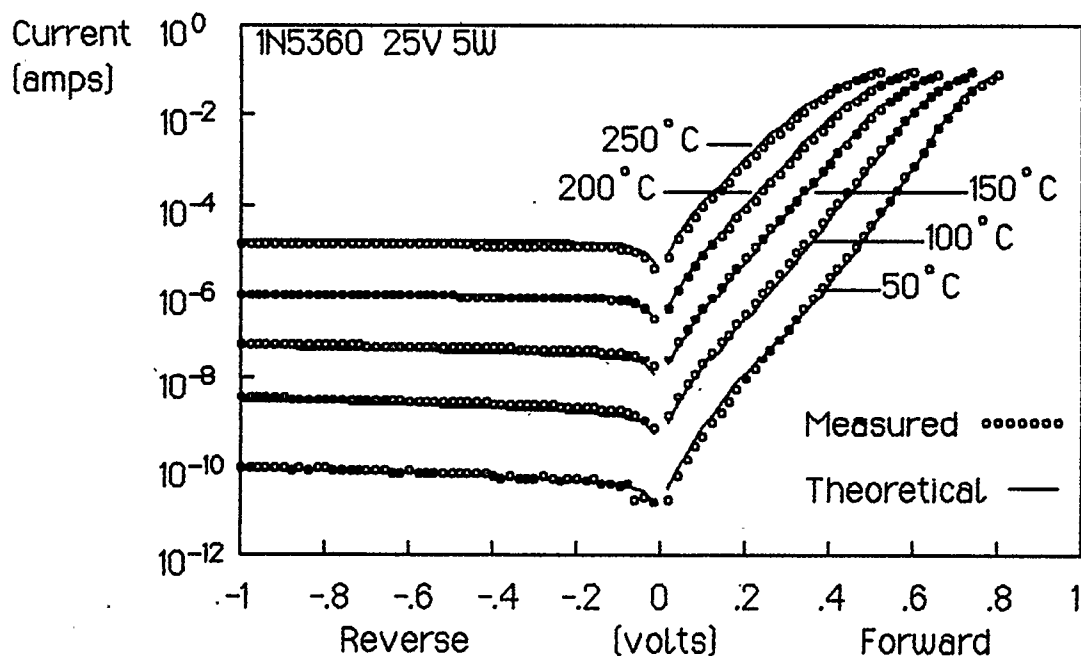


**Figure 7.9** A Comparison of the Comprehensive Diode Model with the Measured Characteristics of a 25V 5W Diode.

and that is in keeping with the generally observed indifference between the low and high injection delay times. Figure 2 of reference [[6]] suggests that  $\tau_n$  can be less than  $\tau_p$ .

In these last two examples it was assumed that  $\tau_n \ll \tau_p$  because it is believed to be this way in the N bulk. However, the lifetimes in the bulk are not generally the same as those in the depletion region; also, if the magnitudes of  $\tau_n$  and  $\tau_p$  are reversed, the fit can be maintained by reversing the sign of  $v_t$ . It is not possible by matching the theoretical model to measured data to uniquely determine  $v_t$ , the sign of  $v_t$ ,  $\tau_n$  and  $\tau_p$ . Therefore, for modelling purposes, it seems reasonable to drop the distinction between the  $\tau$ 's in the depletion region, and to use instead  $\tau_0 \approx \tau_n \approx \tau_p$  and consider  $v_t$  as the absolute value of the trap potential. Since  $2\tau_0 \approx \tau_n + \tau_p$ , then  $\tau_0$  can be thought of as the average of the two lifetimes. This suggests a simplification for the definition of  $\tau_t$ ,

$$\tau_t \equiv \tau_n e^{-\frac{qv_t}{kT}} + \tau_p e^{\frac{qv_t}{kT}} \equiv \tau_0 e^{\frac{qv_t}{kT}}, \quad [7.14]$$

since the term with the positive exponent is larger than the other.

An analytical solution of the refined depletion region RG equation is possible. The second and third terms of the expression for  $\psi - \phi$  given by Equation (5.32) are significantly smaller than the first term; that is

$$\psi - \phi \approx \frac{q\sigma W^2}{8\epsilon} x \quad \text{for } x \leq \frac{W}{2}. \quad [7.15]$$

When this is used in place of Equation (5.32) in the integral form of the refined depletion region RG equation, Equation (7.12), there is no perceptible difference in the numerically integrated theoretical curves of Figures 7.8 and 7.9. Because the depletion region potential distribution of Figure 7.6 is symmetrical, then the quasi Fermi level expressions for p and n dictate that

$$p(x) = n(-x), \quad n(x) = p(-x), \quad n(x) \gg p(x), \quad p(-x) \gg n(-x).$$

Hence, Equation (7.12) can be integrated in two parts: over the P side neglecting  $n$  since  $n \ll p$  in the P side, and over the N side neglecting  $p$  since  $p \ll n$  in the N side. This can be done while maintaining the distinction between  $\tau_n$  and  $\tau_p$ , but since there is little merit in doing so, the problem can be simplified somewhat by using the average lifetime,  $\tau_0$ , which makes the two halves of the integral equal. Applying this technique and substituting Equations (7.14) and (7.15) into (7.12) gives

$$I_{RG} = \frac{A q n_i [e^{qV/kT} - 1]}{\tau_0 e^{qV_t/kT}} 2 \int_0^{W/2} \frac{dx}{1 + e^{\frac{V-2V_t}{2kT/q} - \frac{q a W^2 x}{8 \epsilon kT/q}}}. \quad (7.16)$$

This is easily integrated to give

$$I_{RG} = \frac{A q n_i [e^{qV/kT} - 1]}{\tau_0 e^{qV_t/kT}} 2 \left[ x - \frac{8 \epsilon kT}{q a W^2} \ln \left[ 1 + e^{\frac{V-2V_t}{2kT/q} - \frac{q a W^2 x}{8 \epsilon kT/q}} \right] \right]_0^{W/2} \quad (7.17)$$

For substantial reverse bias the natural log term in this equation vanishes, and  $I_{RG}$  reduces to the standard depletion region RG equation for reversed biased diodes, Equation (7.8). Continuing the solution:

$$I_{RG} = \frac{A q n_i [e^{qV/kT} - 1]}{\tau_0 e^{qV_t/kT}} \frac{8 \epsilon kT}{q a W^2} 2 \left[ \ln \left[ 1 + e^{\frac{V-2V_t}{2kT/q}} \right] - \frac{V-2V_t}{2kT/q} \right]$$

$$= \frac{A q n_i [e^{qV/kT} - 1]}{\tau_0 e^{qV_t/kT}} \frac{2}{3} \frac{W}{\psi_{np}} \frac{kT}{q} 2 \left[ \ln \left[ 1 + e^{\frac{V-2V_t}{2kT/q}} \right] - \frac{V-2V_t}{2kT/q} \right], \quad (7.18)$$

where use has been of the fact that

$$\frac{V-2v_t}{2kT/q} e^{\frac{q a W^2}{B e} \frac{W}{2kT/q}} \gg 1$$

for all values of the applied voltage. Equation (7.18) is the refined depletion region RG equation. When the theoretical curves of Figures 7.8 and 7.9 are redrawn using Equation (7.18) with the same  $\tau_n = \tau_p$  parameters as used before in Equation (7.12), there is no noticeable change.

### 7.3 Surface Leakage Current

Figure 7.10 shows a comparison of the comprehensive diode model and the measured characteristics of a smaller 25V diode, a 1N5253. The

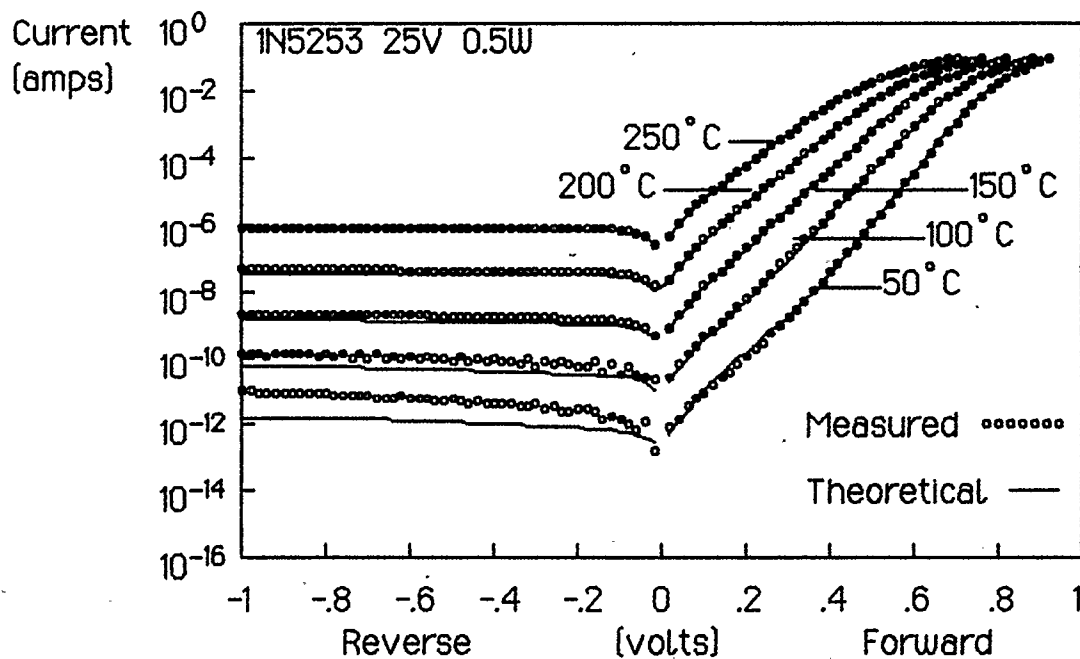


**Figure 7.10A** Comparison of the Comprehensive Diode Model with the Measured Characteristics of a 25V 0.5W Diode.

measured reverse characteristic at the lowest temperature has a greater voltage dependence than that predicted by the model. Even though the surface leakage current is small, it can apparently exceed the reverse diode current at moderate and low temperatures. In Figure 7.11 an additional current component,

$$I_{sl} = \frac{V}{R_{sl}} = \frac{V}{1500 e^{0.5/kT}}, \quad (7.19)$$

has been added to the theoretical model. The temperature dependence assigned to  $R_{sl}$  to achieve the best fit is that which would be expected of a semiconductor oxide material [[13 pp2-51]] used for fabrication of the  $P^+$  diffusion mask and the package. At low temperatures surface leakage dominates the low current domain, and its presence can be recognized by the resistive voltage dependence of the measured current.

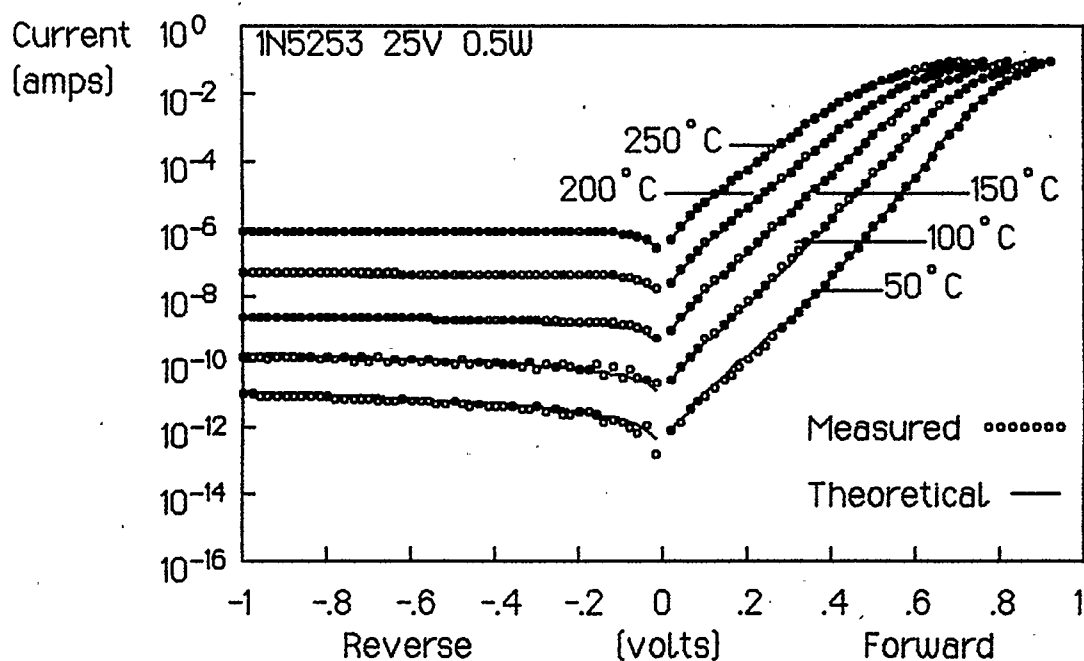


**Figure 7.11** A Comparison of the Measured Characteristics of a 25V 0.5W Diode with the Comprehensive Diode Model and an Added Surface Leakage Current Component.

## 8 CONCLUSION

### 8.1 Summary

The ideal diode equation governs the low injection domain of the forward characteristic where the current exceeds that due to depletion region RG. The ideal or low injection equation for a p<sup>+</sup>n diode is

$$I_p = I_s \left[ e^{qV/kT} - 1 \right].$$

The high injection equation governs the high injection region, and for a p<sup>+</sup>n diode it is given by

$$I_p = I_h e^{qV/2kT}.$$

Both regions can be modelled by the improved diode equation:

$$I_p = I_h \left[ \sqrt{\left[ \frac{I_h}{2I_s} \right]^2 + e^{qV/kT}} - \sqrt{\left[ \frac{I_h}{2I_s} \right]^2 + 1} \right].$$

The high and low injection intercepts,  $I_h$  and  $I_s$ , can be obtained from a measured forward characteristic. To model the diode behavior at all temperatures, the temperature dependence assigned to the intercepts must be

$$I_h \propto \frac{n_i}{T} \quad \text{and} \quad I_s \propto \frac{n_i^2}{T}.$$

Series resistance influences the forward characteristic at high current, and it is accommodated by

$$V = V_a - R_s I_p.$$

When  $I_h$  and  $I_s$  are determined in this way and substituted into the improved diode equation, and when series resistance is accounted for, the resulting model is an excellent mathematical representation of the diode's behavior outside of the influence of depletion region RG.

The high injection intercept can be calculated from known or measured parameters using

$$I_h = e^{-\chi} \sqrt{2 \left[ 1 + \frac{D_p}{D_n} \right]} A q \frac{\sqrt{D_p}}{\sqrt{t_{dH}} \frac{2(1+\chi)}{\sqrt{\pi}}} n_i.$$

The only parameter in this equation that cannot be measured is  $\chi$  which is given by

$$\chi = \frac{1}{4} \left[ \frac{W_b}{L} + e^{W_b/L} - 1 \right].$$

The value of  $\chi$  needed to equate the calculated and measured values of  $I_h$  requires a value for the ratio of  $W_b/L$  that seems to be reasonable.

The low injection intercept can also be calculated using

$$I_s = A q \frac{\sqrt{D_p}}{\sqrt{t_d} \frac{2(1+\chi)}{\sqrt{\pi}}} \frac{n_i^2}{N_{do}}.$$

The only unknown parameter in this equation is  $N_{do}$ . The value of  $N_{do}$  needed to equate the calculated and measured values of  $I_s$  is found to be equal to or slightly lower than the known substrate doping, which is as expected.

The relationship between lifetime and charge storage delay time is the same for high injection as it is for low injection. When calculating the low injection lifetime from the measured low injection delay time, consideration must be given to the effects of non-uniform doping and space charge recovery time.

The generally accepted depletion region RG current equation for forward biased diodes,

$$I_{RG\text{ Fwd}} = A q \frac{W}{\tau} n_i e^{qV/2kT},$$

generates theoretical values that are one to two orders of magnitude greater than the measured currents at room temperature. The integral form of the refined depletion region RG equation for a linearly graded junction,

$$I_{RG} = \frac{A q n_i [e^{qV/kT} - 1]}{\tau_t} \int_{-W/2}^{W/2} \frac{dx}{1 + \frac{e^{qV/2kT}}{\tau_t} [\tau_n e^{-q(\phi - \phi)/kT} + \tau_p e^{q(\phi - \phi)/kT}]},$$

where

$$\tau_t \equiv \tau_n e^{-\frac{qv_t}{kT}} + \tau_p e^{\frac{qv_t}{kT}}$$

can be integrated numerically, and the results agree well with observed currents in both the forward and reverse directions. The range of values assigned to  $v_t$ ,  $\tau_n$  and  $\tau_p$  to equate the measured and theoretical data seem to be reasonable, but the matching procedure does not reveal unique values for these or for the sign of  $v_t$ . To obtain a unique set, use is made of  $\tau_n \approx \tau_p$ , and the absolute value of  $v_t$ .

Without noticeably degrading the model the refined depletion region RG equation can be expressed in closed form as

$$I_{RG} = \frac{A q n_i [e^{qV/kT} - 1]}{\tau_0 e^{qV_t/kT}} \frac{8 \epsilon}{q a W^2} \frac{kT}{q} 2 \left[ \ln \left[ 1 + e^{\frac{V-2V_t}{2kT/q}} \right] - \frac{V-2V_t}{2kT/q} \right]$$

where  $\tau_0$  is used in place of  $\tau_n$  and  $\tau_p$ .

Current that leaks around the junction can be larger than the diode current in the low current region. This leakage current can be modelled by

$$I_{sl} = \frac{V}{R_{sl}} = \frac{V}{C_1 e^{C_2/kT}}$$

and the parameters in this expression required to make  $I_{sl}$  agree with the measured currents are those that would be expected of typical package materials. At low temperatures this leakage current dominates the low current region.

The improved diode equation alone adequately models the forward and reverse characteristics of diodes exposed to high temperatures. At moderate temperatures depletion region RG current dominates the region of small positive bias and negative bias, and the refined depletion region RG equation must be added to the improved diode equation to produce a comprehensive model. Current that leaks around the surface of the diode can dominate the low current region of small diodes at low temperatures, and this is easily modelled by a temperature sensitive parallel resistor.

## 8.2 Applications

It is hoped that this detailed analysis has resulted in a better understanding of the influence that the diode parameters have on the

shape of the DC characteristics. The comprehensive model should be useful to diode designers endeavoring to achieve a particular kind of response. A small computer can be used to plot DC characteristics generated by the comprehensive model for various temperatures, and the effects of changing the parameters can be readily visualized.

Since  $\sigma$  is fairly close to unity, Equation (3.49),

$$\sigma A q \frac{D_p}{L_p} = \frac{I_h}{n_1},$$

can be used to obtain an order of magnitude estimate of the low injection lifetime from the measured high injection intercept, if the diode area is known. Also, Equation (3.49),

$$\sigma N_d = \frac{I_h}{I_s} n_1,$$

can be used to estimate the substrate doping from the ratio of the measured high and low intercepts. A more accurate method is to measure the charge storage delay time, and thereby determine the lifetime, then calculate  $\sigma$  from the first of the above two equations, then calculate  $N_d$  from the second.

The series resistance, which is a measure of the effectiveness of the metal contacts, can be measured by matching the high injection equation to the measured forward characteristic.

The average lifetime in the depletion region and the absolute value of the trap potential can be measured by equating the closed form of the refined depletion region RG equation to measured data. In the forward direction for  $V > 2 v_t$ ,  $v_t$  does not influence the current, and  $\tau_0$  can be chosen to equate the measured and theoretical data. Once  $\tau_0$  has been established, then  $v_t$  can be determined by matching the theoretical and measured data in the reverse direction where  $v_t$  is influential.

If the polarity of  $v_t$  and the ratio of  $\tau_n/\tau_p$  are otherwise known, then there may be reason to retain both  $\tau_p$  and  $\tau_n$  in the integration of the refined depletion region RG equation, and to attempt to determine these from the curve fitting process. But for modelling purposes only this does not seem to be necessary.

A good estimate of pn junction reverse current is useful in calculating the quiescent power supply drain of integrated CMOS structures that contain numerous reverse biased N substrate to P well junctions and reverse biased gate protection diodes.

Circuit simulators such as SPICE could more accurately model pn junctions by replacing the ideal diode model with the comprehensive silicon diode model.

### 8.3 Suggestions for Further Research

The comprehensive silicon diode model could be confirmed at temperatures below 25°C; it is expected to continue to predict diode behavior at very low temperatures.

The comprehensive model should be confirmed for abrupt junction diodes. For this the improved diode equation is unchanged, but it will be necessary to use the abrupt junction potential distribution in the refined depletion region RG equation. A closed form solution should be possible for a p<sup>+</sup>n junction, since it will only be necessary to integrate the depletion region RG equation across the N side of junction where the hole concentration term can be neglected.

Noise measurements [14] could be used to confirm the value obtained for the trap potential from the refined depletion region RG equation.

There could be some merit in applying an analysis similar to that used to

thyristors.

An investigation similar to the one presented here could be conducted for direct recombination gallium arsenide devices.

## 9 LABORATORY INSTRUMENTATION

Three kinds of diode measurements were made:

- DC characteristics,
- charge storage delay time and
- junction capacitance.

The DC characteristics were recorded at temperatures ranging from 25 °C to 250 °C. Charge storage delay times were measured at temperatures of up to 150 °C, and the junction capacitance measurements were performed at room temperature. A Macintosh computer was used to plot and compare the measured data with the theoretical models and to serve as a word processor for the production of this document.

The steady state current voltage characteristic measurement setup is illustrated in Figure 9.1. The Despatch LFD 1-42 oven was used to elevate the temperature of the device under test. Although the oven is

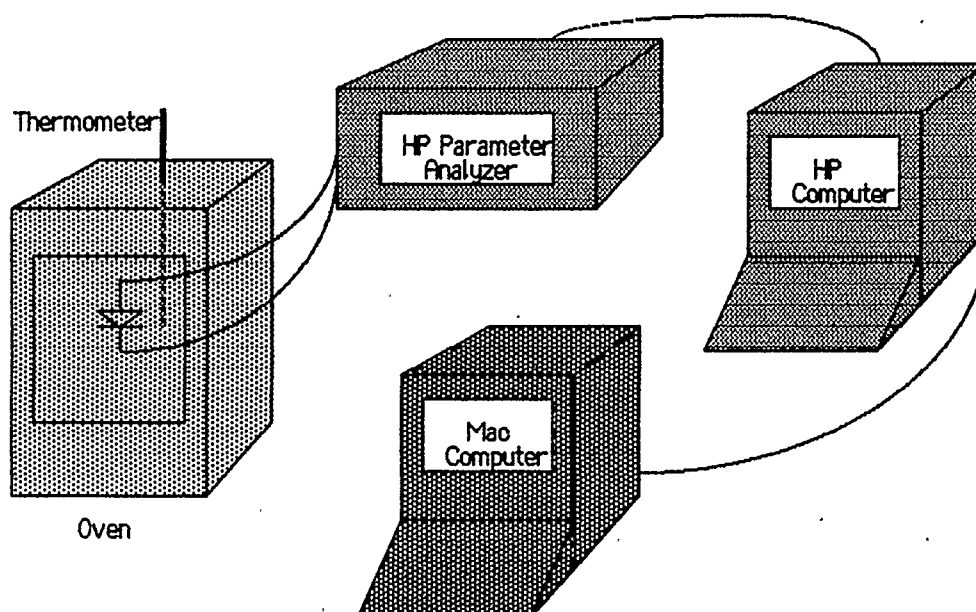


**Figure 9.1** DC Characteristic Data Acquisition

equipped with a digital temperature readout, a scientific thermometer was placed in the oven adjacent to the diode to make sure that the diode had reached the desired temperature.

The voltage and current ranges of the Hewlett Packard 4145A programmable parameter analyzer are  $\pm 100$  volts and about  $10^{-14}$  amps to  $10^{-1}$  amps. The Hewlett Packard 9816 desktop computer was used to interface the HP-IB bus of the parameter analyzer to the RS232 port of the Macintosh computer.

Charge storage delay time measurement was accomplished as shown in Figure 9.2. The square wave voltage across the series combination of the diode and the resistor was maintained at  $\pm 10$  volts. The forward voltage drop across the diode opposes the positive half of the generator voltage and aids the negative half; consequently, the initial reverse current is larger than the forward current. This accounts for a  $\gamma = 1.1$ . To keep the leads short for these tests the diode's temperature was elevated in a small beaker of hot oil rather than in the oven.

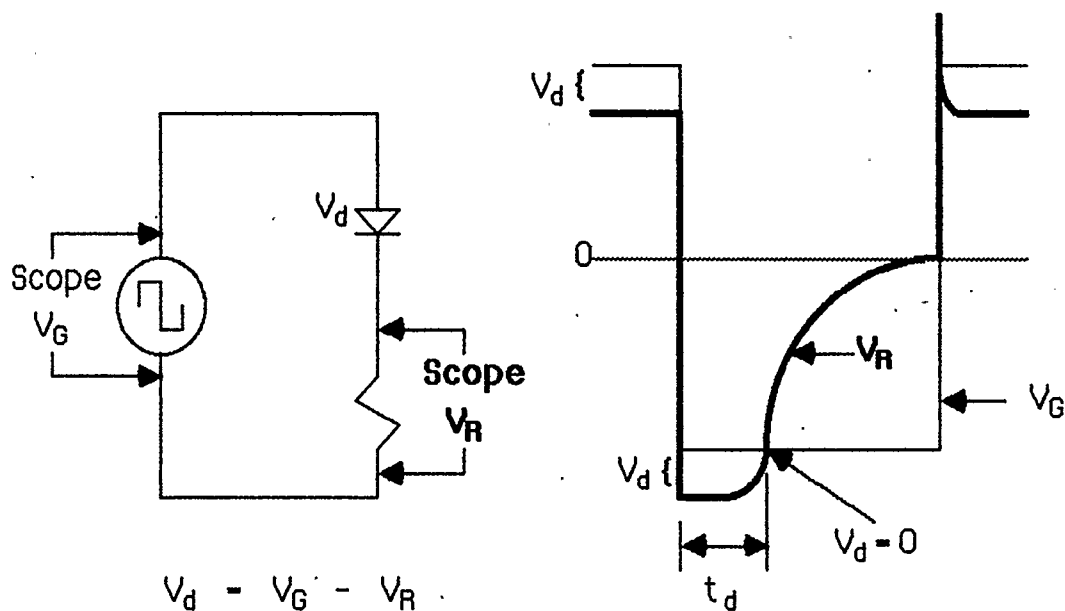


**Figure 9.2** Charge Storage Delay Time Measurement Schematic and Waveforms.

Junction Capacitance was measured using a Hewlett Packard 4262A LCR meter and checked with a Wayne Kerr bridge. The LCR meter was calibrated with several 1% capacitors. The reverse bias voltage source connected in series with the diode was shunted with a 0.01  $\mu$ fd capacitor to short circuit the impedance of the supply and connecting leads.

The instruments used to measure current and voltage are accurate to more than four significant figures. The accuracy of the capacitance measurements is estimated to be better than  $\pm 2\%$ . The temperature was known to within  $\pm 1^\circ$  C. The greatest source of error was the uncertainty in the delay time measurements, but it should be no larger than about  $\pm 5\%$ .

## 10 REFERENCES

- [[1]] Sze, S.M., Semiconductor Devices Physics and Technology, Wiley, N.Y., 1985.
- [[2]] Yang, E.S., Fundamentals of Semiconductor Devices, McGraw-Hill, N.Y., (1978).
- [[3]] Sze, S.M., Physics of Semiconductor Devices, Wiley, N.Y., 1969.
- [[4]] Pierret, R.F., Modular Series on Solid State Devices. Semiconductor Fundamentals, Vol. I, Addison Wesley, Mass, (1983).
- [[5]] Neudeck, G.W., Modular Series on Solid State Devices. The PN Junction Diode, Vol. II, Addison Wesley, Mass, (1983).
- [[6]] Shockley W. and Read W. T., "Statistics of Recombination of Holes and Electrons", *Phys. Rev.*, 87, 835, (1952).
- [[7]] Lax B. and Neustadter S. F., "Transient Response of a p-n Junction", *J. Appl. Phys.*, 25, 1148, (1954).
- [[8]] Kingston R. H., "Switching Time in Junction Diodes and Junction Transistors", *Proc. IRE*, 42, 828, (1954).
- [[9]] Fogiel M., Handbook of Mathematical Formulas Tables Functions Graphs Transforms, Library of Congress Card Number 80-52490.
- [[10]] Girand M., personal communication, Motorola Semiconductor Products Inc., Phoenix, Ariz.

- [[11]] Chang C. Y., Fang Y. K. and Sze S. M., "Specific Contact Resistance of Metal-Semiconductor Barriers", *Solid State Elec.*, 14, 541, (1971).
- [[12]] Yu A. Y. C., "Electron Tunneling and Contact Resistance of Metal-Silicon Contact Barriers", *Solid State Elec.*, 13, 239, (1970).
- [[13]] Considine D. M., Process Instruments and Controls Handbook, McGraw Hill, N. Y., (1974).
- [[14]] Haslett J. W., Kendall E. J. M., "Temperature Dependence of Low - Frequency Excess Noise in Junction - Gate FET's", *IEEE Tran. on Electron Devices*, ED - 19, 8, 943, (1972).
- [[15]] Glaenzer R. H., Jordan A. G., "The Electrical Properties of Dislocations in Silicon, Parts I and II", *Solid State Elec.*, 12, 247, (1969).